HARVARD UNIVERSITY

Graduate School of Arts and Sciences

DISSERTATION ACCEPTANCE CERTIFICATE

The undersigned, appointed by the
Committee on Higher Degrees in Biological Sciences in Public Health
have examined a dissertation entitled

"Alterations in energy metabolism and neurodegeneration as a consequence of DNA damage"

presented by
Lear Elizabeth Brace
candidate for the degree of Doctor of Philosophy
and hereby certify that it is worthy of acceptance.

Signature _____

Dr. Bruce Kristal, Ph.D., Chair, Harvard Medical School and Brigham and Women's Hospital

Signature _____

Dr. Marianne Wessling-Resnick, Ph.D., Harvard T.H. Chan School of Public Health

Signature _____

Dr. Chih-Hao Lee, Ph.D., Harvard T.H. Chan School of Public Health

Signature _____

Dr. Raul Mostoslavsky, M.D., Ph.D., Massachusetts General Hospital

Date: October 20, 2016

ALTERATIONS IN ENERGY METABOLISM AND NEURODEGENERATION AS A CONSEQUENCE OF DNA DAMAGE

A DISSERTATION PRESENTED

BY

LEAR ELIZABETH BRACE

TO

THE PROGRAM IN BIOLOGICAL SCIENCES IN PUBLIC HEALTH

IN PARTIAL FULFILLMENT OF THE REQUIREMENTS

FOR THE DEGREE OF

DOCTOR OF PHILOSOPHY

IN THE SUBJECT OF

BIOLOGICAL SCIENCES IN PUBLIC HEALTH

HARVARD UNIVERSITY

CAMBRIDGE, MASSACHUSETTS

OCTOBER 2016

ADVISER: JAMES MITCHELL LEAR ELIZABETH BRACE

ALTERATIONS IN ENERGY METABOLISM AND NEURODEGENERATION AS A CONSEQUENCE OF DNA DAMAGE

ABSTRACT

The correlation between DNA damage and aging has been discussed since Peter Medawar framed the first modern theory of aging in 1952. In support of a causal relationship between DNA damage and aging, most human segmental progeroid disorders, which share some but not all of the characteristics of aging, are associated with defects in DNA damage repair and signaling processes. One such example is Cockayne syndrome (CS), which is characterized by neurodegeneration, cerebellar ataxia and failure to thrive, caused by inborn defects in key proteins of the transcription-coupled arm of the nucleotide excision DNA repair pathway (NER). Here, we created a new mouse model of CS by combining two different null alleles in the NER pathway. Double homozygous mutant *Csa*|*Xpa*, or CX mice, represent the first mouse model of severe CS that survive the weaning period with high penetrance, solving a recurring problem with previous models. After weaning, CX mice present with progressive loss of adiposity and neurodegenerative complications that accurately mimic the human disease. Investigations into adiposity loss revealed that oxidative phosphorylation, specifically fatty acid oxidation (FAO), is significantly increased upon the chronic accumulation of DNA damage in CX animals *in vivo* and *in vitro,* and also in CS patient cell lines. The

increase in FAO is dependent on PARP-1 activation, driving NAD+/ATP depletion and subsequent activation of AMPK, increasing FAO-related gene expression. We further demonstrate that increased FAO is a general response to DNA damage, as acute doses of numerous genotoxic agents similarly increased fat burning in wildtype mice both *in vitro* and *in vivo.* This metabolic adaptation is also beneficial, as blocking FAO reduced cell viability upon damage and increasing FAO further extended the lifespan of CX mice via a diet reduced in methionine. Investigations of the role of myelin loss in neurodegeneration of CX mice were also performed. Age-dependent loss of myelin, astrogliosis, and increased mRNA expression of enzymes that act to catabolize myelin lipids were observed in CX brains compared to controls. Increased FAO capacity was also observed in CX brain and sciatic nerve, with cultured primary astrocytes of the CX central nervous system identified as the likely cell type responsible for this fat burning. Whether increased FAO by astrocytes contributes to the patchy loss of white matter/myelin in CX nervous tissue and subsequent neurodegeneration remains an outstanding issue. Lastly, we utilized CX mice to analyze potential new endpoints, such as hematopoietic cell growth, circulating liver enzyme levels, and adipocyte dysfunction, as markers of therapeutic interventional efficacy of pharmacological approaches including NAD+ supplementation. The CX mouse model thus represents a valuable tool that accurately models important aspects of human Cockayne syndrome, and may also be used to shed light on the role of DNA damage in physiological aging.

TABLE OF CONTENTS

ACKNOWLEDGMENTS

I would like to express my most sincere gratitude for the individuals that have supported my scientific career over the last twelve years. First and foremost, I would like to thank my adviser, Jay Mitchell, for being an incredibly supportive PI with an infectious excitement for science from whom I learned a great deal. Jay has a tremendous versatility as a mentor, a rare asset that assisted in leading the kooky researchers in our group.

An immense thank you to the members of the Mitchell Lab throughout the years: Chris, Pedro, Jordan, Eylül, Dottie, Sarah, Alban, Humberto, Lauren, Matt, Jo, Luis, and Justin. The energy of the Mitchell lab was consistently high and the laughs overwhelmed any day-to-day frustrations. Special thanks to Chris, who is the nicest and most rational scientist (and human being) I have yet to encounter and was always approachable for advice and assistance, Pedro, for sharing the highs and lows of science from our shared desks even if he did routinely ask me when my rotation was over, and Humberto, for being a walking textbook and having the ability to infuse any room with both momentum and hilarity. The Mitchell lab made it fun to come to lab every day and I thank all members past and present for their friendship and collaboration.

Great thanks to my PQE, DAC, and Thesis committee members: including Vishal Vaidya, Alec Kimmelman, Zhi-Min Yuan, David Sinclair, Ed Nielan, Raul Mostoslavsky, Chih-Hao Lee, Marianne Wessling-Resnick, and Bruce Kristal for their time and support. BPH is a special program, due in large part to the work of Marianne Wessling-Resnick and her guidance and attitude set the pace for my classmates and myself to succeed. I have a great deal of respect for her as a mentor and as a scientist and have always

encouraged all new students to seek out her advice. I would also like to acknowledge Brendan Manning for his direction of the BPH program for the last few years, as well as Deirdre Duckett, Tom Brazda, and Holly Southern for making everything work in this program and being excellent advice-givers.

I started this program in a fantastic group of individuals especially Jemila, Nicole, Rose, Christine, and Kassie. I am perplexed how someone can succeed in his or her PhD without Jemila, because she certainly made mine possible. I cannot thank her enough for her friendship and support and at times being the only person I wanted to talk to in a 5-mile radius. The work she has accomplished in the last five years is staggering and her ability to juggle all of her roles is remarkable and enviable. Nicole Espy is my go-to for life/work advice and dancing away our stressors and the thought of Nicole not being only 2 streets away at any given moment is incredibly upsetting. Thank you also to Kasia, Perrine, Nelson and Kent for their friendship and support through the years in BPH.

Special thanks to the BPH class above me: Peter, Allison, Caeul, Jordan, Michelle, Alex, and Eylül for immediately welcoming me into this program and what felt like (and still is) the greatest group of friends. The additions of Noah, Burak, Sam, and Big Peter only sweetened the pot. As you each trickled out of HSPH, the gloom increased but we will all find a way to stick together even if separated by many states or countries. Alaattin Kaya has been an incredible friend and sounding board for the last few years and our paths will absolutely continue to cross in the future. Thank you to Eric Camire for being the greatest friend for over a decade: your presence throughout both college and our PhDs was extremely reassuring.

I learned how to be a scientist from Fran Perler. From age 17 she taught me the importance of controlled experimentation, effective scientific communication, and the importance of good coffee. I am forever in debt to her calm yet focused direction that made me want to be a scientist. My college chemistry adviser, Faina Ryvkin, further focused my future direction and challenged me on a daily basis. Witnessing her genuine devotion to her students, I learned to love teaching others. Special thanks to Matthew Meyerson and Meyerson lab members, especially Josh Francis, who continues to be my best critic and close friend.

Wonderful friends since childhood surrounded me outside of science and their encouragement and enthusiasm consistently motivated me: thank you to Janna, Breezy, Shannon, Laura, and Andrew. Profound gratitude to the Parlor guys: Jon Olszewski, Max Dougherty, and Garvey Salomon for quick wit, late nights, and frequent distractions from any stressors. Not sure how we got lucky enough to find the three best guys all in one place.

My mother has been my #1 fan from Day One and she and my brother have supported my scientific career wholeheartedly and have kept me grounded and balanced. My extended family, especially the Bussone, Pinciaro, and McGrath families, have been a constant source of encouragement. Brien deserves volumes of praise for his constant support of my efforts in grad school including accompanying me on middle of the night trips into the lab and dealing with the day to day highs and lows of grad school. His self-motivation inspires me to work harder every day and I am forever grateful for his patience and partnership.

DEDICATION

For my mother, brother, and husband

In memory of my father

LIST OF FIGURES

CHAPTER 1

Introduction

Cockayne syndrome: History, diagnosis, and clinical features

Edward Cockayne first described Cockayne syndrome (CS) in 1936 as a disorder of "dwarfism with retinal atrophy and deafness"[1]. Other early accounts of the cardinal features of CS include microcephaly, growth failure, developmental delay, deformed and rigid joints, and calcifications on the brain. However, it was not until the landmark study of Nance and Berry in 1992 that the first comprehensive evaluation of the severe and progressive clinical features of CS was established[2]. Since then, numerous studies have increased our understanding of this multi-system degenerative syndrome[3-7].

Cockayne syndrome is an extremely rare, autosomal recessive disease, with an estimated prevalence of 2.5 per million and an incidence of 1 in 250,000 live births[8]. Cells of CS patients are specifically defective in the transcription-coupled arm of nucleotide excision DNA repair (TC-NER). NER acts to recognize and remove helix-distorting lesions both throughout the global genome (GG-NER) and selectively from actively transcribed genes (TC-NER). CS patients have normally active GG-NER but this pathway is defective in other family members of NER disorders including Xeroderma pigmentosum (XP) and trichothiodystrophy (TTD).

Inborn defects in proteins of NER lead to XP, CS, or TTD though the clinical outcomes are diverse. Patients with XP have extreme light sensitivity and photophobia with high incidence of skin cancers whereas patients with TTD have no cancer prevalence and are of short stature with brittle hair and neurological impairment[9]. Cerebro-occulo-

facio-skeletal syndrome (COFS) is a CS variant that is extremely severe but ultraviolet sensitivity syndrome (UVSS) has mild features, mainly photosensitivity. Rare cases do exist of mixed XP/CS phenotypes linked to mutations in other NER-associated proteins, including XPD, XPB, and XPG, and display severe photosensitivity and cancer-proneness[10]. However, CS itself is not associated with any cancer risk, which is usually seen in DNA repair deficient syndromes[9]. The zero incidence of cancer seen in CS patients is often hypothesized to be due to cellular growth inhibition resulting from increased apoptosis of DNA damaged cells[11] or due to the absence of UV-induced mutagenesis[12] but it remains an unsolved question in the pathology of Cockayne syndrome.

Most CS patients fall into one of two complementation groups: CS-A or CS-B. CS-A patients have mutations in *CSA*/*ERCC8,* while *CSB*/*ERCC6* is mutated in individuals in the CS-B group, which is responsible for roughly 65% of cases[5]. The protein CSA is part of an E3 ubiquitin ligase complex required for the recruitment of transcription-coupled nucleotide excision repair factors to the repair site[13]. CSB is a member of a large protein complex of the SWI2/SNF2 family involved in chromatin remodeling, transcription, and DNA repair[14]. CS proteins have also been implicated in base excision repair, through possible interactions with poly (ADP-ribose) polymerase 1 (PARP-1) and APE-1[15], and in mitochondrial DNA repair, transcription, and proteostasis[8].

In the roughly 120 genetically confirmed CS patients reported in the literature, approximately 78 mutations were found in *CSB* and 30 in *CSA*. In CS patients, all types of mutations have been detected (nonsense, missense, frameshift, splicing, and large deletions), and patients from the same family often show similar phenotypes but there are only a few examples of unrelated CS patients with the same mutations showing similar clinical phenotypes. As a result, the genotype-phenotype correlations continue to be elusive, and there is no specific severity group linked to one particular mutation[5]. Historically, there are three CS severity groups, though recent work has expanded the categories to four: Severe CS (Type II or early-onset CS), Moderate CS (Type I or Classical CS), Mild CS (Type III or Mild/Atypical CS), and Photosensitivity only/adult-onset CS[4]. CS patients in the most severe subtype cannot talk or sit independently, while many with milder forms are able to walk and talk, and even hold jobs[16]. The average lifespan for severe CS is approximately 5 years, moderate is 16 years, and mild 30.3 years[4]. The range of clinical features is extensive and dependent on severity group. CS patients are photosensitive, have wizened faces with sunken eyes due to loss of subcutaneous adipose tissue in the face, which is also seen throughout the entire body. Stature and weight are significantly reduced in CS patients, in parallel to severity group, with the preferential loss of fat over lean tissue. Oral intake is commonly limited as CS patients have difficulty swallowing, and possess frequent gastroesophageal reflux with repeated vomiting. Severe CS patients almost always require a feeding tube. Dental anomalies are also common in CS including dental caries, enamel hypoplasia, and tooth malposition. Athero- and arteriosclerosis is common and can lead to stroke, hypertension, and nephropathy. Renal

failure can occur in CS patients, often secondary to the cardiovascular features and is frequently a marker of poor prognosis and impending death. There is progressive decay of the skeletal system showing osteopenia leading to kyphosis and joint contractures. Liver enzymes, aspartate aminotransferase (AST) and alanine aminotransferase (ALT), are often elevated in serum, consistent with mild liver damage and some cases exist of acute liver failure as cause of death. Most common cause of death is pneumonia or other respiratory problems, with some cases of kidney failure, cardiac arrest, complications of seizures or stroke. These features have been consistently documented since the initial reports in 1936[1] with increased patient numbers and discussion of severity groups from more recent reviews since 1992[2-8,17].

Neurological manifestations in severe CS

In addition to the wide range of complications seen in major organ systems of Cockayne syndrome patients, the neurological defects of the central and peripheral nervous system are also complex and multifaceted. Depending on the severity group, progression of neurological symptoms can range from mild to substantial with the most profound alterations seen in early onset, severe patients. In this group, microcephaly and developmental delay beginning around age 2 are often what initiates diagnosis. The small brain size is likely due to a combination of brain defects and profound atrophy[17]. Motor, language, and cognitive development is delayed, yet even if minimally verbal or nonverbal, CS patents have engaging personalities[17]. Early cerebellar atrophy is often seen

in severe CS, leading to ataxia with tremors and seizures as well as loss of Purkinje layer and granular neurons[18]. Bilateral calcifications are commonly found in the basal ganglia, subcortical white matter, and dentate nucleus in almost all CS patients by the age of 3, but rare cases of confirmed CS are found without evidence of calcification[18]. Though there is no confirmed correlation between the age of the patient and calcification status, the largest calcification deposits are often found in the oldest patients[18]. The progressive loss of vision and hearing contributes significantly to the cognitive dysfunction[17]. However, the progressive loss of myelin integrity in both the central and peripheral nervous system is one of the major key characteristics of CS neurological disease[19], though whether the loss of myelin is developmental, degenerative, or both is disputed.

White matter loss in CS: Dysmyelination vs. demyelination?

CS brains show reduced oligodendrocytes/Schwann cell numbers and a reduction in myelinated fibers, but it remains unclear if CS neurological involvement is primarily due to neurodegeneration stemming from myelin loss with secondary neuronal dysfunction (demyelination), or the failure of oligodendrocyte/Schwann cell differentiation and myelin synthesis (dysmyelination). In CS patients, myelin is preserved in perivascular areas but depleted in a patchy pattern, characterized as "tigroid leukodystrophy"[3]. Although there are reports in CS mouse models supporting defective transcriptional regulation during early development resulting in dysmyelination[20], most of the evidence stems from imaging of COFS patients and Type II CS that reflect delayed

myelin formation[21,22]. Myelin becomes progressively diffuse and irregular in both the central and peripheral nervous system of CS patients, indicating that both myelinating cell types, oligodendrocytes and Schwann cells are involved in the disease process[3,17]. Furthermore, investigations in human CS patients and mouse models demonstrate evidence of aberrant myelin collapse such as rolled and redundant myelin, increased swelling/inclusions in cytoplasm of oligodendrocytes, and progressive loss of nerve conduction velocity (NCV), indicating that myelin loss is not a developmental impediment but is a progressive and segmental demyelinating process[17].

Histology of patient sciatic and sural nerves reflects reduced number of myelinated fibers, onion bulb formations, denervated Schwann cell clusters, Schwann cell nuclei, and evidence of remyelination efforts[17,23]. In particular, onion bulb formations are consistent with attempted repair of nerve segments that have undergone previous myelin loss, suggestive of demyelination/remyelination rather than dysmyelination[17]. The loss of myelin in the peripheral nerves consistently worsens in CS patients, which can lead to muscle atrophy, and loss of sensory and motor control. As a result, progressive peripheral neuropathy, measured either in sciatic or sural nerves, has been demonstrated in almost all CS types with various age of onset by NCV measurements[8]. The gradual and progressive decline in peripheral NCV seen in CS mimics the slowing seen in normal aging. In humans, NCV decreases with advancing age[24,25], consistent with progressive loss of both small and large myelinated fiber density[26]. NCV also declines in the last third of life in wildtype mice[27]. The slowing of NCV in CS patients attests to the progression of

demyelinating neuropathy[28], which eventually leads to secondary axonal degeneration and muscle atrophy.

Mouse models of Cockayne syndrome

Mouse models of CS have been generated from each of the CS-associated genes (*Csa, Csb, Xpd, Xpb, Xpg*) in an attempt to understand the underlying etiology of pleiotropic disease symptoms, as well as potentially to understand the role of DNA damage in the aging process. However, phenocopying of human disease symptoms in particular, or the normal mouse aging process more generally, has met with varying degrees of success. Mice with *Csa* or *Csb* alleles engineered to genetically mimic presumed null alleles observed in human CS patients show extremely mild symptoms with a relatively normal lifespan of approximately 2.5 years and a minor neurodegenerative phenotype including age-related photoreceptor loss[29] and spiral ganglion cell loss leading to loss of hearing, as well as reduced subcutaneous fat and mitochondrial dysfunction late in life[30-32]. Interestingly, combined *Csa*/*Csb* double mutant mice have a normal lifespan, and cells from these animals had similar UV sensitivity to the single knockouts[33]. Despite the mild organismal phenotype, fibroblasts from these mice display hypersensitivity to UV similar to that observed in CS patient cells. Such a lack of correlation between DNA repair capacity and organismal phenotype is common amongst NER-associated disorders, suggesting that the lesions themselves may not be the driving force behind disease symptoms.

NER progeria models with perinatal lethality: Crossing *Csa*$^{-/-}$ or *Csb*$^{m/m}$ mouse models into genetic backgrounds with additional defects in additional NER-associated repair factors results in a consistent pattern of severe phenotypes that more closely resembles severe CS and is collectively known as "NER progeria". The main features of NER progeria include dwarfism, cerebellar ataxia, failure to thrive, and death before weaning. The first such models described was *Csb*$^{m/m}$ crossed with GG-NER deficient *Xpa* knockout mice, which on its own has no overt progeroid phenotypes despite an increased risk of UV or DMBA-induced skin cancer[34,35]. *Csb*$^{m/m}$/*Xpa*$^{-/-}$ mice, as well as other combinations of CS and XP proteins and termed C+X, reliably mimic CS phenotypes as described below but are limited in use as death before weaning is a persistent result[34-36].

NER progeroid mice, including C+X mice, are generally born at Mendelian frequencies and appear indistinguishable from single knockout and wildtype controls, consistent with normal embryonic development. However, postnatal growth and development are impaired. By postnatal day 14, when mice begin transitioning from mother's milk to solid food, C+X mice achieved their maximum body weight. After this, body weight declines by approximately 25-50% by 3 weeks, with the mice succumbing to death before weaning with high penetrance[34-36].

In addition to small size and short lifespan, a number of the phenotypes of NER progeria are notable with respect to their similarity to either CS or normal aging. These

include loss of adiposity, kyphosis, cerebellar ataxia and progressive loss of motor control including tremors and spasticity[34-36]. On a histological level, these latter symptoms manifest as defects in postnatal cerebellar development, including increased apoptosis in the granular layer, Purkinje cell loss, and failed Purkinje arborization and retinal degeneration[34-36]. Nonetheless, as most CS patients do not die during the immediate postnatal developmental period, the relevance of these phenotypes to either CS or normal aging has been questioned[37].

Other NER progeria models include *Xpd*$^{XPCS/XPCS}$/*Xpa*$^{-/-}$ [38], *Xpd*$^{TTD/TTD}$/*Xpa*$^{-/-}$ [39] *Xpg* [40], *Xpf* [41] and *Ercc1* [42,43], as well as *Csa*$^{-/-}$/*Xpa*$^{-/-}$ [44], and *Csb*$^{m/m}$/*Xpc*$^{-/-}$ [36]. There is considerable overlap in phenotype between these mouse models, especially in neurological dysfunction, though pathogenesis differs. For reasons that remain unclear, cultured fibroblasts from some NER progeria models display premature senescence (e.g. *Xpg, Xpf and Ercc1*), while other do not (*Csa* or *Csb* combined with *Xpa* or *Xpc*)[37]. This could be attributed to the additional functions of these proteins outside of NER, which in the case of *Xpf*/*Ercc1* (but not *Xpb*) could be in telomere maintenance[45].

NER progeria that survives weaning: Importantly, there is another class of mouse models of genetic NER deficiency that display the same postnatal developmental phenotypes described above, but do not die prior to weaning with high penetrance. The first such model described is *Ercc1*$^{\Delta/-}$, a compound heterozygote with one hypomorphic and one null *Ercc1* allele, which survives about 4-6 months[43]. Another model with similar

characteristics is the compound heterozygous $Xpd^{TTD/XPCS}$ in an *Xpa* null background[37]. Both mouse models display progressive neurological phenotypes, reduced adiposity, failure to thrive, and a reduced lifespan though they are not categorically considered models of Cockayne syndrome as ERCC1 also plays a role in crosslink and double-stranded break repair, and XPD can be associated with cancer predisposition. The combined C+X mouse models of severe CS more closely resemble both the genetic and phenotypic outcomes in the human syndrome but the reduced lifespan of 3-4 weeks is extremely limiting. Though $Ercc1^{\Delta/-}$ and $Xpd^{TTD/XPCS}/Xpa^{-/-}$ are considered poor models of Cockayne syndrome, they do provide hints at the potential for the weaning period, much like the perinatal period, to represent a phase of increased stress. This may point to the weaning period representing a developmental bottleneck and modulation of stress resistance or dietary intake may allow for survival, further increasing the relevance of these severe mouse models of CS.

Current treatments and potential interventions for CS patients

There is currently no general treatment for Cockayne syndrome patients. In the most severe cases, children are often diagnosed around the age of 2 and do not survive more than a few years. Children with moderate CS survive into teenage years and the mildest cases until the 3rd or 4th decade. The existing palliative goals are to maximize the quality of life and to manage symptoms. Current therapies include cochlear implants for hearing, cataract surgeries, high SPF sunscreen, physical therapy, and feeding tube

insertion. Along with physical therapy for joint stiffness, botox injections and surgery have shown improvements[3].

As of today, no pharmacological treatment has halted or even slowed the progression of the disease, though some patients have seen minor improvements in tremors and fine motor movements with carbidopa-levodopa therapy, a treatment that synthesizes dopamine in the brain and is combined with an anti-nausea medication[46]. Another treatment, Prodarsan, a putative antioxidant and free radical scavenging drug, was Phase I/II tested in CS patients with long bone growth as the primary study endpoint, however trials were halted during enrollment and collection of baseline data prior to testing of the drug.

Currently, clinical trials have been proposed to test another promising intervention for CS patients: repletion of NAD+ levels. Such trials are based on recently published studies in mouse models of XP as well as CS, demonstrating the depletion of NAD+ upon PARP-1 overactivation[47,48]. PARP-1 is an enzyme responsible for catalyzing the conversion of NAD+ to chains of poly-ADP-ribose (PAR) and nicotinamide upon binding to sites of DNA damage. PARP-1 activation is also known to increase with age, potentially correlating with the accumulation of DNA damage[49,50]. Recent work showed that levels of NAD+ decline with age and supplementation with NAD+ precursors or use of pharmacological inhibition of PARP-1 can extend lifespan of worms, improve mitochondrial dysfunction in DNA repair disorders, and improve tissue functionality to a

"youthful" state[47,49,51]. The NAD+ dependent deacetylase, SIRT1, is required for these benefits[49,51]. Similarly, two weeks of treatment with nicotinamide riboside (NR), a NAD+ precursor, in a severe mouse model of CS, *Csa*$^{-/-}$/*Xpa*$^{-/-}$, increased the NAD+ content of cerebellar mitochondria and improved numerous mitochondrial phenotypes such as increased ROS and mitochondrial membrane potential levels[47]. NR can also reverse deficits in muscle mass, strength, and exercise capacity in mice deficient in Nampt, an essential enzyme in the NAD+ salvage pathway[52]. Together, these data support the use of NAD+ precursors or PARP-1 inhibition for treatment of CS. Though not yet published, preliminary human clinical trials claim using ChromaDex® NR in healthy human volunteers increased NAD+ levels (US Clinical trial #NCT02303483, NCT02300740 NCT02191462, NCT02678611). ChromaDex® is currently seeking FDA approval for NR trials in CS patients.

Various dietary interventions with demonstrated efficacy in CS mouse models, including dietary restriction and high fat diet, have also been considered for improving healthspan and lifespan of CS patients. Dietary restriction (DR) is defined as reduced food intake without malnutrition. DR was first described in the 1930's to extend longevity in rats[53], and since then, extension of lifespan has been demonstrated in multiple species from yeast to worms, flies, rodents, and non-human primates[54]. Numerous nutrient sensing pathways have been implicated to be involved in the regulation of lifespan by DR, including AMPK, mTOR, insulin/insulin like growth factor (IGF) signaling, sirtuins, GCN2, and the transsulfuration pathway of hydrogen sulfide production[54,55], although the

exact molecular mechanisms underlying DR benefits remain mostly unknown. In two NER progeria models, *Ercc1*$^{\Delta/-}$ and *Xpg*$^{-/-}$, 30% DR increased lifespan by approximately 200% of the normal 4-6 month lifespan[56]. In CSB mice with a relatively mild progeroid phenotype[31], 8 months of feeding a high fat diet (HFD) was protective against age-associated loss of spiral ganglion cells and associated hearing loss[48]. In contrast, 40% restriction of total calories failed to provide any benefit in hearing loss of *Csb*$^{m/m}$ mice[48]. HFD-fed CSB mice showed increased ketone body levels and increased SIRT1 activity and in nematode models of CSB loss, ketone body as well as PARP inhibitor treatment slightly but significantly increased lifespan[48]. Though minor benefits were met with ketone body treatment, testing the efficacy in more relevant mouse models will better inform on its relevance as a CS therapy.

Links between nuclear DNA damage repair and energy metabolism

While damage to nuclear DNA can be recognized and repaired by numerous overlapping repair pathways, overwhelming DNA damage can cause necrotic cell death in large part due to depletion of cellular energy stores. Mitochondrial DNA damage can also affect energy metabolism through perturbations in mitochondrial function and many of the nuclear repair pathway proteins are also present in the mitochondria[57]. The classic example of DNA damage altering metabolism occurs via activation of PARP-1 in response to single stranded DNA breaks. PARP-1 utilizes NAD+ as a co-factor to poly ADP-ribosylate target proteins in the vicinity of a DNA lesion. In the face of overwhelming

PARP-1 activation, this key intermediate in energy metabolism is depleted, with pleiotropic consequences on subsequent ATP generation. As discussed in greater detail below, PARP-1 can also influence cellular energy metabolism through additional mechanisms, including indirect or direct effects on mitochondrial homeostasis[58], as well as transcriptional regulation of genes involved in metabolism such as *NRF-1, FOXO*, and *PPARγ*, independent of its role in DNA damage signaling[59-61].

Despite this well-established ability of severe DNA damage to impact cellular energy metabolism, much less is known about the consequences of sub-lethal or chronic DNA damage on energy metabolism, particularly on the organismal level. Nonetheless, there is abundant evidence that such a relationship exists. For example, Hutchinson-Gilford Progeria syndrome (HGPS), which is characterized on a cellular level by defects in nuclear architecture resulting in chromosomal instability and activation of DNA damage responses[62,63], presents on the organismal level with growth retardation, failure to thrive, decreased signaling through the GH/IGF-1/axis, decreased body fat, atherosclerosis and a lifespan of an average 13 years[64-66]. Defects in the DNA damage signaling kinase ATM cause ataxia telangiectasia (A-T), a rare disorder characterized by elevated cancer, cerebellar ataxia, and immune dysfunction[67], but also presenting with insulin resistance and low insulin receptor affinity[68]. Similar links between DNA damage signaling and insulin signaling are conserved in mouse models of AT[69]. ATM is also a sensor of ROS and can mediate mitochondrial ROS signaling to extend lifespan in yeast[70,71] and has been

shown to activate the pentose phosphate pathway, further linking DNA repair processes and cellular energy metabolism[72].

Other examples of connections between DNA damage and energy metabolism involve proteins with dual roles in control of both processes, including the tumor suppressor p53 and the sirtuin SIRT6. The p53 protein is activated by genotoxic stress through AMPK and mTOR signaling pathways and is known to transcriptionally regulate components of oxidative phosphorylation, and the expression of both glucose transporters and fatty acid synthase[73]. SIRT6 is a nuclear histone deacetylase that is known to play a role in DNA repair via activation of PARP-1 to enhance repair of double stranded breaks[74], and acts as a tumor suppressor to regulate cancer metabolism via transcriptional repression of HIF-1 dependent gluconeogenic gene targets as well as regulating ribosomal gene expression[75]. Mice deficient in SIRT6 develop fatal hypoglycemia resulting from enhanced glucose uptake in brown adipose tissue and muscle and, like NER progeroid mice, lose subcutaneous fat, supporting SIRT6's role in lipid and glucose homeostasis[76]. In contrast, mice that overexpress SIRT6 are protected against dietary and age-associated metabolic defects and have an extended lifespan[77].

Interestingly, not all the perturbations in energy metabolism associated with DNA damage are associated with negative outcomes. Many different NER-deficient mouse models display phenotypes typically associated with extended longevity because of either interventional DR or genetic hypopituitary dwarfism[37,78-80]. For example, *Csa*$^{-/-}$ and *Csb*$^{m/m}$

(but not *Xpa* or *Xpc* mice) display protection from high fat diet-induced obesity, reduced adiposity, and improved insulin sensitivity[78]. They are also resistant to renal ischemia reperfusion injury, a form of acute inflammatory and oxidative stress, although whether this is related to changes in energy metabolism remains unclear[81]. The severe mouse models of CS also possess many symptoms that overlap with dietary restricted animals, including reduced circulating levels of glucose, insulin, and IGF-1[78], as well as reduced growth hormone receptor (GHR) mRNA levels in many tissues consistent with systemic downregulation of the GH/IGF-1 axis[34,37,82]. In DR, the reduction in insulin/IGF-1 signaling is an adaptive response to the stress of nutrient/energy deficiency associated with longevity extension and other benefits such as stress resistance[83,84]. However, whether it represents an adaptive or maladaptive response to damage accumulation from endogenous genotoxic stress remains unclear. Interestingly, defects in IGF-1 signaling are not exclusive to NER disorders, but are also found in Seckel syndrome, a disorder caused by defective ATR and stalled cell cycle checkpoints, though whether this is a constitutive defect or an adaptation is unclear[85,86].

Effects of PARP-1 activation on energy metabolism, aging and disease

Historically, PARP-1 is best known for its role in DNA repair. As the progressive accumulation of damage to both nuclear and mitochondrial DNA increases with age, it may also play a prominent role in the aging and aging-associated disease[87,88]. This is thought to occur primarily via depletion of NAD+, which in addition to a decline in

NAD+ biosynthesis[89], contributes to the general decline in NAD+ levels observed during aging[60,90]. Due to its role as a cofactor of multiple enzymes in glycolysis, fatty acid oxidation, and oxidative phosphorylation, reduced NAD+ likely has direct consequences on cellular energy metabolism. However, reduced NAD+ also has important indirect effects on energy production via the NAD+-dependent deacetylase, SIRT1, which deacetylates and activates PGC1α, the master regulator of mitochondrial biogenesis[90], whereas SIRT6-dependent acetylation of GCN5 acetylates PGC1α and reduces gluconeogenic gene expression[91]. PARP-1 mediated loss of SIRT1 function and the subsequent reduction in the mitochondrial transcription factor, TFAM, further contributes to the downregulation of mitochondrial biogenesis in a PGC1α-independent manner[51]. It also promotes oxidative damage to complex I of the electron complex chain, downregulation of antioxidant defense pathways, increasing mitochondrial membrane potential, and further preventing mitochondria turnover by mitophagy[50,57]. Over time, chronic low-level DNA damage and PARP-1 activation can thus inhibit mitochondrial turnover, perturbing energy homeostasis.

PARP-1 overactivation has been found in numerous human diseases including chronic heart failure, stroke, Parkinson's disease (PD), and Alzheimer's disease (AD)[92]. Interestingly, overexpression of SIRT1 is neuroprotective against mouse models of AD[93] and Huntington's disease (HD)[94,95]. The defect in mitophagy can be suppressed by treatment with either PARP-1 inhibitors or supplementation of NAD+ levels[47]. Individuals

with XP, A-T, and CS are also thought to have a compromised balance of PARP-1 and SIRT1 function resulting in inefficient mitophagy[47].

In addition to its function as a poly (ADP-ribose) polymerase, PARP-1 also functions in different pathways including DNA repair and transcriptional control of metabolism[96] with broader effects on tumorigenesis, inflammation, and cell differentiation[97]. For example, PARP-1 and 2 interact with many nuclear receptor transcription factors, such as FOXO and PPARγ, to regulate mitochondrial and fat oxidation genes, though genetic manipulation of one member often results in upregulation of others and as a result, ADP-ribosylation activity is frequently not required[60,61].

NAD+ metabolism and neurodegeneration

There are several examples for NAD+ playing a major role in neuroprotection. In a mouse model called Wallerian degeneration slow, *WldS*, animals show an increased protection against axonal degradation in both the central and peripheral nervous system due to a triplication of the NMNAT1 gene, a key enzyme in NAD+ salvage that is expressed mainly in skeletal muscle, heart, and liver but almost undetectable in the brain[98-101]. Supplementation by nicotinamide mononucleotide (NMN) or NR has also been shown to protect against axonal degeneration after axotomy, noise-induced hearing loss in rodents, and hearing loss due to manganese toxicity[102-105]. A recent drug screen

performed in rodents *in vivo* to determine small molecules that enhance hippocampal neurogenesis identified P7C3, an allosteric activator of Nampt, the rate-limiting enzyme in the NAD+ salvage pathway[106,107]. Later derivatives of the drug showed neuroprotective activity in mouse models of PD, amytrophic lateral sclerosis, and traumatic brain injury[108-110]. Neuroprotection has been the main topic of study using PC73, though it may also influence other aging-related diseases as aged rats maintained body weight longer upon treatment with the drug[107]. Supplementation of NAD+ levels with precursors NR or NMN are known to have protective effects on the abundance and function of respiratory chain complexes[51] and against age-related glucose metabolism impairment[89], which suggests a systemic influence of DNA damage on the regulation of energy metabolism. Clearly, the manipulation of NAD+ and its consuming enzymes are of great interest in efforts for disease prevention, especially in neurodegeneration, and lifespan extension.

Thesis Summary

This thesis reports on how sub-lethal levels of DNA damage impact energy metabolism and neurodegeneration using models of Cockayne syndrome and chemo-/radio-therapeutic genotoxic stress. In **Chapter 2,** we present the characterization of the first mouse model of severe Cockayne syndrome, CX mice, with a lifespan of approximately 5 months that phenocopies metabolic defects such as loss of adiposity and the progressive neurodegeneration. In **Chapter 3,** we investigate the relationship between DNA damage accumulation and alterations in growth and energy metabolism. Using CX mice as a model of chronic DNA damage and WT mice and cells treated with acute

genotoxic agents, we observed an increase in fatty acid oxidation that was mediated by PARP-1 activation, ATP and NAD+ loss, and AMPK activation. This adaptation is determined to be beneficial and cell autonomous and could contribute to the loss of adipose tissue seen in CX mice as well as in CS patients. In **Chapter 4,** we examine the severe and progressive neurodegenerative symptoms routinely observed in CS patients using the CX mouse model. In addition to the poor histological findings in both the central and peripheral nervous system, we observe patchy demyelination that worsens with age and contributes to neuronal and axonal loss. We also establish that nervous tissue similarly has increased fatty acid oxidation in CX mice and that the loss of fatty myelin sheaths could stem from focal areas of increased fat burning via myelin catabolism. In **Chapter 5,** we utilize the CX mouse model to investigate potential endpoints that could be used to determine disease progression upon therapeutic interventions. In **Chapter 6**, we end with concluding remarks and a discussion of our results.

REFERENCES

1. Cockayne EA. Dwarfism with retinal atrophy and deafness. *Arch Dis Child.* 1936;11(61):1-8.

2. Nance MA, Berry SA. Cockayne syndrome: review of 140 cases. *Am J Med Genet.* 1992;42(1):68-84.

3. Rapin I, Weidenheim K, Lindenbaum Y, et al. Cockayne syndrome in adults: review with clinical and pathologic study of a new case. *J Child Neurol.* 2006;21(11):991-1006.

4. Natale V. A comprehensive description of the severity groups in Cockayne syndrome. *Am J Med Genet A.* 2011;155A(5):1081-1095.

5. Laugel V. Cockayne syndrome: the expanding clinical and mutational spectrum. *Mech Ageing Dev.* 2013;134(5-6):161-170.

6. Kubota M, Ohta S, Ando A, et al. Nationwide survey of Cockayne syndrome in Japan: Incidence, clinical course and prognosis. *Pediatr Int.* 2015;57(3):339-347.

7. Wilson BT, Stark Z, Sutton RE, et al. The Cockayne Syndrome Natural History (CoSyNH) study: clinical findings in 102 individuals and recommendations for care. *Genet Med.* 2016;18(5):483-493.

8. Karikkineth AC, Scheibye-Knudsen M, Fivenson E, Croteau DL, Bohr VA. Cockayne syndrome: Clinical features, model systems and pathways. *Ageing Res Rev.* 2016.

9. Lehmann AR. DNA repair-deficient diseases, xeroderma pigmentosum, Cockayne syndrome and trichothiodystrophy. *Biochimie.* 2003;85(11):1101-1111.

10. Lindenbaum Y, Dickson D, Rosenbaum P, Kraemer K, Robbins I, Rapin I. Xeroderma pigmentosum/cockayne syndrome complex: first neuropathological study and review of eight other cases. *Eur J Paediatr Neurol.* 2001;5(6):225-242.

11. Caputo M, Frontini M, Velez-Cruz R, Nicolai S, Prantera G, Proietti-De-Santis L. The CSB repair factor is overexpressed in cancer cells, increases apoptotic resistance, and promotes tumor growth. *DNA Repair (Amst).* 2013;12(4):293-299.

12. Reid-Bayliss KS, Arron ST, Loeb LA, Bezrookove V, Cleaver JE. Why Cockayne syndrome patients do not get cancer despite their DNA repair deficiency. *Proc Natl Acad Sci U S A.* 2016;113(36):10151-10156.

13. Fousteri M, Vermeulen W, van Zeeland AA, Mullenders LH. Cockayne syndrome A and B proteins differentially regulate recruitment of chromatin remodeling and repair factors to stalled RNA polymerase II in vivo. *Mol Cell.* 2006;23(4):471-482.

14. Troelstra C, van Gool A, de Wit J, Vermeulen W, Bootsma D, Hoeijmakers JH. ERCC6, a member of a subfamily of putative helicases, is involved in Cockayne's syndrome and preferential repair of active genes. *Cell.* 1992;71(6):939-953.

15. Wong HK, Muftuoglu M, Beck G, Imam SZ, Bohr VA, Wilson DM, 3rd. Cockayne syndrome B protein stimulates apurinic endonuclease 1 activity and protects against agents that introduce base excision repair intermediates. *Nucleic Acids Res.* 2007;35:4103-4113.

16. Morris DP, Alian W, Maessen H, et al. Cochlear implantation in Cockayne syndrome: our experience of two cases with different outcomes. *Laryngoscope.* 2007;117(5):939-943.

17. Weidenheim KM, Dickson DW, Rapin I. Neuropathology of Cockayne syndrome: Evidence for impaired development, premature aging, and neurodegeneration. *Mech Ageing Dev.* 2009;130(9):619-636.

18. Koob M, Laugel V, Durand M, et al. Neuroimaging in Cockayne syndrome. *AJNR Am J Neuroradiol.* 2010;31(9):1623-1630.

19. Mizuguchi M, Itoh M. A 35-year-old female with growth and developmental retardation, progressive ataxia, dementia and visual loss. *Neuropathology.* 2005;25(1):103-106.

20. Revet I, Feeney L, Tang AA, Huang EJ, Cleaver JE. Dysmyelination not demyelination causes neurological symptoms in preweaned mice in a murine model of Cockayne syndrome. *Proc Natl Acad Sci U S A.* 2012;109(12):4627-4632.

21. Del Bigio MR, Greenberg CR, Rorke LB, Schnur R, McDonald-McGinn DM, Zackai EH. Neuropathological findings in eight children with cerebro-oculo-facio-skeletal (COFS) syndrome. *J Neuropathol Exp Neurol.* 1997;56(10):1147-1157.

22. Pasquier L, Laugel V, Lazaro L, et al. Wide clinical variability among 13 new Cockayne syndrome cases confirmed by biochemical assays. *Arch Dis Child.* 2006;91(2):178-182.

23. Ohnishi A, Mitsudome A, Murai Y. Primary segmental demyelination in the sural nerve in Cockayne's syndrome. *Muscle Nerve.* 1987;10(2):163-167.

24. Taylor PK. Non-linear effects of age on nerve conduction in adults. *J Neurol Sci.* 1984;66(2-3):223-234.

25. Suzuki M. Peripheral neuropathy in the elderly. *Handb Clin Neurol.* 2013;115:803-813.

26. Tohgi H, Tsukagoshi H, Toyokura Y. Quantitative changes with age in normal sural nerves. *Acta Neuropathol.* 1977;38(3):213-220.

27. Verdú E, Ceballos D, Vilches JJ, Navarro X. Influence of aging on peripheral nerve function and regeneration. *J Peripher Nerv Syst.* 2000;5(4):191-208.

28. Leech RW, Brumback RA, Miller RH, Otsuka F, Tarone RE, Robbins JH. Cockayne syndrome: clinicopathologic and tissue culture studies of affected siblings. *J Neuropathol Exp Neurol.* 1985;44(5):507-519.

29. Jaarsma D, van der Pluijm I, van der Horst GT, Hoeijmakers JH. Cockayne syndrome pathogenesis: lessons from mouse models. *Mech Ageing Dev.* 2013;134(5-6):180-195.

30. Kamenisch Y, Fousteri M, Knoch J, et al. Proteins of nucleotide and base excision repair pathways interact in mitochondria to protect from loss of subcutaneous fat, a hallmark of aging. *J Exp Med.* 2010;207(2):379-390.

31. Scheibye-Knudsen M, Ramamoorthy M, Sykora P, et al. Cockayne syndrome group B protein prevents the accumulation of damaged mitochondria by promoting mitochondrial autophagy. *J Exp Med.* 2012;209:855-869.

32. van der Horst GT, van Steeg H, Berg RJ, et al. Defective transcription-coupled repair in Cockayne syndrome B mice is associated with skin cancer predisposition. *Cell.* 1997;89(3):425-435.

33. de Waard H, de Wit J, Andressoo JO, et al. Different effects of CSA and CSB deficiency on sensitivity to oxidative DNA damage. *Mol Cell Biol.* 2004;24(18):7941-7948.

34. van der Pluijm I, Garinis GA, Brandt RM, et al. Impaired genome maintenance suppresses the growth hormone--insulin-like growth factor 1 axis in mice with Cockayne syndrome. *PLoS Biol.* 2007;5(1):e2.

35. Murai M, Enokido Y, Inamura N, et al. Early postnatal ataxia and abnormal cerebellar development in mice lacking Xeroderma pigmentosum Group A and Cockayne syndrome Group B DNA repair genes. *Proc Natl Acad Sci U S A.* 2001;98(23):13379-13384.

36. Laposa RR, Huang EJ, Cleaver JE. Increased apoptosis, p53 up-regulation, and cerebellar neuronal degeneration in repair-deficient Cockayne syndrome mice. *Proc Natl Acad Sci U S A.* 2007;104(4):1389-1394.

37. van de Ven M, Andressoo JO, Holcomb VB, et al. Adaptive stress response in segmental progeria resembles long-lived dwarfism and calorie restriction in mice. *PLoS Genet.* 2006;2:e192.

38. Andressoo JO, Mitchell JR, de Wit J, et al. An Xpd mouse model for the combined xeroderma pigmentosum/Cockayne syndrome exhibiting both cancer predisposition and segmental progeria. *Cancer Cell.* 2006;10(2):121-132.

39. de Boer J, Andressoo JO, de Wit J, et al. Premature aging in mice deficient in DNA repair and transcription. *Science.* 2002;296(5571):1276-1279.

40. Harada YN, Shiomi N, Koike M, et al. Postnatal growth failure, short life span, and early onset of cellular senescence and subsequent immortalization in mice lacking the xeroderma pigmentosum group G gene. *Mol Cell Biol.* 1999;19(3):2366-2372.

41. Tian M, Shinkura R, Shinkura N, Alt FW. Growth retardation, early death, and DNA repair defects in mice deficient for the nucleotide excision repair enzyme XPF. *Mol Cell Biol.* 2004;24(3):1200-1205.

42. McWhir J, Selfridge J, Harrison DJ, Squires S, Melton DW. Mice with DNA repair gene (ERCC-1) deficiency have elevated levels of p53, liver nuclear abnormalities and die before weaning. *Nat Genet.* 1993;5(3):217-224.

43. Weeda G, Donker I, de Wit J, et al. Disruption of mouse ERCC1 results in a novel repair syndrome with growth failure, nuclear abnormalities and senescence. *Curr Biol.* 1997;7(6):427-439.

44. van der Horst GT, Meira L, Gorgels TG, et al. UVB radiation-induced cancer predisposition in Cockayne syndrome group A (Csa) mutant mice. *DNA Repair (Amst).* 2002;1(2):143-157.

45. Zhu XD, Niedernhofer L, Kuster B, Mann M, Hoeijmakers JH, de Lange T. ERCC1/XPF removes the 3' overhang from uncapped telomeres and represses formation of telomeric DNA-containing double minute chromosomes. *Mol Cell.* 2003;12(6):1489-1498.

46. Neilan EG, Delgado MR, Donovan MA, et al. Response of motor complications in Cockayne syndrome to carbidopa-levodopa. *Arch Neurol.* 2008;65(8):1117-1121.

47. Fang EF, Scheibye-Knudsen M, Brace LE, et al. Defective mitophagy in XPA via PARP-1 hyperactivation and NAD(+)/SIRT1 reduction. *Cell.* 2014;157:882-896.

48. Scheibye-Knudsen M, Mitchell SJ, Fang EF, et al. A High-Fat Diet and NAD(+) Activate Sirt1 to Rescue Premature Aging in Cockayne Syndrome. *Cell Metab.* 2014;20:840-855.

49. Mouchiroud L, Houtkooper RH, Auwerx J. NAD^+ metabolism: a therapeutic target for age-related metabolic disease. *Crit Rev Biochem Mol Biol.* 2013;48(4):397-408.

50. Cantó C, Houtkooper RH, Pirinen E, et al. The NAD(+) precursor nicotinamide riboside enhances oxidative metabolism and protects against high-fat diet-induced obesity. *Cell Metab.* 2012;15(6):838-847.

51. Gomes AP, Price NL, Ling AJ, et al. Declining NAD(+) induces a pseudohypoxic state disrupting nuclear-mitochondrial communication during aging. *Cell.* 2013;155(7):1624-1638.

52. Frederick DW, Loro E, Liu L, et al. Loss of NAD Homeostasis Leads to Progressive and Reversible Degeneration of Skeletal Muscle. *Cell Metab.* 2016;24(2):269-282.

53. McCay CM, Crowell MF, Maynard LA. The effect of retarded growth upon the length of life span and upon the ultimate body size. 1935. *Nutrition.* 1989;5(3):155-171; discussion 172.

54. Fontana L, Partridge L, Longo VD. Extending healthy life span--from yeast to humans. *Science.* 2010;328(5976):321-326.

55. Hine C, Mitchell JR. Calorie restriction and methionine restriction in control of endogenous hydrogen sulfide production by the transsulfuration pathway. *Exp Gerontol.* 2015;68:26-32.

56. Vermeij WP, Dollé ME, Reiling E, et al. Restricted diet delays accelerated ageing and genomic stress in DNA-repair-deficient mice. *Nature.* 2016;537(7620):427-431.

57. Fang EF, Scheibye-Knudsen M, Chua KF, Mattson MP, Croteau DL, Bohr VA. Nuclear DNA damage signalling to mitochondria in ageing. *Nat Rev Mol Cell Biol.* 2016;17(5):308-321.

58. Cantó C, Auwerx J. Interference between PARPs and SIRT1: a novel approach to healthy ageing? *Aging (Albany NY).* 2011;3(5):543-547.

59. Schiewer MJ, Knudsen KE. Transcriptional roles of PARP1 in cancer. *Mol Cancer Res.* 2014;12(8):1069-1080.

60. Bai P, Houten SM, Huber A, et al. Poly(ADP-ribose) polymerase-2 [corrected] controls adipocyte differentiation and adipose tissue function through the regulation of the activity of the retinoid X receptor/peroxisome proliferator-activated receptor-gamma [corrected] heterodimer. *J Biol Chem.* 2007;282(52):37738-37746.

61. Sakamaki J, Daitoku H, Yoshimochi K, Miwa M, Fukamizu A. Regulation of FOXO1-mediated transcription and cell proliferation by PARP-1. *Biochem Biophys Res Commun.* 2009;382(3):497-502.

62. Verstraeten VL, Broers JL, Ramaekers FC, van Steensel MA. The nuclear envelope, a key structure in cellular integrity and gene expression. *Curr Med Chem.* 2007;14(11):1231-1248.

63. Liu B, Wang J, Chan KM, et al. Genomic instability in laminopathy-based premature aging. *Nat Med.* 2005;11(7):780-785.

64. Marino G, Ugalde AP, Fernandez AF, et al. Insulin-like growth factor 1 treatment extends longevity in a mouse model of human premature aging by restoring somatotroph axis function. *Proc Natl Acad Sci U S A.* 2010;107:16268-16273.

65. Al-Shali KZ, Hegele RA. Laminopathies and atherosclerosis. *Arterioscler Thromb Vasc Biol.* 2004;24(9):1591-1595.

66. Merideth MA, Gordon LB, Clauss S, et al. Phenotype and course of Hutchinson-Gilford progeria syndrome. *N Engl J Med.* 2008;358(6):592-604.

67. Shackelford RE. Pharmacologic manipulation of the ataxia-telangiectasia mutated gene product as an intervention in age-related disease. *Med Hypotheses.* 2005;65(2):363-369.

68. Lavin MF. An unlikely player joins the ATM signalling network. *Nat Cell Biol.* 2000;2(12):E215-217.

69. Miles PD, Treuner K, Latronica M, Olefsky JM, Barlow C. Impaired insulin secretion in a mouse model of ataxia telangiectasia. *Am J Physiol Endocrinol Metab.* 2007;293:E70-74.

70. Schroeder EA, Raimundo N, Shadel GS. Epigenetic silencing mediates mitochondria stress-induced longevity. *Cell Metab.* 2013;17(6):954-964.

71. Guo Z, Kozlov S, Lavin MF, Person MD, Paull TT. ATM activation by oxidative stress. *Science.* 2010;330(6003):517-521.

72. Cosentino C, Grieco D, Costanzo V. ATM activates the pentose phosphate pathway promoting anti-oxidant defence and DNA repair. *EMBO J.* 2010;30:546-555.

73. Zhang XD, Qin ZH, Wang J. The role of p53 in cell metabolism. *Acta Pharmacol Sin.* 2010;31(9):1208-1212.

74. Mao Z, Hine C, Tian X, et al. SIRT6 promotes DNA repair under stress by activating PARP1. *Science.* 2011;332(6036):1443-1446.

75. Sebastián C, Zwaans BM, Silberman DM, et al. The histone deacetylase SIRT6 is a tumor suppressor that controls cancer metabolism. *Cell.* 2012;151(6):1185-1199.

76. Mostoslavsky R, Chua KF, Lombard DB, et al. Genomic instability and aging-like phenotype in the absence of mammalian SIRT6. *Cell.* 2006;124:315-329.

77. Kanfi Y, Peshti V, Gil R, et al. SIRT6 protects against pathological damage caused by diet-induced obesity. *Aging Cell.* 2010;9(2):162-173.

78. van de Ven M, Andressoo JO, Holcomb VB, et al. Extended longevity mechanisms in short-lived progeroid mice: identification of a preservative stress response associated with successful aging. *Mech Ageing Dev.* 2007;128(1):58-63.

79. Andressoo JO, Weeda G, de Wit J, et al. An Xpb mouse model for combined xeroderma pigmentosum and cockayne syndrome reveals progeroid features upon further attenuation of DNA repair. *Mol Cell Biol.* 2009;29(5):1276-1290.

80. Wijnhoven SW, Beems RB, Roodbergen M, et al. Accelerated aging pathology in ad libitum fed Xpd(TTD) mice is accompanied by features suggestive of caloric restriction. *DNA Repair (Amst).* 2005;4(11):1314-1324.

81. Susa D, Mitchell JR, Verweij M, et al. Congenital DNA repair deficiency results in protection against renal ischemia reperfusion injury in mice. *Aging Cell.* 2009;8(2):192-200.

82. Niedernhofer LJ, Garinis GA, Raams A, et al. A new progeroid syndrome reveals that genotoxic stress suppresses the somatotroph axis. *Nature.* 2006;444:1038-1043.

83. Longo VD, Finch CE. Evolutionary medicine: from dwarf model systems to healthy centenarians? *Science.* 2003;299(5611):1342-1346.

84. Rincon M, Muzumdar R, Atzmon G, Barzilai N. The paradox of the insulin/IGF-1 signaling pathway in longevity. *Mech Ageing Dev.* 2004;125(6):397-403.

85. Ducos B, Cabrol S, Houang M, Perin L, Holzenberger M, Le Bouc Y. IGF type 1 receptor ligand binding characteristics are altered in a subgroup of children with intrauterine growth retardation. *J Clin Endocrinol Metab.* 2001;86(11):5516-5524.

86. Schmidt A, Chakravarty A, Brommer E, et al. Growth failure in a child showing characteristics of Seckel syndrome: possible effects of IGF-I and endogenous IGFBP-3. *Clin Endocrinol (Oxf).* 2002;57(2):293-299.

87. López-Otín C, Blasco MA, Partridge L, Serrano M, Kroemer G. The hallmarks of aging. *Cell.* 2013;153(6):1194-1217.

88. Bürkle A, Virág L. Poly(ADP-ribose): PARadigms and PARadoxes. *Mol Aspects Med.* 2013;34(6):1046-1065.

89. Yoshino J, Mills KF, Yoon MJ, Imai S. Nicotinamide mononucleotide, a key NAD(+) intermediate, treats the pathophysiology of diet- and age-induced diabetes in mice. *Cell Metab.* 2011;14(4):528-536.

90. Imai S, Guarente L. NAD+ and sirtuins in aging and disease. *Trends Cell Biol.* 2014;24(8):464-471.

91. Dominy JE, Lee Y, Jedrychowski MP, et al. The deacetylase Sirt6 activates the acetyltransferase GCN5 and suppresses hepatic gluconeogenesis. *Mol Cell.* 2012;48(6):900-913.

92. Pacher P, Szabo C. Role of the peroxynitrite-poly(ADP-ribose) polymerase pathway in human disease. *Am J Pathol.* 2008;173(1):2-13.

93. Kim D, Nguyen MD, Dobbin MM, et al. SIRT1 deacetylase protects against neurodegeneration in models for Alzheimer's disease and amyotrophic lateral sclerosis. *EMBO J.* 2007;26(13):3169-3179.

94. Jeong H, Cohen DE, Cui L, et al. Sirt1 mediates neuroprotection from mutant huntingtin by activation of the TORC1 and CREB transcriptional pathway. *Nat Med.* 2012;18(1):159-165.

95. Jiang M, Wang J, Fu J, et al. Neuroprotective role of Sirt1 in mammalian models of Huntington's disease through activation of multiple Sirt1 targets. *Nat Med.* 2012;18(1):153-158.

96. Luo X, Kraus WL. On PAR with PARP: cellular stress signaling through poly(ADP-ribose) and PARP-1. *Genes Dev.* 2012;26(5):417-432.

97. Krishnakumar R, Kraus WL. The PARP side of the nucleus: molecular actions, physiological outcomes, and clinical targets. *Mol Cell.* 2010;39(1):8-24.

98. Emanuelli M, Carnevali F, Saccucci F, et al. Molecular cloning, chromosomal localization, tissue mRNA levels, bacterial expression, and enzymatic properties of human NMN adenylyltransferase. *J Biol Chem.* 2001;276(1):406-412.

99. Mack TG, Reiner M, Beirowski B, et al. Wallerian degeneration of injured axons and synapses is delayed by a Ube4b/Nmnat chimeric gene. *Nat Neurosci.* 2001;4(12):1199-1206.

100. Conforti L, Wilbrey A, Morreale G, et al. Wld S protein requires Nmnat activity and a short N-terminal sequence to protect axons in mice. *J Cell Biol.* 2009;184(4):491-500.

101. Sasaki Y, Vohra BP, Lund FE, Milbrandt J. Nicotinamide mononucleotide adenylyl transferase-mediated axonal protection requires enzymatic activity but not increased levels of neuronal nicotinamide adenine dinucleotide. *J Neurosci.* 2009;29(17):5525-5535.

102. Brown KD, Maqsood S, Huang JY, et al. Activation of SIRT3 by the NAD^+ precursor nicotinamide riboside protects from noise-induced hearing loss. *Cell Metab.* 2014;20(6):1059-1068.

103. Sasaki Y, Araki T, Milbrandt J. Stimulation of nicotinamide adenine dinucleotide biosynthetic pathways delays axonal degeneration after axotomy. *J Neurosci.* 2006;26(33):8484-8491.

104. Wang L, Ding D, Salvi R, Roth JA. Nicotinamide adenine dinucleotide prevents neuroaxonal degeneration induced by manganese in cochlear organotypic cultures. *Neurotoxicology.* 2014;40:65-74.

105. Gerdts J, Brace EJ, Sasaki Y, DiAntonio A, Milbrandt J. SARM1 activation triggers axon degeneration locally via NAD^+ destruction. *Science.* 2015;348(6233):453-457.

106. Pieper AA, Xie S, Capota E, et al. Discovery of a proneurogenic, neuroprotective chemical. *Cell.* 2010;142(1):39-51.

107. Wang G, Han T, Nijhawan D, et al. P7C3 neuroprotective chemicals function by activating the rate-limiting enzyme in NAD salvage. *Cell.* 2014;158(6):1324-1334.

108. De Jesús-Cortés H, Xu P, Drawbridge J, et al. Neuroprotective efficacy of aminopropyl carbazoles in a mouse model of Parkinson disease. *Proc Natl Acad Sci U S A.* 2012;109(42):17010-17015.

109. Tesla R, Wolf HP, Xu P, et al. Neuroprotective efficacy of aminopropyl carbazoles in a mouse model of amyotrophic lateral sclerosis. *Proc Natl Acad Sci U S A.* 2012;109(42):17016-17021.

110. Yin TC, Britt JK, De Jesús-Cortés H, et al. P7C3 neuroprotective chemicals block axonal degeneration and preserve function after traumatic brain injury. *Cell Rep.* 2014;8(6):1731-1740.

CHAPTER 2

Lifespan extension by dietary intervention in a mouse model of Cockayne Syndrome uncouples early postnatal development from segmental progeria

This chapter is a reproduction of a published manuscript with minor modifications:

Lear E. Brace[1], Sarah C. Vose[2], Dorathy F. Vargas[1], Shuangyun Zhao[3], Xiu-Ping Wang[3], James R. Mitchell.[1] (2013), Lifespan extension by dietary intervention in a mouse model of Cockayne Syndrome uncouples early postnatal development from segmental progeria. Aging Cell, 12: 1144–1147.

[1]Department of Genetics and Complex Diseases, Harvard T.H. Chan School of Public Health, 655 Huntington Ave, Boston, MA 02115.
[2]Vermont Departments of Health, Environmental Health, Burlington, Vermont, United States
[3]Department of Developmental Biology, Harvard School of Dental Medicine, 188 Longwood Avenue, Boston, MA 02115.

Author Contributions:
L.E.B. and J.R.M. wrote the manuscript. L.E.B. and J.R.M. designed experiments. L.E.B. and S.C.V. performed experiments, assisted by D.F.V. S.Z. and Z.-P.W. analyzed teeth.

ABSTRACT

Cockayne Syndrome (CS) is a rare autosomal recessive segmental progeria characterized by growth failure, lipodystrophy, neurological abnormalities and photosensitivity but without skin cancer predisposition. CS life expectancy ranges from 5 to 16 years for the two most severe forms (Types II and I, respectively). Mouse models of CS have thus far been of limited value due either to very mild phenotypes, or premature death during postnatal development prior to weaning. The cause of death in severe CS models is unknown but has been attributed to extremely rapid aging. Here, we found that providing mutant pups with soft food from as late as postnatal day 14 allowed survival past weaning with high penetrance independent of dietary macronutrient balance in a novel CS model (*Csa*$^{-/-}$|*Xpa*$^{-/-}$). Survival past weaning revealed a number of CS-like symptoms including small size, progressive loss of adiposity and neurological symptoms, with a maximum lifespan of 19 weeks. Our results caution against interpretation of death before weaning as premature aging, and at the same time provide a valuable new tool for understanding mechanisms of progressive CS-related progeroid symptoms including lipodystrophy and neurodysfunction.

INTRODUCTION, RESULTS, & DISCUSSION

Proteins altered in CS, including CSA and CSB, share a common function in transcription-coupled nucleotide excision DNA repair (TC-NER) in the nucleus and base excision repair (BER) of mitochondrial DNA[1]. TC-NER specifically removes lesions in DNA that obstruct RNA polymerases and block transcription, and is distinguished from Global Genome NER (GG-NER), which operates throughout the genome to eliminate helix-distorting DNA damage[2]. CSA and CSB are required for removal of RNA polymerase stalled at the site of a lesion in order for the repair reaction to occur[3]. CS proteins are also localized to mitochondria and are thought to recruit and stabilize BER proteins to repair complexes in the inner mitochondrial membrane. Human CS cells exhibit an altered redox balance with increased intracellular ROS and mitochondrial dysfunction[4]. Whether this reflects indirect effects of unrepaired DNA damage, or a more direct role of CS proteins in redox balance remains unknown. NER proteins also participate in a number of transcription related processes including initiation and elongation[5]. Mutations in other NER-related genes (*XPD, XPG, XPB*) can also cause CS in combination with symptoms of Xeroderma Pigmentosum (XP), most notably pigmentation abnormalities and elevated skin cancer in UV-exposed skin, resulting in the combined disorder XPCS[6]. CS includes a spectrum of severities with life expectancies ranging from 5 years for the most severe form (early onset Type II including Cerebro-Oculo-Facio-Skeletal Syndrome, COFS)[7], 16.1 for moderate (classical Type I) and 30.3 for atypical (mild, late onset Type III)[8].

Numerous mouse models of CS (*Csb*$^{m/m}$, *Csa*$^{-/-}$) and XPCS (*Xpd*$^{XPCS/XPCS}$) have been established, however with a generally milder phenotype than CS[9]. Further inhibition of NER by crossing these models into backgrounds lacking the GG-NER-specific protein XPC, or XPA which is common to both sub-pathways, results in a more severe disorder, NER progeria, that more closely resembles the small size, lipodystrophy and neurological complications of CS[9]. A hallmark of severe NER progeria in *Csb*$^{-/-}$|*Xpa*$^{-/-}$[10,11], *Xpd*$^{XPCS/XPCS}$|*Xpa*$^{-/}$ [12], *Csb*$^{-/-}$|*Xpc*$^{-/-}$[13] and *Xpg*$^{-/-}$ [14] mutant models is death before weaning at approximately 3 weeks of age. Attempts to extend lifespan past the weaning period by such interventions as reducing litter size, moistening the food[11], providing surrogate mothers[15] or extending the nursing period[12] have so far proven unsuccessful.

We generated double homozygous mutants by intercrossing *Csa*$^{-/-}$|*Xpa*$^{+/-}$ or *Csa*$^{+/-}$|*Xpa*$^{-/-}$ mice. *Csa*$^{-/-}$|*Xpa*$^{-/-}$ (CX) mice were born at Mendelian ratios and were indistinguishable at birth from controls. By postnatal day 5, CX mice were visually smaller in size compared to WT or single KO littermates. By postnatal day 12, clenching of the hind limbs, indicative of neurological dysfunction, was evident. As with other progeroid NER mice, CX mice reached a peak weight at approximately two weeks of age, followed by a decline in fitness, failure to thrive, and premature death with nearly 100% penetrance by postnatal day 28. Control heterozygous and single homozygous mutant CSA (*Csa*$^{-/-}$) and XPA (*Xpa*$^{-/-}$) mice developed normally as reported previously[16,17].

Despite the fact that CX mutants nursed and had milk in their stomachs observable upon sacrifice between days 14 and 21, white adipose but not brown adipose tissue weights were reduced relative to body weight on postnatal day 10 (Figure 2.1 a). Serum triglycerides and blood glucose were also reduced (Figure 2.1 b, c). We hypothesized that a nutritional deficiency might contribute to death at weaning, and reasoned that increasing the energy density of the milk by supplementing lactating dams with a high fat diet may ameliorate this mutant phenotype. Feeding pregnant dams a high fat diet (HFD, 60% calories from fat) vs. standard chow (22% calories from fat) increased triglycerides in their milk without significantly altering protein content (Figure 2.2) and thus increasing total calories. Consistent with our hypothesis, HFD feeding of lactating dams rescued premature death in CX mice with high penetrance (Figure 2.1 d). However, counter to our hypothesis, a control low fat diet (LFD) with only 10% calories from fat also rescued premature death (Figure 2.1 d) without significantly increasing triglycerides or total calories in the milk (Figure 2.2).

Because both diets (HFD, LFD) that rescued death before weaning were composed of refined ingredients, we next hypothesized that a contaminant or toxin present in the standard chow, a grain-based diet made with unrefined ingredients, might interact with the congenital DNA repair deficiency and cause premature death. To address this, we pulverized refined and unrefined pellets, and prepared them in a final 1% semi-solid agar form separately or in a 3:1 ratio. Regardless of the composition of the diet, CX mutant litters receiving agar-based diets survived weaning with high penetrance (Figure 2.1 d).

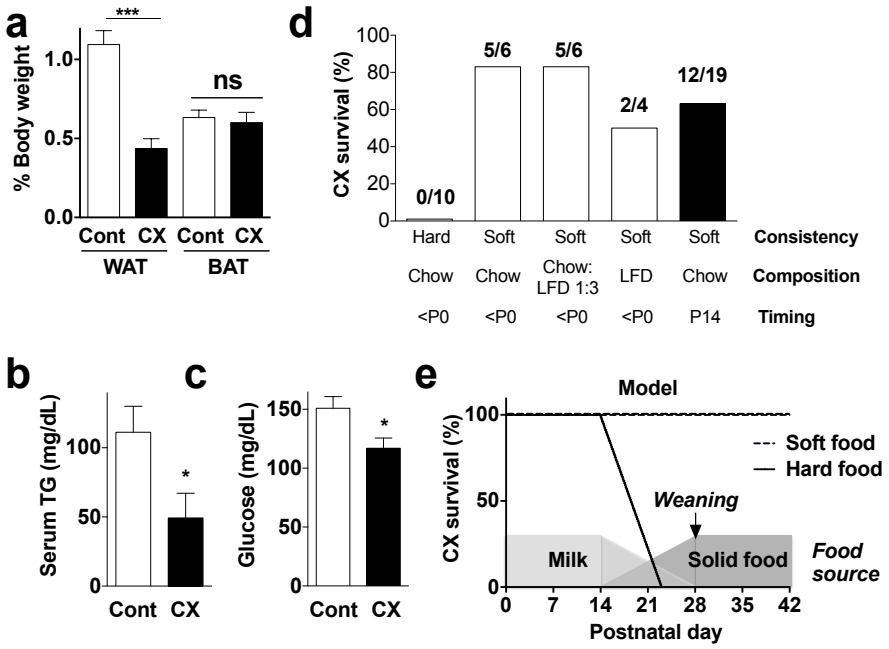

Figure 2.1: Death before weaning as a result of starvation. a. White and brown adipose tissue (WAT, BAT) expressed as a percent of total body weight in 10-day-old control (Cont, n=4) and CX (n=5) animals as indicated. Asterisks indicate significance by Student's T test between the indicated groups; *** p<0.0001. **b.** Triglycerides (TG) measured in serum of control (n=6) and CX (n=4) mice at postnatal day 14; *p<0.05 by Student's T test. **c.** Blood glucose measured in control (n=12) and CX (n=12) mice between P7 and P14; *p<0.05 by Student's T test. **d.** Survival of CX mice past weaning at P28. Diets of the indicated consistency (hard pellets vs. pulverized pellets in soft agar form) and composition (standard chow, refined LFD, or a 1:3 mixture of the two) were present from before birth (<P0) or from P14 as indicated. The number of surviving/total CX mice in each diet group is indicated above the bar. **e**. Model for a bottleneck in CX mouse development comprising an inability to consume hard food during the transition from milk to solids beginning around P14. Presentation of soft food at this time can prevent malnutrition and death. Beyond this bottleneck, neither consistency nor macronutrient balance affects longevity.

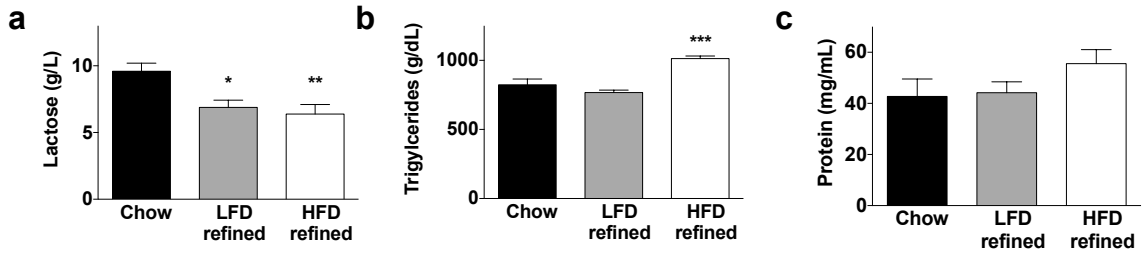

Figure 2.2. Modulation of macronutrient content of milk by diet. a-c. Milk was collected from anesthetized dams injected with oxytocin (2.5 IU/mouse) and frozen prior to analysis of triglycerides, lactose, and protein (BCA) according to manufacturer's instructions. Milk from dams fed an unrefined chow diet (Chow), refined low-fat diet (LFD) or refined high-fat diet (HFD) analyzed for concentration of lactose (**a**), triglycerides (TG, **b**) or total protein (**c**). Asterisks indicate the significance of the difference between the indicated group and the chow diet group (n=4-5/group) according to a one-way ANOVA with post-hoc Dunnett multiple comparison testing; ***p<0.0001, **p<0.001, *p<0.05.

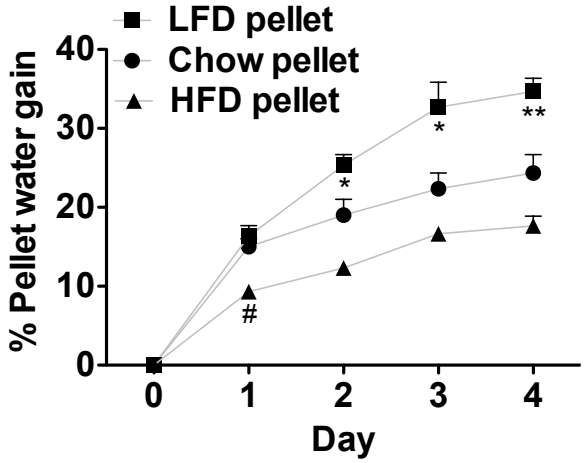

Figure 2.3. Propensity of LFD pellets to absorb moisture. Percentage increase in water weight of the indicated pelleted diet in triplicate over time in a humid environment. Asterisks and hash marks indicate the significance of the difference between low fat diet (LFD) and high fat diet (HFD), respectively, vs. the chow diet according to a one-way ANOVA with post-hoc Bonferroni multiple comparison testing on the indicated day; */# p<0.05, ** p<0.01.

These data are inconsistent with a toxin in unrefined chow or differences in macronutrient content between refined and unrefined diets as causative of premature death in CX mice. Instead, they suggest a defect in the ability to transition from mother's milk to solid food unless that food is soft. Consistent with this, HFD pellets are soft due to their high fat content, and LFD pellets, although initially hard, readily absorbed water (Figure 2.3) and became soft in the hopper within days, likely due to the absorbance of humidity from the cage. To directly test the potential role of soft food during the transition from milk to solids, we presented litters with standard chow in soft agar form from postnatal day 14, coincident with this transition in C57BL/6 mice (http://jaxmice.jax.org/literature/factsheet/LT0001_Pups.pdf). Twelve out of 19 CX mice survived weaning at 28 days (Figure 2.1 d). We conclude the CX mutants that cannot transition to solid food during this developmental window die of malnutrition (Figure 2.1 e).

CX mutants weaned at four weeks of age onto chow in soft agar form had an average lifespan of ~16 weeks (Figure 2.4 a). Five CX mutants weaned onto hard pelleted chow displayed similar longevity (data not shown); the requirement for soft food is thus likely to occur only during an early developmental window. CX mutants weaned onto HFD had slightly extended mean but not maximal lifespan relative to LFD or chow (Figure 2.4 a). CX mutants remained smaller than control littermates throughout their lifespans (Figure 2.4 b, c). Similar to pre-weaned mice, CX mutants weaned onto a chow diet had reduced adiposity, consisting of ~2% of body weight through most of their adult

life. Mutants on a HFD from 7 wks of age achieved higher adiposity of ~5%, but failed to maintain it towards the end of their lifespan (Figure 2.4 d). Lean % body mass was maintained independent of diet or loss of adiposity; organ weights were also maintained relative to body weight except for a reduction in WAT, while heart, lung and brain were slightly increased (Figure 2.5).

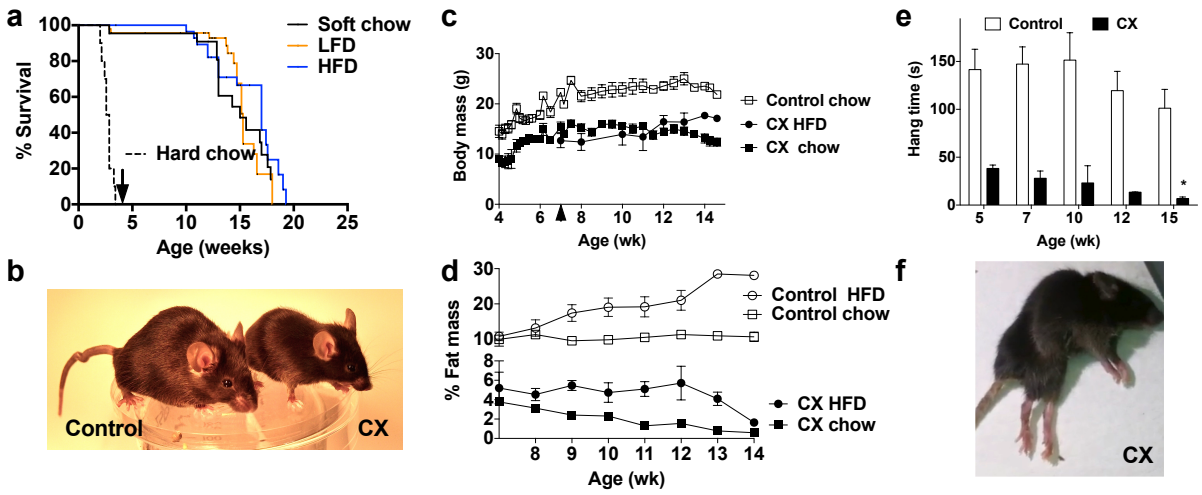

Figure 2.4: Progressive lipodystrophy and neurological complications in a new mouse model of Type I/II CS. a. Kaplan Meier analysis of CX mice born to dams fed hard chow pellets (dotted line, n=10) or soft diets as indicated (LFD, n=47; HFD, n=29; chow agar, n=22). Arrow indicates weaning at 4 weeks of age. **b**. Representative image of CX and control littermates at 14 wks of age. **c**. Body weights of CX and control mice weaned onto chow pellets at 4 wks or CX mice switched to HFD at 7 wks (arrowhead); n=3/group. **d.** Body fat percentage of CX and control mice fed HFD or chow pellets over the indicated time period (n=3/group)**. e**. Grip strength of CX and control mice at the indicated age (n=3/genotype/age) as determined by the length of time hanging on a wire. Asterisks indicate significance according to a one-way ANOVA followed by Dunnett's multiple comparison test vs. the 5 week time point within genotype (* $p<0.05$); between genotype comparisons were significant ($p<0.05$) at each timepoint by one-way ANOVA and Tukey's multiple comparison test. **f**. Representative image of 16 wk old CX mouse displaying hind-limb paralysis, lipodystrophy and kyphosis.

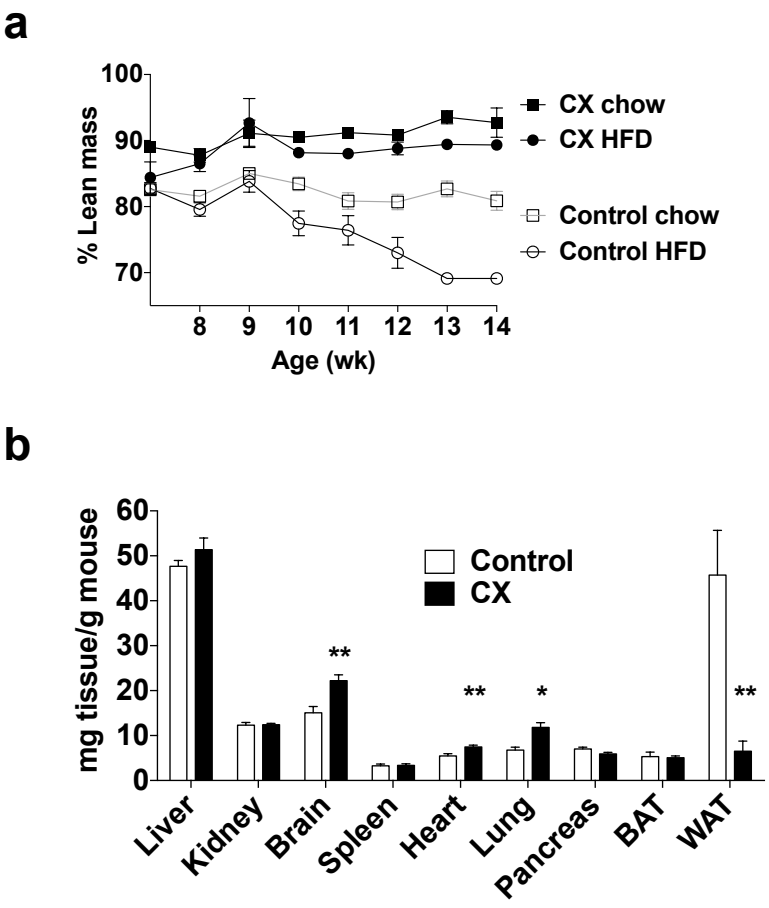

Figure 2.5. Normal lean body mass as a function of weight in CX mutants. a. Lean body mass of the indicated genotype and dietary group (n=3/group) as determined by longitudinal weekly NMR and expressed as a percentage of body weight. **b**. Organ weights upon sacrifice of 105 day old mice of the indicated genotype on chow pellets expressed relative to total body weight; n=4/group. Asterisks indicate the significance of the difference between CX and control tissue by Student's T test; ** $p<0.01$, * $p<0.05$.

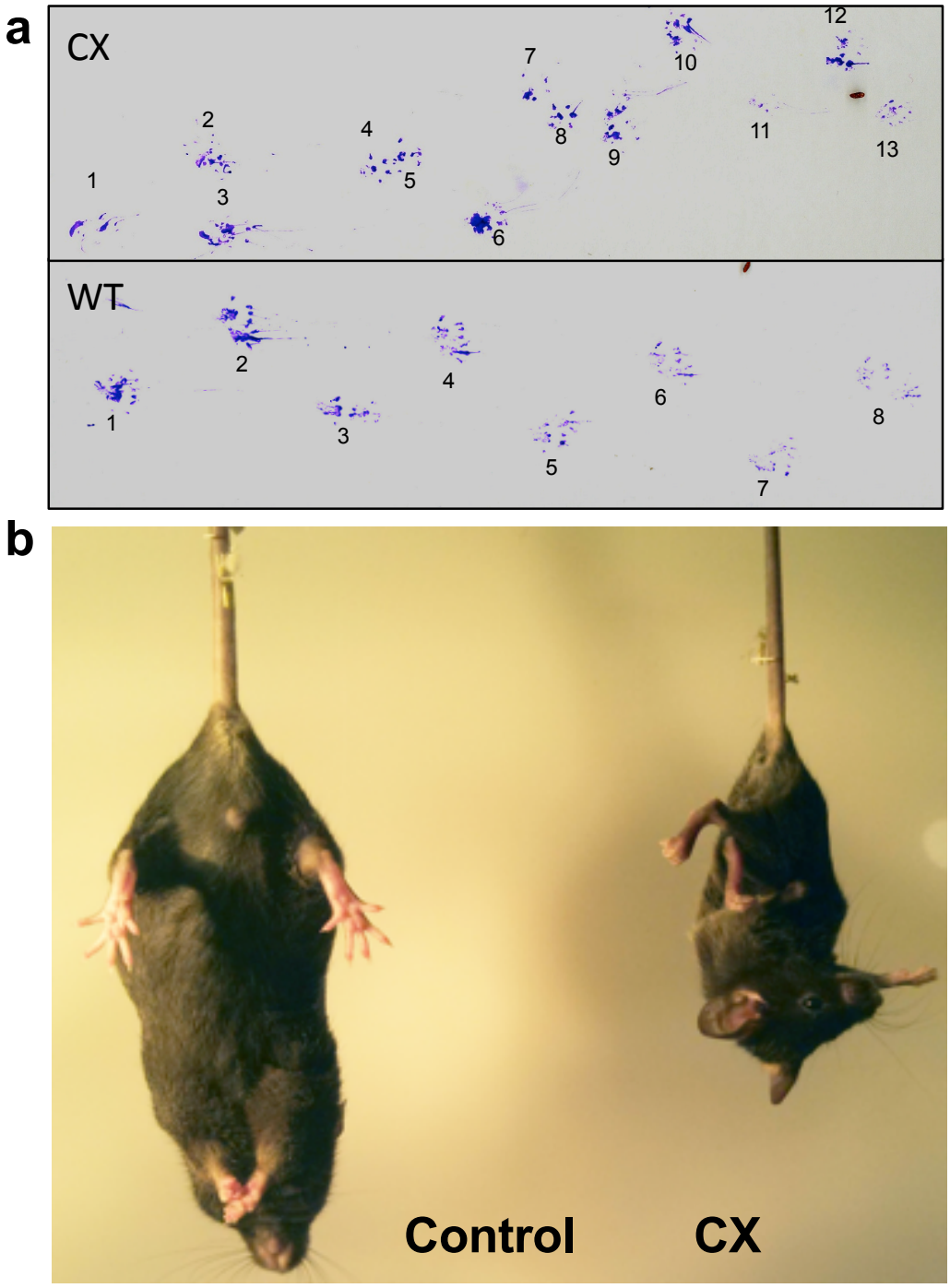

Figure 2.6. Neurological abnormalities in CX mice. a. Gait of CX and control mice. Fore and hind paws were painted with non-toxic tempera paint and then the mouse was placed on a Whatman paper-lined runway (length 50 cm, width 10 cm, height 13 cm). **b**. Tail hang test with age-matched control and CX mice as indicated. Note the abnormal clenching of the hind and fore limbs in the CX mouse.

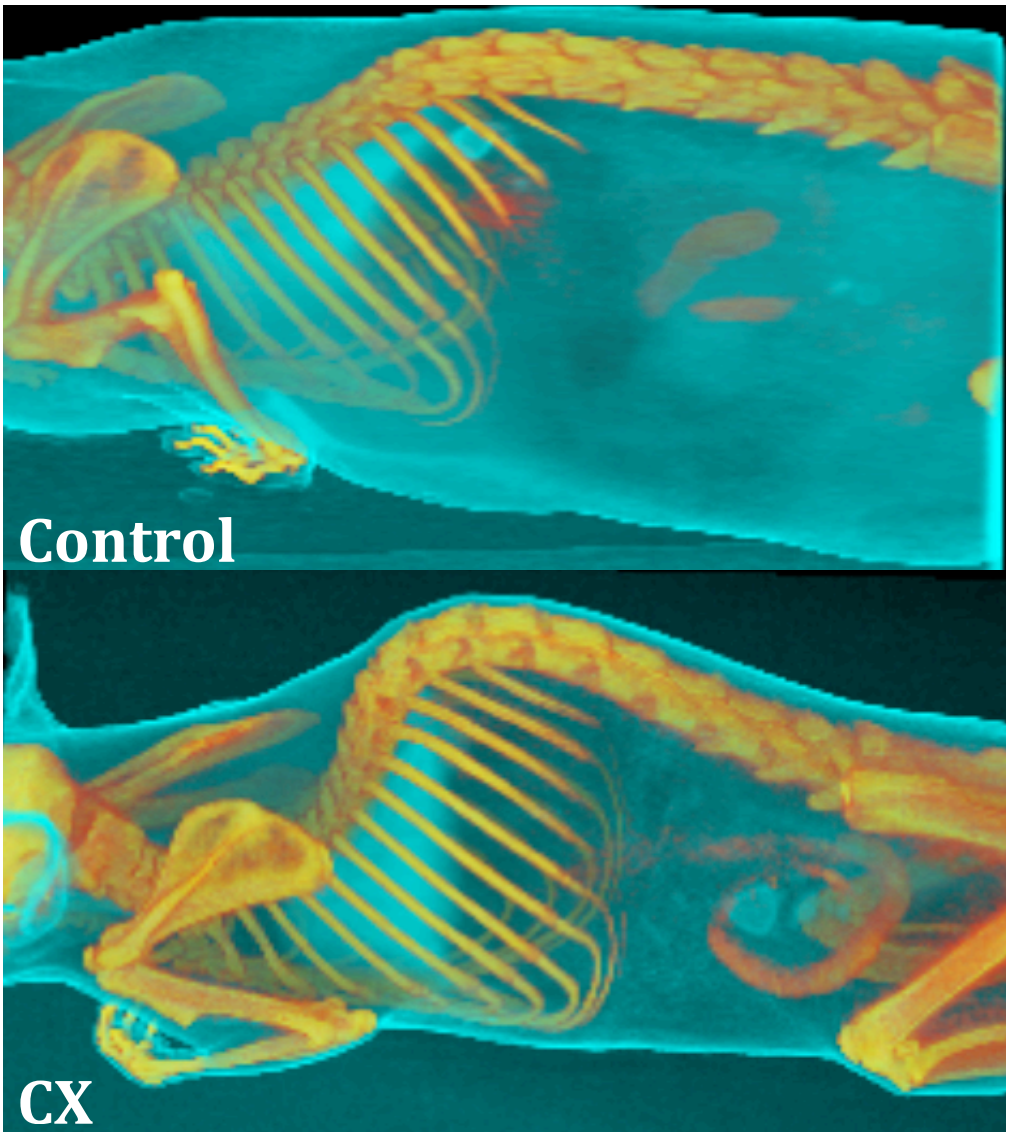

Figure 2.7. Kyphosis in CX mice. Representative computed tomography images of 18 week old Control and CX mice. 18-week-old mice were anesthetized and scanned with a GE Explore CT 120 scanner. Data capture and reconstructions were done using Osirix software.

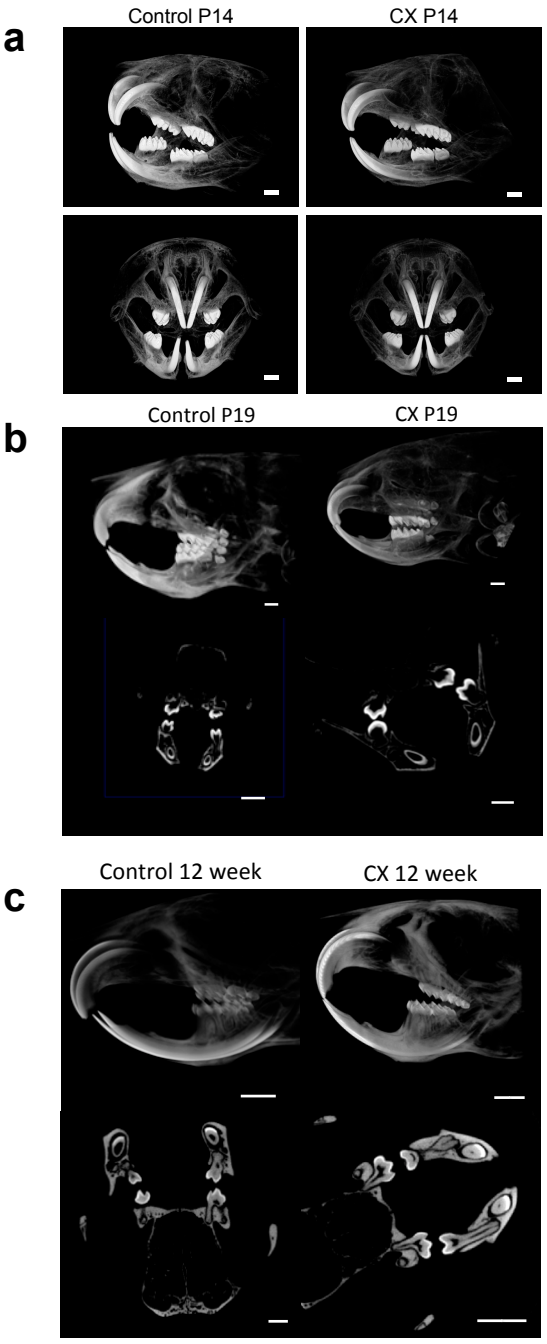

Figure 2.8. Normal tooth development in CX mutants. a-c. Representative images of bone density by computed tomography in CX and Control mice at postnatal day 14 (P14, **a**), P19 (**b**) and 12 weeks (**c**). No defects in tooth development or incisors were noted at any age. Scale bar = 10mm. Mice were perfused with 4% paraformaldehype (PFA) in PBS, heads removed and stored in 4% PFA/PBS at 4°C, and scanned with micro-CT (Xradia, USA) with settings of 60kV, 8W, and 12.390µm pixel size for P14 mouse heads; 80kV, 8W, and 23.814µm for P19 and 12-week-old mouse heads.

Neurological involvement was observed on several levels, including abnormal gait consistent with cerebellar ataxia, inappropriate hind limb clasping in a tail hang test (Figure 2.6) and progressive reduction in grip strength (Figure 2.4 e) culminating in uncoordinated hind limb movement, dystonia, and eventual paralysis (Figure 2.4 f). Other symptoms typical of progeroid disorders were also observed, including kyphosis (Figure 2.7). The reasons underlying these progressive progeroid symptoms are unknown, and they could not be rescued by feeding refined or high energy-density diets (Figure 2.4 a). Taken together, our data indicate that early postnatal death hampering existing models of severe CS resulted from malnutrition and could be rescued with soft food during the critical developmental transition from milk to solid food (Figure 2.1 e). Surviving animals were smaller in size and had progressive adipose and neurological features reminiscent of CS.

Why were CX mice unable to transition normally to solid food? Prolonged survival on a soft food diet after weaning was previously observed in an inducible mouse model of Hutchinson-Gilford Progeria Syndrome with apparent dental abnormalities[18]. Oral anomalies are frequently noted in CS patients[19-21]; however, analysis of bone density in CX teeth revealed no defects in tooth development, enamel, emergence of incisors or molars, or differences in root length during the developmental window of P14 to P19 or later in life (Figure 2.8). CS patients typically have problems eating, possibly due to a neuromuscular deficit, such as restricted mandibular range of motion that can hinder chewing[22], or coordination of chewing and swallowing (E. Nielan, personal

communication). As a result, many are fed soft food and/or receive nutrition via a gastrojejunostomy feeding tube. Future experiments will be required to address the underlying causes of feeding problems in CS patients, as well as the developmental defect in eating hard chow pellets observed in CX mice, and any potential connection between the two.

Why is rescue of death before weaning in CX mice important? This is the first severe CS model to survive weaning with high penetrance, allowing for the analysis of key progeroid features of CS, including progressive loss of adiposity and neurological dysfunction, and their potential relationship to DNA repair insufficiency outside of the window of early development. It also cautions against the use of lifespan extension beyond weaning as a means to score efficacy of experimental interventions until the cause of the inability to switch to solid food is better understood[11].

MATERIALS & METHODS

Mice Mice carrying *Xpa* and/or *Csa* knockout alleles in a C57BL/6 background were maintained under standard laboratory conditions (temperature 20–24 °C, relative humidity 50–60%, 12 h light/12 h dark) and allowed free access to water and standard chow pellets (PicoLab 5058, Purina) unless otherwise indicated. All animal experiments were performed with the approval of the appropriate institutional animal care and use committee.

Diets PicoLab 5058 chow (Purina) consists of unrefined ingredients including wheat, corn, soybean, fish, yeast, and porcine fat, with 23%, 22% and 55% calories from protein, fat and carbohydrates, respectively. High fat (60% calories, D12492) and low fat (10% calories, D12450B) diets (Research Diets, New Brunswick, NJ) consist of refined ingredients (casein, corn starch, maltodextrin 10, sucrose, soybean oil, lard). Agar-based food was prepared by pulverizing pellets of PicoLab 5058 or D12450B and mixing 100g with 100mL of a 2% agar solution. Water absorption of food pellets was determined in a humidified chamber (80% relative humidity) by weighing pellets daily.

Grip strength test Mice were allowed to hang for 180 seconds on a 55cm wide x 2mm thick wire secured 35cm over soft bedding. The length of time hanging was recorded in three trials with at least 5 minutes rest in between each trial.

Body composition Fat and lean mass were assessed by non-invasive nuclear magnetic resonance (NMR) in awake animals (EchoMRI, Echo Med Systems, Houston, TX, USA).

Blood Measurements *Glucose:* Freshly drawn tail vein blood was analyzed with a hand-held blood glucose monitor (One Touch; Johnson & Johnson) according to the manufacturer's instructions. *Triglycerides:* Serum was analyzed using the Serum Triglyceride Determination Kit (Sigma) according to manufacturer's instructions.

Statistics Data analyses were performed in GraphPad Prism 5.0 and presented as the mean +/- SEM unless otherwise noted.

ACKNOWLEDGEMENTS

This work was funded in part by NIH training grants (Interdisciplinary Genes and Environment T32ES016645; Radiation Biology T32CA009078), the Glenn Foundation for Medical Research and the Luke O'Brien Foundation. We thank Ediz Calay for technical assistance and Raul Mostoslovsky, Edward Nielan and Jaan-Olle Andressoo for insightful discussions.

REFERENCES

1. Sykora P, Wilson DM, 3rd, Bohr VA. Repair of persistent strand breaks in the mitochondrial genome. *Mech Ageing Dev.* 2012;133(4):169-175.

2. Hoeijmakers JH. DNA damage, aging, and cancer. *The New England journal of medicine.* 2009;361(15):1475-1485.

3. Fousteri M, Mullenders LH. Transcription-coupled nucleotide excision repair in mammalian cells: molecular mechanisms and biological effects. *Cell research.* 2008;18(1):73-84.

4. Scheibye-Knudsen M, Ramamoorthy M, Sykora P, et al. Cockayne syndrome group B protein prevents the accumulation of damaged mitochondria by promoting mitochondrial autophagy. *J Exp Med.* 2012;209(4):855-869.

5. Brooks PJ. Blinded by the UV light: How the focus on transcription-coupled NER has distracted from understanding the mechanisms of Cockayne syndrome neurologic disease. *DNA Repair (Amst).* 2013.

6. Cleaver JE, Lam ET, Revet I. Disorders of nucleotide excision repair: the genetic and molecular basis of heterogeneity. *Nat Rev Genet.* 2009;10(11):756-768.

7. Suzumura H, Arisaka O. Cerebro-oculo-facio-skeletal syndrome. *Advances in experimental medicine and biology.* 2010;685:210-214.

8. Natale V. A comprehensive description of the severity groups in Cockayne syndrome. *American journal of medical genetics Part A.* 2011;155A(5):1081-1095.

9. van de Ven M, Andressoo JO, Holcomb VB, et al. Extended longevity mechanisms in short-lived progeroid mice: identification of a preservative stress response associated with successful aging. *Mech Ageing Dev.* 2007;128(1):58-63.

10. Murai M, Enokido Y, Inamura N, et al. Early postnatal ataxia and abnormal cerebellar development in mice lacking Xeroderma pigmentosum Group A and Cockayne syndrome Group B DNA repair genes. *Proc Natl Acad Sci U S A.* 2001;98(23):13379-13384.

11. van der Pluijm I, Garinis GA, Brandt RM, et al. Impaired genome maintenance suppresses the growth hormone--insulin-like growth factor 1 axis in mice with Cockayne syndrome. *PLoS Biol.* 2006;5(1):e2.

12. Andressoo JO, Mitchell JR, de Wit J, et al. An Xpd mouse model for the combined xeroderma pigmentosum/Cockayne syndrome exhibiting both cancer predisposition and segmental progeria. *Cancer Cell.* 2006;10(2):121-132.

13. Laposa RR, Huang EJ, Cleaver JE. Increased apoptosis, p53 up-regulation, and cerebellar neuronal degeneration in repair-deficient Cockayne syndrome mice. *Proc Natl Acad Sci U S A.* 2007;104(4):1389-1394.

14. Harada YN, Shiomi N, Koike M, et al. Postnatal growth failure, short life span, and early onset of cellular senescence and subsequent immortalization in mice lacking the xeroderma pigmentosum group G gene. *Mol Cell Biol.* 1999;19(3):2366-2372.

15. de Boer J, Andressoo JO, de Wit J, et al. Premature aging in mice deficient in DNA repair and transcription. *Science.* 2002;296(5571):1276-1279.

16. van der Horst GT, Meira L, Gorgels TG, et al. UVB radiation-induced cancer predisposition in Cockayne syndrome group A (Csa) mutant mice. *DNA Repair (Amst).* 2002;1(2):143-157.

17. de Vries A, van Oostrom CTM, Hofhuis FMA, et al. Increased susceptibility to ultraviolet-B and carcinogens of mice lacking the DNA excision repair gene *XPA*. *Nature.* 1995;377:169-173.

18. Sagelius H, Rosengardten Y, Hanif M, et al. Targeted transgenic expression of the mutation causing Hutchinson-Gilford progeria syndrome leads to proliferative and degenerative epidermal disease. *J Cell Sci.* 2008;121(Pt 7):969-978.

19. Schneider PE. Dental findings in a child with Cockayne's syndrome. *ASDC journal of dentistry for children.* 1983;50(1):58-64.

20. Horbelt CV. Robinow syndrome, Cockayne syndrome, and Pfeiffer syndrome: an overview of physical, neurological, and oral characteristics. *General dentistry.* 2010;58(1):14-17.

21. Sorin MS. Cockayne's syndrome: dental findings and management. *The Journal of clinical pediatric dentistry.* 1994;18(4):299-302.

22. Boraz RA. Cockayne's syndrome: literature review and case report. *Pediatric dentistry.* 1991;13(4):227-230.

CHAPTER 3

Increased oxidative phosphorylation in response to acute and chronic DNA damage

This chapter is a reproduction of a published manuscript with minor modifications:

Lear E. Brace[1], Sarah C. Vose[2], Kristopher Stanya[1], Rose M. Gathungu[3], Vasant R. Marur[3], Alban Longchamp[1], J. Humberto Treviño-Villarreal[1], Pedro Mejia[1], Dorathy Vargas[1], Karen Inouye[1], Roderick T. Bronson[4], Chih-Hao Lee[1], Edward Neilan[5], Bruce S. Kristal[3], James R. Mitchell.[1]* Increased oxidative phosphorylation in response to acute and chronic DNA damage. npj Aging and Mechanisms of Disease 2, 2016.

[1] Department of Genetics and Complex Diseases, Harvard T.H. Chan School of Public Health, 655 Huntington Ave, Boston, MA 02115, USA
[2] Vermont Departments of Health, Environmental Health Division, 108 Cherry St, Burlington, Vermont, 05402, USA
[3] Departments of Neurosurgery, Harvard Medical School, Brigham and Women's Hospital, 221
Longwood Avenue, Boston, MA 02115, USA
[4] Rodent Histopathology Laboratory, Harvard Medical School, 77 Avenue Louis Pasteur, Boston, MA 02115, USA
[5] Genetics and Metabolism, Boston Children's Hospital, Harvard Medical School, Boston, MA 02115, USA

Author contributions

L.E.B., S.C.V, and J.R.M. designed experiments. L.E.B. S.C.V, K.S., R.M.G., A.L., J.H.T.V., P.M., D.V., and K.I., performed the experiments. L.E.B., V.R.M., R.T.B., C-H.L., E.N., B.S.K., and J.R.M. analyzed the data. L.E.B. and J.R.M. wrote the paper.

ABSTRACT

Accumulation of DNA damage is intricately linked to aging, aging-related diseases and progeroid syndromes such as Cockayne syndrome (CS). Free radicals from endogenous oxidative energy metabolism can damage DNA, however the potential of acute or chronic DNA damage to modulate cellular and/or organismal energy metabolism remains largely unexplored. We modeled chronic endogenous genotoxic stress using a DNA repair-deficient $Csa^{-/-}|Xpa^{-/-}$ mouse model of CS. Exogenous genotoxic stress was modeled in mice *in vivo* and primary cells *in vitro* treated with different genotoxins giving rise to diverse spectrums of lesions, including ultraviolet radiation, intrastrand crosslinking agents and ionizing radiation. Both chronic endogenous and acute exogenous genotoxic stress increased mitochondrial fatty acid oxidation (FAO) on the organismal level, manifested by increased oxygen consumption, reduced respiratory exchange ratio, progressive adipose loss and increased FAO in tissues *ex vivo*. In multiple primary cell types, the metabolic response to different genotoxins manifested as a cell-autonomous increase in oxidative phosphorylation (OXPHOS) subsequent to a transient decline in steady-state NAD+ and ATP levels, and required the DNA damage sensor PARP-1 and energy-sensing kinase AMPK. We conclude that increased FAO/OXPHOS is a general, beneficial, adaptive response to DNA damage on cellular and organismal levels, illustrating a fundamental link between genotoxic stress and energy metabolism driven by the energetic cost of DNA damage. Our study points to therapeutic opportunities to mitigate detrimental effects of DNA damage on primary cells in the context of radio/chemotherapy or progeroid syndromes.

INTRODUCTION

The process of generating energy through mitochondrial oxidative phosphorylation inevitably results in production of free radicals that can damage cellular macromolecules, including DNA. Consistent with this, interventions that increase oxidative phosphorylation (OXPHOS) (e.g. fasting) can also lead to an increase in free radical generation, at least transiently[1]. Because of the potential detrimental effects of free radical damage, cells have evolved a variety of mechanisms of detoxification, many of which respond to oxidative stress in an inducible fashion. For example, the transcription factor NRF2 controlling expression of key enzymes in the glutathione pathway is itself activated by oxidative and electrophilic stressors[2]. On the other hand, because energy generation through aerobic glycolysis rather than OXPHOS could potentially limit further oxidative DNA damage accumulation[3], altering metabolism could be another potential strategy to limit free radical damage. As proof of principle, a number of cell types can rapidly shift between OXPHOS and glycolysis depending on environmental cues, for example upon antigen stimulation in the case of immune cells[4], although the potential of DNA damage to contribute to this process remains untested.

DNA damage can also be energetically costly, for example upon activation of the DNA damage response protein, PARP-1. PARP-1 binds directly to single stranded DNA and generates chains of poly-ADP-ribose (PAR) in response to breaks that occur directly or indirectly upon ultraviolet radiation (UV)[5], ionizing radiation (IR)[6], topoisomerase

inhibition[7] or DNA alkylation[8]. PARP-1 activation by massive DNA damage leads directly to NAD+ depletion and subsequently to ATP depletion and cell death via necrosis[9] or apoptosis[10]. While this demonstrates the indirect potential of DNA damage to alter cellular energy levels, with profound downstream consequences on cell fate[11], the molecular mechanisms underlying PARP-1 induced ATP loss remain unresolved[12]. One possibility is through depletion of NAD+, a key metabolite in both glycolytic and oxidative energy metabolism.

While the PARP-1 example serves to illustrate the high energetic cost of excessive DNA damage, how cells respond to perturbations in energy homeostasis induced by sublethal doses of DNA damage remains poorly characterized. One clue is the discovery that genotoxic stressors including UV-C, IR[13], and cisplatin[14] can activate the AMP-activated protein kinase (AMPK), which acts to restore energy balance by inhibiting ATP-consuming processes and activating processes to generate ATP[15]. AMPK is regulated allosterically by AMP, but also requires phosphorylation by upstream kinases such as LKB1 and CaMKKβ[15] or p53 transcriptional targets, sestrin 1/2[16]. Currently, neither the mechanism by which DNA damage activates AMPK, nor the consequences of such activation, are clearly understood.

Thus, while it is clear that the byproducts of normal energy metabolism can cause DNA damage, and that DNA damage can impact cellular energy metabolism, whether and how DNA damage itself exerts feedback control over energy metabolism is poorly

characterized, particularly on the organismal level. Here, we set out to directly test the potential of DNA damage to affect energy metabolism, and to identify common adaptive metabolic changes on the cellular and organismal levels in response to both chronic and acute DNA damage.

For chronic damage, we utilized a mouse model of the congenital DNA repair deficiency disorder, Cockayne syndrome (CS). CS is characterized by growth failure, loss of adiposity, neurodegeneration, and photosensitivity without prevalence of skin cancer[17]. It is caused by alterations in proteins including CSA or CSB that share a common function in transcription-coupled nucleotide excision repair (NER) of bulky, helix-distorting lesions, for example those caused by UV light that sterically hinder RNA polymerases and block transcription[18]. Recently, we reported a mouse model of CS lacking both *Csa* and *Xpa,* another NER gene, (heretofore referred to as CX) that recapitulates many aspects of the human progeria[19]. As a model of acute genotoxic stress, we subjected wildtype (WT) mice and cells with genotoxins (UV-C, IR, mitomycin C (MMC) and irinotecan) giving rise to diverse spectrums of DNA lesions. Here, we report that multiple forms of acute and chronic genotoxic stress engender a PARP-1 dependent metabolic switch characterized by increased fatty acid oxidation (FAO) and OXPHOS as an adaptive response to maintain energy homeostasis on both organismal and cell-autonomous levels.

RESULTS

Perturbations in energy metabolism indicative of improved metabolic fitness in CX mice

A number of mouse models with severe symptoms of CS ("NER progeria" in mice), display apparent alterations in systemic metabolism during postnatal development, including loss of adiposity, perturbations of the post-natal GH-IGF-1 axis and hypoglycemia contributing to death before weaning[20]. Using the CX mouse model that survives weaning with high penetrance[19], we first characterized changes in adiposity, glucose and lipid homeostasis as markers of whole-body energy metabolism. Although physically smaller than Control (includes WT, CSA single KO, and XPA single KO) mice, CX mice increased in body mass during postnatal development at a similar rate. Maximal body mass was attained by 8wks and was stable for ~5wks before onset of terminal senescent weight loss over the remainder of the lifespan (Figure 3.1a). Body fat in CX mice calculated as either a percentage of body weight (Figure 3.1b) or in absolute grams (Supplemental Figure 3.1a) paralleled body weight, peaking ~8wks and declining after 13wks. Although the absolute lean mass declined with age in CX mice (Supplemental Figure 3.1b), the percentage lean mass remained stable between 13-20wks (Figure 3.1c). CX mice fed a high fat diet (HFD) failed to normalize relative and absolute weights of subcutaneous or perigonadal white adipose (WAT) depots compared to controls (Figure 3.1d, Supplemental Figure 3.1c), consistent with the failure of HFD feeding to rescue CX

longevity[19]. Progressive histological investigation of WAT from CX mice showed a decline in mature adipocyte size (Figure 3.1e), but no visible evidence of crown-like structures indicative of inflammatory macrophage activation by H&E or in WAT from 16wk CX mice as shown by F4/80 immunohistochemistry (Supplemental Figure 3.1d) or fluorescence associated cell sorting (FACS) analysis of F4/80+/CD11b+ stromal vascular fraction (SVF) (Supplemental Figure 3.1e). These data suggest altered functionality of CX WAT rather than loss of cellularity due to inflammation.

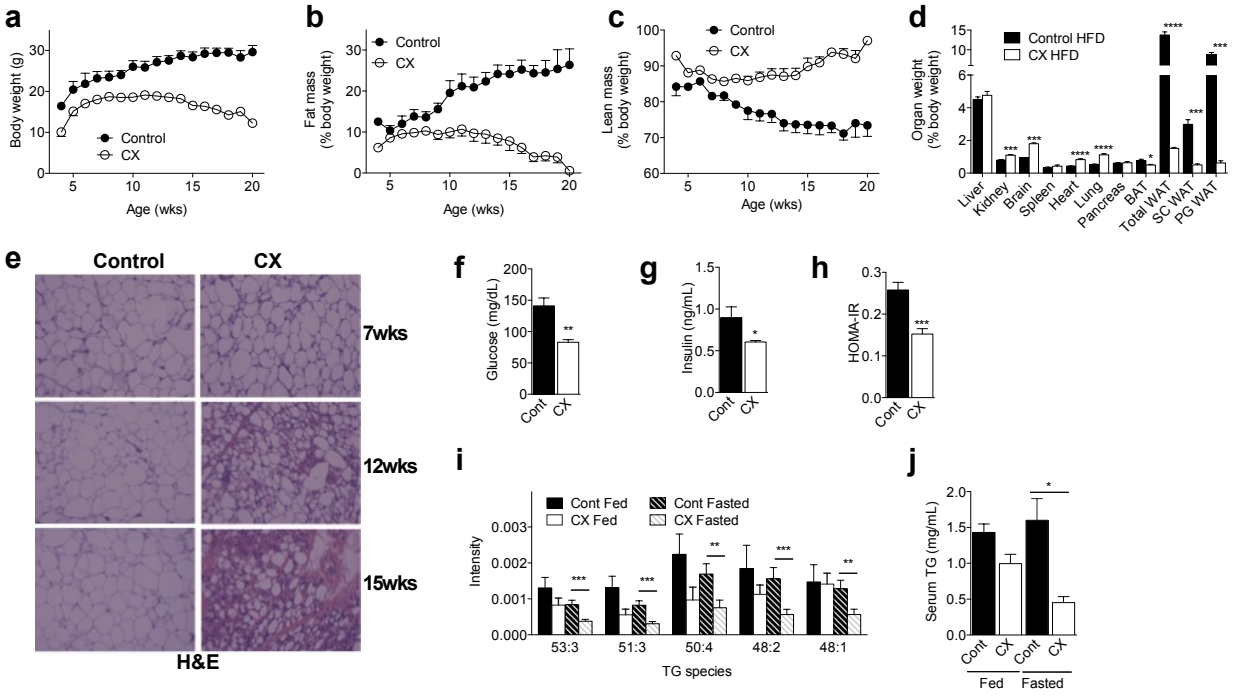

Figure 3.1: Perturbations in energy metabolism indicative of improved metabolic fitness in CX mice. a-c. Changes in body weight **(a)**, percentage fat **(b)** and lean mass **(c)** over time in CX and control mice (n=14-16/group). **d.** Organ weights upon sacrifice of 14wk mice on a HFD expressed as a percentage body weight, n=4/group; Student's T test. **e**. H&E staining of paraffin-embedded perigonadal WAT from control and CX mice. **f-h.** Blood glucose **(f)**, serum insulin levels **(g)**, and HOMA-IR **(h)** of 12-16wk Control and CX mice (n=7-11/genotype); Students T test. **i.** Relative intensity of the indicated triglyceride (TG) species in serum from fed or fasted CX or control mice by unbiased lipidomics (CX=5/group, control=10/group); 2-way ANOVA with Bonferroni post-test. **j.** Total serum TG in fasted and fed WT and CX mice (n=3/group); Student's T test. *p<0.05, **p<0.01, ***p<0.001, ****p<0.0001.

In 14-16wk CX mice, fasted blood glucose and insulin levels were significantly reduced (Figure 3.1f, g), leading to an improved HOMA-IR (Figure 3.1h). Insulin challenge trended towards increased glucose disposal in 14wk CX mice (Supplemental Figure 3.1f), and glucose tolerance tests revealed no difference (Supplemental Figure 3.1g), suggestive of improved whole-body insulin sensitivity but reduced capacity for stimulated insulin secretion in CX mice, similar to long-lived models such as growth hormone receptor knockout mice[21]. Circulating leptin levels in the fasted state were significantly decreased in CX vs. Control mice (Supplemental Figure 3.1h) but adiponectin levels were unchanged (Supplemental Figure 3.1i). Analysis of serum lipids using unbiased mass spectrometry revealed significant differences in multiple lipid species in the fasted state and a trend towards a reduction in the fed state in 16wk CX mice relative to both WT and single KO controls, including a number of individual triglyceride (TG) species (Figure 3.1i, Supplemental Figure 3.1j). Measurement of bulk serum TG in a separate cohort of Control and CX mice confirmed a significant reduction in the fasted state (Figure 3.1j).

Increased FAO in CX mice *in vivo* and cells *in vitro*

Reduced adiposity, improved glucose homeostasis and reduced circulating lipids are characteristics of the pro-longevity intervention known as dietary restriction (DR), defined as reduced food intake without malnutrition, and linked an overall metabolic shift to FAO[22]. Previously, DR-like phenotypes including improved insulin sensitivity and

increased oxidative stress resistance have been observed in CS mouse models[23]. We used indirect calorimetry to test the hypothesis that FAO was increased in CX mice despite *ad libitum* access to food. CX mice consumed more O_2 (Figure 3.2a) and produced more CO_2 (Figure 3.2b) than control littermates, but without significant differences in physical activity (Supplemental Figure 3.2a) or food intake (Supplemental Figure 3.2b). Importantly, a reduced respiratory exchange ratio (RER), indicative of preferential use of fat or protein relative to carbohydrate, was observed (Figure 3.2c, Supplemental Figure 3.2c), but only during the dark phase and despite normal intake of a nutritionally complete diet with 70% calories in the form of carbohydrates. Ketone bodies were appropriately elevated in both fasted Control and CX mice, suggestive of an intact fasting response in CX mice without evidence of malabsorption (Supplemental Figure 3.2d).

Gene expression profiling of skeletal muscle from fasted CX relative to Control mice revealed a significant increase in many FAO-related genes (Figure 3.2d). Consistently, soleus muscle from CX mice had a significantly elevated capacity to oxidize the radiolabeled 16C-saturated fatty acid palmitate relative to controls (Figure 3.2e). Interestingly, soleus from CSA KO animals with a much milder metabolic phenotype displayed a trend toward increased FAO capacity, while soleus from XPA KO mice with no reported metabolic phenotype did not. *Ex vivo* FAO capacity was also significantly increased in livers of CX mice relative to controls (Figure 3.2f).

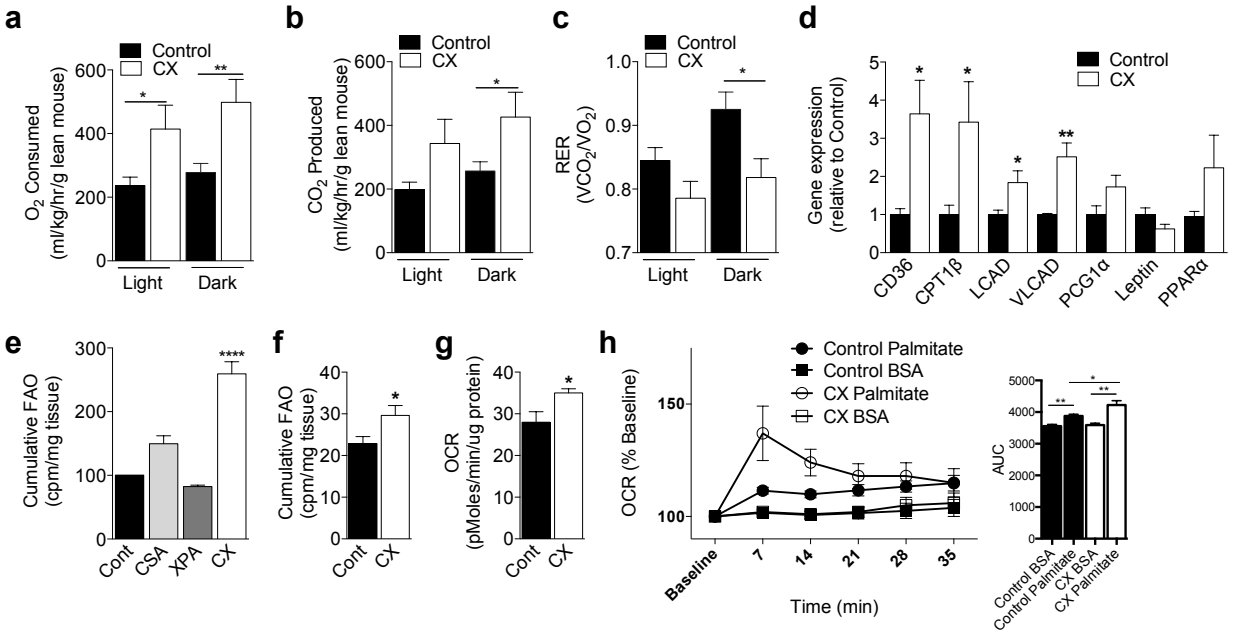

Figure 3.2: Increased FAO in CX mice *in vivo* and in cells *in vitro*. a-c. Indirect calorimetry of 8-14wk Control and CX mice (n=12/group) showing O_2 consumed **(a),** CO_2 produced **(b)** and RER (**c**) all corrected by lean body mass; Students T test. **d.** Gene expression of 12-16wk Control and CX muscle (n=6/group); Student's T test. **e.** Cumulative FAO of tritiated palmitate of soleus muscle from 16wk mice (n=5-8/group); 1-way ANOVA with Dunnett's post-test. **f.** Cumulative FAO of tritiated palmitate of liver of 16wk mice (n=5-8/group); Student's T test. **g.** Basal OCR of MDFs measured by Seahorse Cell Metabolism Analyzer in 3 independent lines of each genotype; Student's T test. **h.** OCR expressed as a percentage of baseline within cell line of Control and CX MDFs by Seahorse after addition of 200μM BSA-conjugated Palmitate with area under the curve analysis (AUC) inset at right (n=4 lines/genotype), Student's T test. *p<0.05, **p<0.01, ***p<.001, ****p<0.0001.

Because FAO can be driven by substrate availability *in vivo*, we next asked if increased FAO capacity was an intrinsic property of CX cells. To this end, primary, low-passage dermal fibroblasts (MDFs) were isolated from tails of pre-weaning heterozygote WT and CX mice. We note that cells from CS patients and related rodent models do not show defects in cellular proliferation or onset of premature cellular senescence[24], nor did we observe this in CX cells.

Under standard serum-free Seahorse media conditions with 11mM glucose, CX MDFs had a higher oxygen consumption rate (OCR) than control cells (Figure 3.2g), consistent with increased mitochondrial OXPHOS, and slightly but not significantly reduced extracellular acidification rate (ECAR) indicative of aerobic glycolysis (Supplemental Figure 3.2e). Both measures were normalized to total cellular protein content, a marker of cell viability, which was not different amongst genotypes (Supplemental Figure 3.2f); mitochondrial content was slightly but not significantly increased in CX MDFs relative to Control cells (Supplemental Figure 3.2g). Under low glucose conditions (2.5mM), addition of the fatty acid palmitate increased OCR to a significantly higher level in CX MDFs compared to Control cells (Figure 3.2h). Thus, increased OXPHOS activity appears to be a cell-intrinsic property of CX cells independent of the substrate, glucose or fatty acid that is available for oxidation.

Increased FAO is a cell-autonomous, adaptive response triggered by genotoxic stress in CX cells

Because increased FAO in CX cells/animals could be due to changes distinct from accumulated unrepaired DNA lesions, for example defects in transcriptional regulation associated with some forms of CS[25], we next tested the potential of DNA damage to directly impact OXPHOS/FAO capacity. To this end, MDFs were challenged with UV-C to induce bulky DNA lesions without generation of free radicals that can damage lipids and proteins. Twenty-four hours after a relatively low dose of 4J/m² UV-C vs. mock treatment,

OCR was significantly increased as a function of UV-C exposure in CX MDFs under conditions favoring FAO (2.5mM glucose, addition of palmitate; Figure 3.3a, AUC inset) or glucose oxidation (11mM glucose, without palmitate; Figure 3.3b), consistent with metabolic substrate flexibility as observed above. OCR readings were normalized to total protein content calculated from the same cells immediately after the final reading; protein content was not significantly altered by low-dose UV-C in this time frame (Supplemental Figure 3.3a). Mitochondrial content normalized to total protein was increased slightly but significantly upon UV-C in both cell types (Supplemental Figure 3.3b), and thus unlikely to be causative of the specific increase in OCR upon UV-C in CX MDFs. ECAR was significantly reduced in UV-C treated CX cells compared to untreated WT cells (Supplemental Figure 3.3c).

Direct measurements of FAO capacity in dermal fibroblast cultures from CX mice (Figure 3.3c), as well as CSA and CSB primary human diploid fibroblasts (HDF; Figure 3.3d), revealed significant increases 24hrs after UV-C irradiation. Increased FAO capacity was not specific to dermal fibroblasts, but was also observed upon UV-C irradiation in CX-derived pre-adipocytes (Supplemental Figure 3.3d). Consistent with the potential for increased FAO/OXPHOS to impact energy homeostasis upon genotoxic stress, steady-state ATP levels did not differ significantly amongst genotypes in unirradiated cells, but were significantly higher 24hrs post irradiation in CX cells (Figure 3.3e), potentially reflecting increased energy production, decreased energy expenditure, or both. Taken together, these data support a model in which increased FAO/OXPHOS is a cell-

autonomous adaptation to both endogenous and exogenous genotoxic stress in CX cells with the potential to impact energy homeostasis.

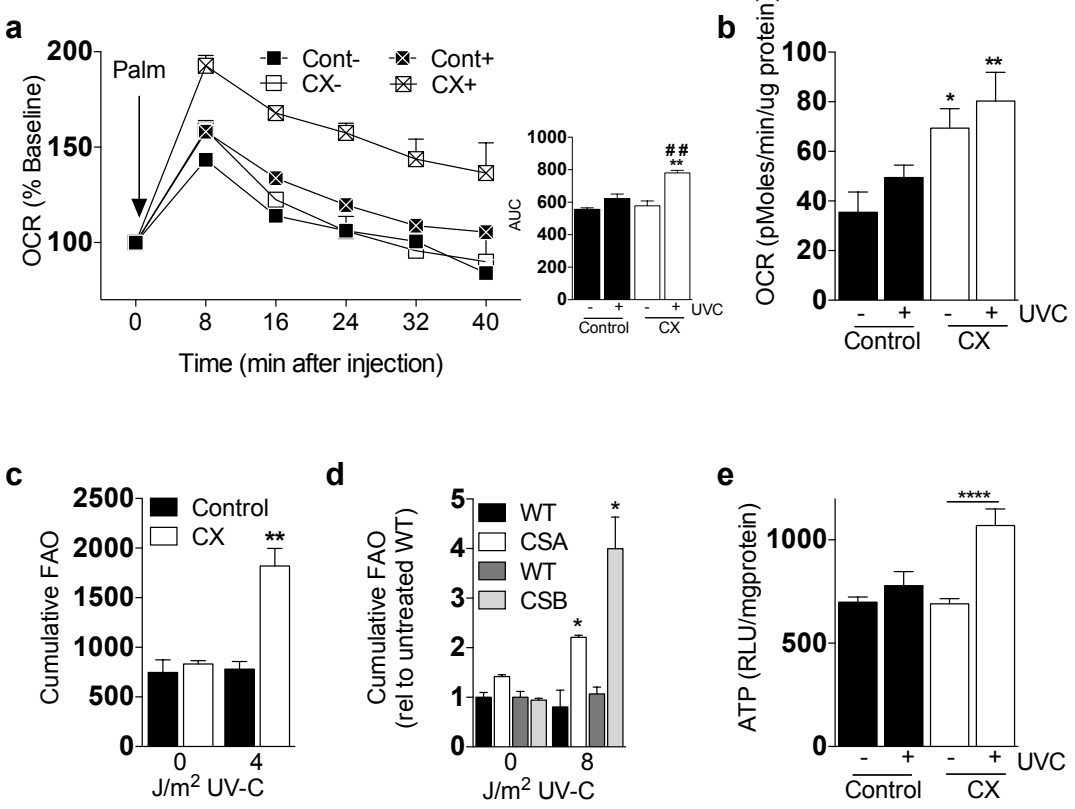

Figure 3.3: Increased FAO is a cell-autonomous, adaptive response triggered by genotoxic stress in CX cells. a. OCR over time after the injection of 200μM BSA-conjugated palmitate in the indicated genotypes (n=3 independent MDF lines/genotype) 24hrs post 4J/m² UV-C or mock treatment (+ or -, respectively) with AUC analysis at right; Student's T test between genotypes within UV treatment group**; Student's T test within genotype between +/- UV treatment$^{\#\#}$. **b.** OCR of MDFs (3 lines/genotype) 24hrs after 4J/m² UV-C or mock treatment; 1way ANOVA between genotypes within treatment group with Dunnett's post-test. **c.** Cumulative FAO of tritiated palmitate over a 4hr period, 24hrs after treatment of MDFs (n=3 lines/genotype) with indicated dose of UV-C; Student's T test between genotypes within UV dose. Primary human CSA and CSB **(d)** dermal fibroblasts treated as in **c**; Student's T test between genotypes within UV dose. **e.** Steady-state ATP levels of MDFs 24hrs after exposure to 0 or 4J/m² UV-C; Student's T test within genotype between +/- UV treatment. *p<0.05, **p<0.01, ****p<0.0001, $^{\#\#}$p<0.01.

Increased FAO is a general response to acute genotoxic stress

We next asked if the observed increase in FAO was a specific property of NER deficiency, or a general response to UV-C. Because WT cells tolerate the low doses of UV-C used to characterize metabolic changes in CX cells, we exposed WT MDFs and HDFs to higher UV-C doses (20 and 24J/m^2, respectively) and measured the time-dependent increase in radiolabeled palmitate oxidation. Although no differences in the capacity to burn fatty acid were observed between irradiated and unirradiated MDFs within the first two hours after UV-C exposure, by 10hrs irradiated MDFs had oxidized significantly more fatty acid (Figure 3.4a) despite an overall time-dependent decrease in oxidation rates (Supplemental Figure 3.4a) likely due to unfavorable culturing conditions (e.g. low glucose, no serum) required for FAO measurements. Additional independent WT MDF and HDF cultures showed similar cumulative increases in FAO between 2 and 10hrs after high-dose UV-C exposure (Figure 3.4b; Supplemental Figure 3.4b, c) coincident with an increase in expression of FAO-related genes 6hrs after exposure in WT MDFs (Figure 3.4c).

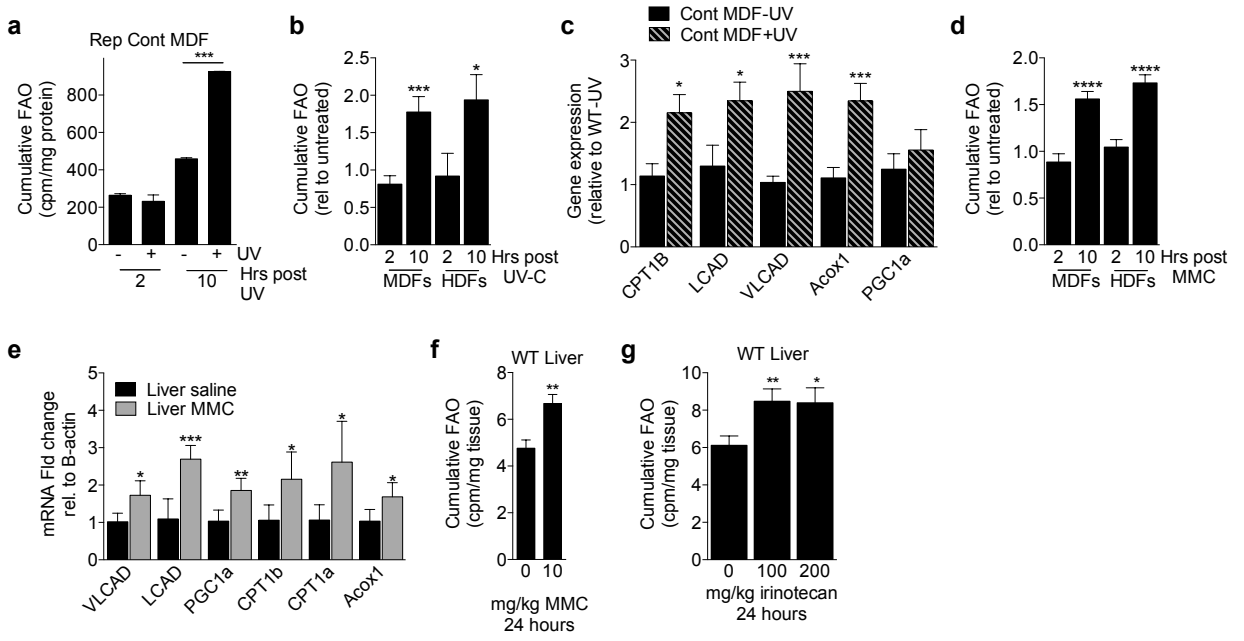

Figure 3.4: Increased FAO is a general response to acute genotoxic stress. a. Cumulative FAO of tritiated palmitate of a representative control MDF line (Rep Cont MDF) over the indicated time period after exposure to 0 or 20J/m² UV-C; Student's T test between treatment groups within time point. **b.** Cumulative FAO of tritiated palmitate of 2 additional UV-C treated control MDF lines expressed relative to untreated at the indicated time point post-irradiation, and of 3 UV-C treated WT HDF lines relative to untreated at the indicated time; Student's T test. **c.** mRNA expression of FAO-related genes in control MDFs 6hrs after exposure to 20J/m² UV-C expressed relative to mock irradiated cells; Student's T test. **d.** Cumulative FAO of tritiated palmitate of three independent MDF and HDF lines exposed to 40μM MMC expressed relative to untreated at the indicated time point; Student's T test. **e, f.** Gene expression of FAO-related genes (**e**) and FAO capacity (**f**) in liver from 8wk WT mice injected IP with 10mg/kg MMC or saline and harvested after 24 hours (n=4/group); Student's T test between treatment groups. **g.** FAO capacity of liver from 8wk WT mice injected IP with 100 or 200mg/kg irinotecan or saline and harvested after 24 hours (n=4/group); Students T test. *p<0.05, **p<0.01, ***p<0.001, ****p<0.0001.

Having established that increased FAO occurs upon high doses of UV-C irradiation of WT cells, we next asked if increased FAO is specific to helix-distorting UV lesions or a more general response to genotoxic stress. Treatment with the crosslinking agent mitomycin C (MMC) resulted in a similar increase in FAO in WT and CX MDFs (Supplemental Figure 3.4d) as well as in WT MDFs and HDFs (Figure 3.4d; Supplemental

Figure 3.4e, f). Interestingly, ionizing radiation (IR), which induces mostly oxidative lesions and some double stranded DNA breaks, failed to increase FAO capacity in MDFs at doses of 4.6 and 10Gy, but significantly increased FAO capacity at 100Gy (Supplemental Figure 3.4g, h). All cumulative measurements were normalized to cellular protein in the same well (Supplemental Figure 3.4i-k).

Lastly, we asked if increased FAO is a physiological response to DNA damage *in vivo,* for example in the context of genotoxic chemotherapy. To this end, 9wk old WT mice were treated with a single chemotherapeutic dose of MMC. One day later, MMC-treated mice displayed significantly increased FAO-related gene expression in liver and muscle (Figure 3.4e, Supplemental Figure 3.4l) and an increased FAO capacity in liver *ex vivo* (Figure 3.4f). Another chemotherapeutic, irinotecan (topoisomerase I inhibitor), also increased FAO capacity in liver and muscle 24hrs after treatment (Figure 3.4g, Supplemental Figure 3.4m), suggesting increased FAO is a general response to genotoxic stress in primary cells *in vitro* and tissues *in vivo*.

PARP-1-dependent NAD+/ATP depletion and AMPK activation link DNA damage to increased FAO

How does DNA damage trigger a metabolic switch to increased FAO/OXPHOS? Because FAO provides reducing equivalents for efficient ATP generation via mitochondrial OXPHOS, we hypothesized that the rapid increase in FAO/OXPHOS was

an adaptive response to increased energy demands upon genotoxic stress. Consistent with this, steady-state ATP levels were transiently reduced in WT MDFs and HDFs within 30-60min of UV-C or MMC treatment, returning to initial levels within 60-90min (Figure 3.5a, Supplemental Figure 3.5a).

Multiple genotoxins result in activation of PARP-1[13], which consumes NAD+ to synthesize poly-ADP ribose (PAR) chains on target proteins surrounding DNA breaks. The resulting NAD+ depletion can mediate ATP loss through multiple mechanisms, including inhibition of ATP generation by glycolysis for which NAD+ is a key cofactor[12]. To test the potential of PARP-1 activation to contribute to ATP depletion, we first confirmed its activity by measuring PAR accumulation and NAD+ depletion in WT vs. PARP-1 KO primary dermal fibroblasts subject to genotoxic stress. Increased PARylation was observed in the nucleus by immunofluorescence (Supplemental Figure 3.5b) and in whole cell extracts by Western blot (Figure 3.5b, Supplemental Figure 3.5c, d) within minutes of MMC or UV-C treatment and coincident with a significant reduction in NAD+ levels (Figure 3.5c) in WT but not PARP-1 KO cells.

Importantly, transient ATP depletion and increased FAO capacity observed upon two different forms of genotoxic stress in WT cells were both absent in PARP-1 KO cells (Figure 3.5d, e, Supplemental Figure 3.5e, f). These data suggest that PARP-1 may serve as the molecular link between DNA damage and energy metabolism across a spectrum of

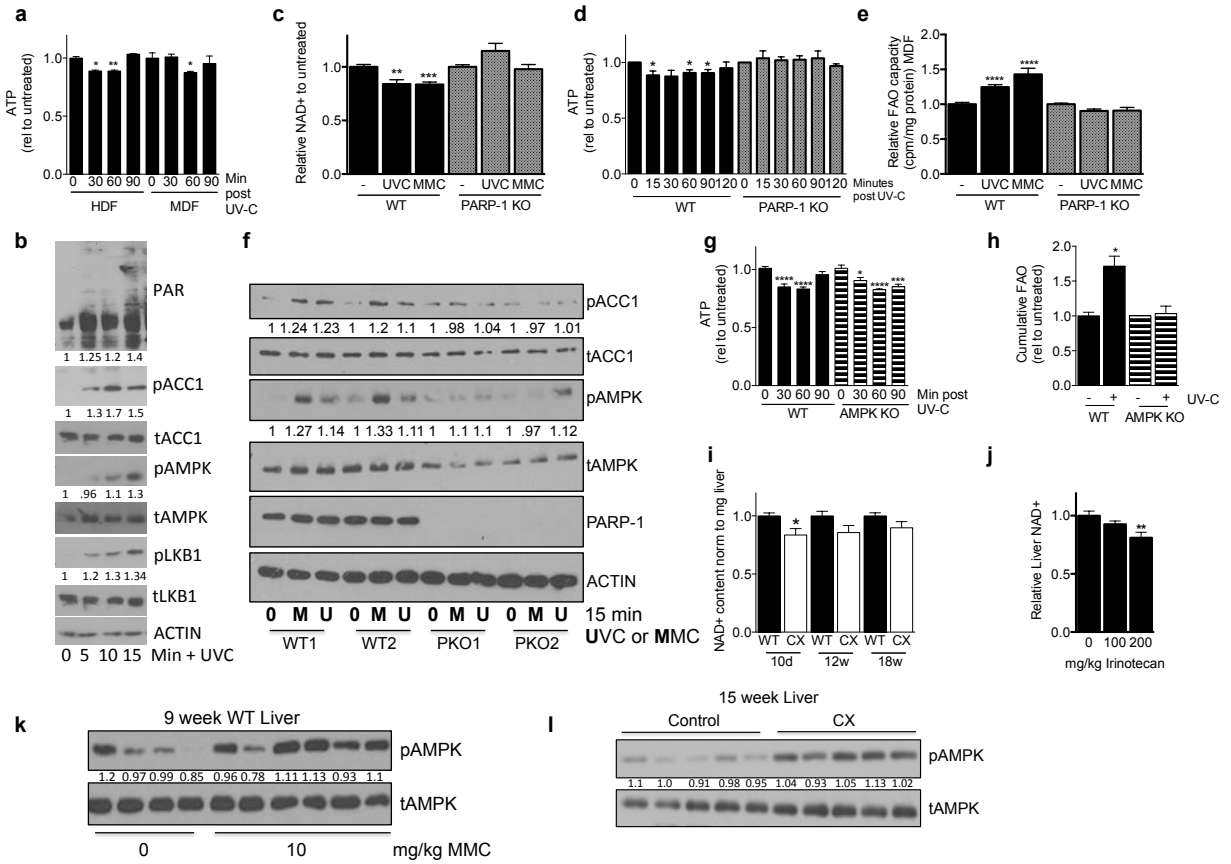

Figure 3.5: PARP-1-dependent NAD+/ATP depletion and AMPK activation link DNA damage to increased FAO. a. Steady-state ATP levels of WT HDFs/MDFs after UV-C exposure (24J/m² for HDF, 20J/m² for MDFs); 1way ANOVA with Dunnett's multiple comparisons test. **b.** Western blot of WT MDFs collected after 20J/m² UV-C at indicated times. **c.** Relative NAD+ content measured in WT and PARP-1 KO MDFs (n=4-8 lines/geno) 5 min after treatment with 20J/m² UV-C or 40μM MMC; Student's T test relative to untreated within genotype. **d.** Steady-state ATP levels of WT and PARP-1 KO MDFs (n=3-4 lines/geno) over a time course after 20J/m² UV-C; 1way ANOVA with Dunnett's multiple comparisons test**. e.** Relative cumulative FAO in WT and PARP-1 KO MDFs 10hrs after exposure to 20J/m² UV-C or 40μM MMC (n=3-4 lines/geno); Student's T test relative to untreated within genotype. **f.** Western blot of 2 WT and PARP-1 KO MDFs collected 15 minutes after exposure to +/-40μM MMC or 20J/m² UV-C. **g.** Steady-state ATP levels of WT and AMPKα1KO MDFs over time course +/- 20J/m² UV-C (n=3-4 lines/geno); 1way ANOVA with Dunnett's multiple comparisons test. **h.** Relative cumulative FAO in WT and AMPKα1KO MDFs 10hrs after exposure to 20J/m² UV-C (n=3 lines/geno); Student's T test relative to untreated within genotype. **i.** Relative NAD+ content in livers from WT and CX mice (n=3-4/geno) at the indicated ages; Student's T test between genotypes within age. **j.** Relative NAD+ content in WT livers from mice treated with 100 or 200mg/kg irinotecan or saline and harvested after 24 hours(n=4/grp); Student's T test relative to untreated. **k.** Western blot of livers from 8wk WT mice injected IP with MMC or saline and harvested after 24hrs (n=4/grp). **l.** Western blot of 15wk WT and CX livers. *p<0.05, **p<0.01, ***p<0.001, ****p<0.0001.

DNA lesions, likely by binding to a DNA damage repair intermediate common to these different lesions.

AMPK controls metabolic adaptations to ATP depletion including decreased energy expenditure, altered substrate utilization and increased energy efficiency production via OXPHOS[15]. Consistent with a role for AMPK in metabolic reprogramming in response to DNA damage, MDFs subject to genotoxic stress displayed a rapid, time-dependent increase in phosphorylated/activated AMPK (Figure 3.5b) in a PARP-1-dependent manner (Figure 3.5f, Supplemental Figure 3.5d).

To test the requirement for AMPK in metabolic reprogramming upon genotoxic stress, we used primary dermal fibroblasts isolated from WT and AMPKα1KO mice, which lacked detectable expression of the AMPK catalytic subunit (Supplemental Figure 3.5g). Steady-state ATP levels were reduced in both WT and AMPKα1 KO MDFs in response to 20J/m^2 UV-C or 40μM MMC, but returned to baseline within two hours only in WT cells (Figure 3.5g, Supplemental Figure 3.5h), consistent with the inability of AMPKα1 KO cells to maintain energy homeostasis. AMPKα1 KO MDFs also failed to activate FAO within 10hrs of various genotoxin treatments as in WT cells (Figure 3.5h, Supplemental Figure 3.5i, j) without consistent effects on cell viability (Supplemental Figure 3.5k-m).

To test the potential relevance of PARP-1-mediated NAD+ depletion and AMPK activation in metabolic reprogramming in response to acute or chronic DNA damage *in vivo,* we analyzed livers from CX vs. WT mice at different ages, and from WT mice 24 hours after treatment with a chemotherapeutic genotoxin, irinotecan or MMC. In all cases, we observed reduced steady-state NAD+ levels (Figure 3.5i, j) and increased phospho-AMPK (Figure 3.5k, l).

Increased FAO is a beneficial adaptive response to genotoxic stress

To determine if increased FAO is a beneficial or maladaptive response to genotoxic stress, we determined cellular hypersensitivity to genotoxic stress *in vitro* in the presence or absence of the FAO inhibitor, etomoxir. In addition to hypersensitivity to 20J/m² UV-C, CX MDFs displayed reduced viability upon etomoxir treatment in both mock and UV-C treated groups (Figure 3.6a), consistent with beneficial effects of increased FAO upon both chronic and acute genotoxic stress. A similar hypersensitivity to UV-C and MMC was observed in AMPKα1KO MDFs relative to WT cells (Figure 3.6b) at doses that increased FAO in WT cells.

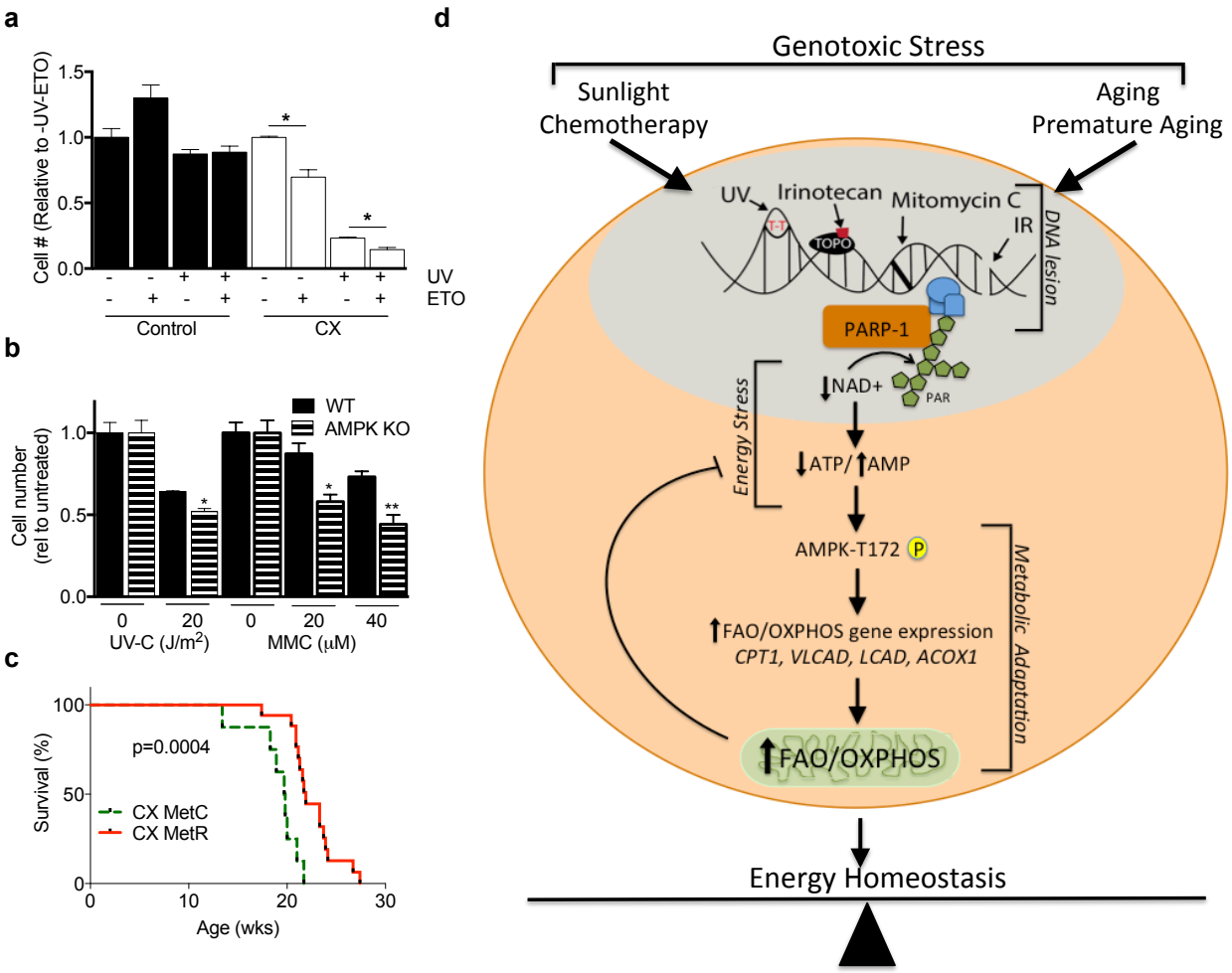

Figure 3.6: Increased FAO is a beneficial adaptive response to genotoxic stress. a. Relative MDF cell number 24hrs after 20Jm/² UV-C and/or 40μM Etomoxir treatment (n=2 independent MDF lines/genotype in duplicate); Student's T test between indicated groups. **b.** Relative cell number of WT and AMPKα1KO MDFs 24hrs after UV-C or MMC (n=2 MDF lines/genotype in duplicate); Student's T test vs. untreated within genotype and treatment. *p<0.05, **p<0.01. **c.** Kaplan Meier survival plots of CX mice on MetR (n=17) and MetC (n=8) diets; log-rank test p=0.0004. **d.** Model of relationship between DNA damage and maintenance of cellular and organismal energy homeostasis. Acute and chronic genotoxic stress activate PARP-1, depleting steady-state ATP and NAD+ levels, activating AMPK and increasing FAO/OXPHOS to restore energy homeostasis

Because blocking whole-body FAO *in vivo* is technically challenging and potentially toxic, we probed the *in vivo* role of FAO by testing the hypothesis that increased FAO is a beneficial adaptive response to chronic DNA damage in CX mice. To this end, we employed

a diet limited for the essential amino acid methionine, which, like DR, promotes a metabolic shift to FAO[26]. After 2wks of methionine restriction (MetR), RER was decreased in CX relative to control mice during the dark phase (Supplemental Figure 3.6a) without affecting activity (Supplemental Figure 3.6b) or food intake (Supplemental Figure 3.6c), consistent with an increase in FAO. Separate cohorts of CX and WT mice on MetR diets from ~6wks also displayed a reduction of body weight (Supplemental Figure 3.6d) and specifically of the percentage fat mass (Supplemental Figure 3.6e), with a reciprocal increased percentage lean mass (Supplemental Figure 3.6f) relative to within-genotype controls on the control (MetC) diet. Absolute fat and lean mass also displayed similar trends between genotypes (Supplemental Figure 3.6g, h). Despite total body fat at or below the level of detection by EchoMRI in the MetR CX group from ~15wks of age, MetR significantly increased median and maximum lifespan of CX mice by approximately 2 and 5 weeks, respectively (mean 19.8wks MetC vs. 21.9wks MetR; maximum 21.7wks MetC vs. 27.4wks MetR; log-rank test p=0.0004) (Figure 3.6c). Although the effects of MetR are pleiotropic and extend beyond increased FAO, we can clearly conclude that neither increased FAO nor loss of adiposity exacerbate CX symptoms *in vivo*; on the contrary, the pro-longevity effects of MetR in this short-lived DNA repair deficient model are consistent with increased FAO as a beneficial, adaptive response to chronic genotoxic stress *in vivo*.

Taken together, these data support a model in which an AMPK-dependent increase in FAO/OXPHOS is an adaptive response to DNA damage-mediated PARP-1 activation that promotes maintenance of NAD+/ATP energy homeostasis and cell survival (Figure 3.6 d).

DISCUSSION

Increased FAO/OXPHOS is a cell autonomous response to DNA damage

Here, we identified a novel link between DNA damage and adaptive cellular/organismal energy metabolism involving an increase in FAO in particular and OXPHOS in general. This connection was observed upon acute treatment of WT animals with a variety of genotoxins giving rise to distinct spectrums of DNA lesions, as well as in a model of chronic genotoxic stress induced by congenital DNA repair deficiency. It was also observed upon treatment of different types of primary cells, both human and mouse, with these different genotoxins. Based on these considerations, we conclude that this metabolic response represents a general, cell-autonomous response to acute and chronic genotoxic stress.

Why do cells increase OXPHOS upon DNA damage, and what is the molecular mechanism linking DNA damage to altered energy metabolism? Our data suggest that multiple different DNA lesions (or potentially common repair intermediates) activate

PARP-1, and that PARP-1 dependent activation of AMPK serves as the link between DNA damage and adaptive changes in NAD+ and ATP energy metabolism. Although PARP-1 activation is directly linked to NAD+ depletion, the definitive cause of ATP loss upon PARP-1 activation remains elusive. Several non-mutually exclusive possibilities have been described. NAD+ biosynthesis, either *de novo* or via the salvage pathway, is an ATP-dependent process, although its contribution to ATP depletion has recently been contested[12]. Free PAR that is rapidly removed from PARylated proteins can bind to and inhibit hexokinase-1, thus blocking ATP production via glycolysis[12]. Furthermore, free AMP released upon PAR degradation, for example by PARG, could compete with ADP for binding to the adenine nucleotide transporter and further diminish ATP production; consistent with such a possibility, methylnitronitrosoguanidine- (MNNG) induced PAR accumulation and PARG activation results in a time-dependent increase in AMP concentrations and a concomitant decrease in ATP in HeLa cells[27]. Regardless of the mechanism, each of these could affect ATP levels and thus promote AMPK activation, which contributes to energy homeostasis by blocking anabolic ATP consuming processes and increasing efficient energy production via mitochondrial OXPHOS, including increased FAO. Although AMPK was previously shown to be activated by phosphorylation upon DNA damage[28], this is the first demonstration of a role for energy stress itself in DNA damage-related AMPK activation.

It is important to note that while we observed an increase in FAO/OXPHOS as a common response to multiple genotoxic stressors in a variety of primary cells *in vitro*, as

well as in models of acute and chronic DNA damage *in vivo*, this response was not uniform across doses of all agents. For example, although 100 Gy IR activated FAO, 5-10 Gy failed to activate FAO despite inducing considerable DNA damage and activating cellular senescence[29]. This could be explained in part by the previous observation that PARP-1 activation upon IR only occurs above 20Gy[6]. Furthermore, low-dose IR (<0.1 Gy) activates a HIF1α-dependent beneficial adaptive response involving increased glucose uptake and glycolysis *in vivo*[30]. DNA damage can also block mitochondrial glutamine anaplerosis via a SIRT4-dependent mechanism, limiting cell proliferation, although whether this has any effect on the balance between oxidative and glycolytic energy metabolism is not known[31]. Future experiments will be required to determine if and how other forms of DNA damage or DNA repair deficiencies perturb energy metabolism.

Increased FAO/OXPHOS is a beneficial adaptive response to DNA damage

Changes in FAO can be driven either by metabolic inflexibility, for example upon insulin resistance[32] or other constitutive defects in glucose metabolic regulation[33], or as an adaptive response to environmental cues, ranging from differential substrate availability in response to normal feeding/fasting cycles[34] or overall restricted food intake[35]. Our data in the CX model, including improved HOMA-IR *in vivo* and increased oxygen consumption in cells independent of energy substrate *in vitro,* are inconsistent with metabolic inflexibility. However, two observations made in this study strongly suggest

that increased FAO/OXPHOS is a beneficial adaptive response to genotoxic stress. First, blocking AMPK or FAO reduced cell viability upon genotoxic stress; second, increasing FAO extended lifespan in a short-lived mouse model of chronic genotoxic stress.

Interestingly, previous studies on XPA as well as CX mice point to PARP-1 hyperactivation and NAD+ depletion driving mitochondrial dysfunction subsequent to defective SIRT1-dependent mitophagy[36]. Similarly, age-related accumulation of damaged mitochondria has been observed in the CSB mouse model[37]. While these findings may appear at odds with the beneficial metabolic adaptations involving overlapping molecular pathways as described here, they are not necessarily mutually exclusive. We suggest that adaptive changes in energy metabolism may precede constitutive defects in mitochondrial function, but are insufficient to prevent such defects because they fail to address the fundamental defect in DNA repair. Future studies will be required to address this and other possibilities. Nonetheless, our findings have important translational implications for conditions driven by chronic or acute DNA damage as discussed below.

For CS and related progeroid syndromes, these results have implications for our understanding of pleiotropic disease symptoms as well as potential treatment options. Loss of subcutaneous fat is often observed in segmental progeroid disorders such as CS, and has been generally interpreted as a maladaptive response to the rapid aging process. Reduced adiposity and increased FAO in CX mice is unlikely due to any underlying defect in glucose homeostasis, as the response to glucose challenge was normal, and HOMA-IR

improved, in CX mice. Instead, our data suggest that loss of adiposity is a constituent of the beneficial adaptive response driven in part by increased fat burning. Consistent with this interpretation, the MetR diet significantly extended longevity of short-lived CX mice despite a further reduction of adiposity. Interestingly, HFD feeding rescues age-dependent hearing loss in a CS model with mild symptoms relative to CX mice[38]. At face value, beneficial results from varying dietary interventions, HFD and MetR, appears paradoxical. However, under the working assumption that DNA damage-driven energy stress is a major contributor to both hearing loss and reduced lifespan, it then follows that improved maintenance of energy homeostasis either by energy supplementation (HFD) or increased energy efficiency (MetR) could both have beneficial effects. Future experiments will be required to determine if this metabolic adaption to genotoxic stress is present in CS patients and potentially other diseases and their corresponding mouse models with defects in genome maintenance[39]. However, existing data collectively suggest that strategies to improve energy homeostasis, either by pharmacologic (NAD+ supplementation, PARP-1 inhibitors) or dietary (DR, MetR, ketogenic diet) means, represent exciting new avenues toward mitigation of disease symptoms.

Finally, our findings here have implications for interventional approaches to protect against clinically relevant stressors involving genotoxic stress, ranging from radio/chemotherapeutics to oxidative stress associated with ischemia reperfusion injury. Dietary preconditioning is one such prophylactic approach involving short-term DR or fasting prior to chemotherapy or surgical stress that significantly reduces detrimental side

effects of these interventions[40-42]; however, the mechanisms of protection remain unclear. Our data suggest the possibility that activation of FAO/OXPHOS by diet prior to genotoxic stress may contribute to protection by preserving energy homeostasis and cell viability, and further that this mechanism may function more effectively when activated prior to the onset of DNA damage.

MATERIALS & METHODS

Mice All mouse experiments were performed with the approval of the Harvard Medical Area Institutional Animal Care and Use Committee. Mice carrying *Xpa* and/or *Csa* knockout alleles in a C57BL/6 background, AMPKα1 (Jackson 014141 bred with E2a-cre) knockout mice in a C57BL/6 background, and PARP-1 knockout mice (Jackson 002779) on a 129S background were maintained under standard laboratory conditions (temperature 20–24 °C, relative humidity 50–60%, 12hr light/12hr dark) and allowed free access to food (Research Diets, New Brunswick, NJ, USA, D12450B with 10% calories from fat, 18% from casein and 72% from carbohydrate) and water unless otherwise indicated as described previously [19]. Other diets utilized include facility chow pellets (PicoLab 5058, Purina, St. Louis, MO, USA), high fat diet (Research diets, 60% calories from fat), and a 1% agar-based diet using D12450BSpx (Research Diets, New Brunswick, NJ, USA) and individual crystalline amino acids (Ajinomoto, Tokyo, Japan) in proportions to those in casein. MetR diets contained 1.5g Met/kg food and lacking Cys [43] compared to MetC diet with the same amino acid composition except for 4.5g Met/kg food. Mitomycin C (MMC) and irinotecan

treatment of WT mice was performed by IP injection with 10mg/kg MMC (Cayman Chemical, Ann Arbor, MI, USA) or 100/200mg/kg irinotecan (Sigma, St. Louis, MO, USA) in saline.

Cell lines Mouse dermal fibroblasts (MDFs) were passaged in 20% FBS in DMEM + Penicillin/Streptomycin (P/S). Primary human dermal fibroblasts (HDFs) from CS-B patients were a gift from PJ Brooks (CSB: GM00739C, WT: RB4492); CS-A HDFs were purchased from Coriell Cell Repository (CSA: AG10213, WT: AG10215, AG12726; CSB: AG12724) and passaged in 15% FBS DMEM + P/S. All cell lines were incubated in 5% CO_2 and 3% O_2. MDFs were treated with 4 or 20J/m^2 UV-C and HDFs at 8 or 24J/m^2; both were treated with 4.6, 10 or 100Gy IR, 40μM MMC, 40μM Compound C, and 40μM Etomoxir (Sigma, St. Louis, MO, USA). Cell survival was measured by the relative change in cell number as measured on a hemocytometer following plating of an equal number of cells per line.

Seahorse Cellular oxygen consumption rate (OCR) and extracellular acidification rate (ECAR) were measured using the Seahorse Cell Metabolism Analyzer XF96. Cells were untreated or irradiated as described above and plated at a density of 18,000 cells/well in a 96-well plate. After 24hrs, media changed to unbuffered XF assay media with 11mM glucose, 2mM glutamine and pyruvate at pH7.4 and basal OCR and ECAR measured for blocks of 2 minutes mixing and 5 minutes measuring. For palmitate assays, cells were treated +/- UV-C, plated at 18,000 cells/96 well and 24hrs later media changed to KHB

buffer (0.5mM KCl, 11.1mM NaCl, 0.2mM $MgSO_4$, 0.14mM NaH_2PO_4, 500µM Carnitine pH7.4) with 2.5mM glucose. After 3 readings at 2 minutes mixing and 5 minutes measuring, either BSA or BSA-conjugated palmitate was injected at 200µM final concentration, and 5 more readings recorded. All plates were normalized to protein content as measured after Seahorse by BCA.

FAO in tissues Soleus and liver were removed, weighed and placed in KH buffer containing 25 mM $NaHCO_3$, 118mM NaCl, 4.7mM KCl, 1.2mM $MgSO_4$, 1.2mM NaH_2PO_4, 1.2mM $CaCl_2$ and glucose (2.5mM). The tissues were kept in buffer on ice until all dissections were completed. Each tissue then transferred to KH buffer plus 2% Fatty acid free BSA and 2.5mM glucose, with 2µCi ^{3}H palmitic acid (Perkin Elmer, Cambridge, MA, USA) and incubated at 37ºC for 1hr. The buffer was collected and hydrolyzed ^{3}H palmitic acid (as ^{3}H water) was extracted. 100µL of buffer was added to 100µL of 10% trichloroacetic acid (TCA), vortexed, incubated at RT for 15 min, spun at 16,000rpm for 10min, and the supernatant collected into a new tube. TCA (5%; 100µL) and 40µL BSA (10%) was added to the supernatant, vortexed, incubated at RT for 15min, spun at 16,000 rpm for 10min, and the supernatant transferred to a new tube. Chloroform:methanol (2:1, 750µL) was added to the supernatant, along with KCl: HCl (2 M each, 300µL), vortexed and spun at 16,000 rpm for 10min. The upper layer (~600µL) was collected into 5ml EcoLume, mixed, and counted in a liquid scintillation counter. After subtracting background cpm, the sample cpm was divided by the tissue weight to determine FAO capacity.

Body composition and metabolic parameters An EchoMRI device (Echo Medical System, Houston TX) was used to determine lean and fat mass. Insulin tolerance tests were performed after a 4-5 hour fast by injection of 0.5 units insulin/kg body weight into the peritoneum. Glucose tolerance tests were performed after 4-6hrs fast by injection of 2mg/kg glucose IP. Blood glucose was measured before and after from tail blood at indicated time-points using the OneTouch glucose monitoring system (Lifescan, Milpitas, CA). Serum insulin (Alpco, Salem, NH, USA), leptin (R&D Systems, Minneapolis, MN, USA) and adiponectin (R&D Systems, Minneapolis, MN, USA) were measured by ELISA. Serum triglycerides (Sigma, St. Louis, MO, USA) and beta-hydroxybutyrate (Pointe Scientific, Canton, MI, USA) were measured by enzymatic kits. HOMA-IR was determined using the mouse serum insulin ELISA kit (Alpco, Salem, NH, USA).

MDF isolation MDFs from preweaning WT, CSA, XPA, CX, and PARP-1 knockout mice and 20wk WT and AMPKα1KO mice were isolated as described previously [24]. Briefly, tail skin was removed and minced using a razor blade in the presence of 1.6mg/ml collagenase II in 20% FBS DMEM P/S and incubated overnight in one well of a 6-well plate at 37°C in a 5% CO_2 and 3% O_2 incubator. After ~16 hours, the minced tissue was pipetted up and down 50 times, passed through a 70μM filter, spun down and resuspended in the above media without collagenase. After a day or two, cells were trypsinized and replated in 2 wells of a 6 well plate. Cells were expanded after culture to 90% confluency and utilized between passage 3 and 5.

Indirect calorimetry Animals were placed in metabolic cages (Comprehensive Lab Animal Monitoring System (CLAMS), Columbus Instruments, Columbus, OH, USA) for 2 days and data collected from the beginning of the first light cycle. Oxygen consumption and carbon dioxide production were normalized to total lean mouse weight. The respiratory exchange ratio (RER) was determined by the ratio of CO_2 produced (VCO_2) over O_2 consumed (VO_2), both corrected for lean mass. RER values were averaged during the light and dark cycles on a per animal basis. Food consumed was corrected for lean mass of mouse over the 2 day period.

Pre-adipocyte isolation and FACS Subcutaneous fat pads from WT, CSA, XPA, and CX mice at 14-16wks of age were isolated, washed in PBS and minced. Tissue was digested for 60 minutes with 1mg/ml Collagenase II in HBSS with 7.5% FBS then passed through a 70μM filter and spun at 400g for 10 minutes. The floating adipocytes were removed and the pelleted stromal vascular fraction (SVF) was resuspended in erythrocyte lysis buffer (154mM NH_4Cl, 5.7mM K_2HPO_4, 0.1mM EDTA) for 10 minutes. The cells were then pelleted again, washed in PBS, and resuspended in 1:1 DMEM:Ham's F12 + P/S and 10% FBS. Media was changed every 2-3 days until 90% confluency was reached in about 7 days. For FACS analysis, erythrocytes were removed from SVF and 1 million cells were blocked with CD16/32 monoclonal antibody and stained for 30 minutes at $4^{o}C$ in the dark with F4/80 FITC and CD11b PeCy7 (at 1:100) all from BioLegend (San Diego, CA, USA).

Cells were washed and acquired immediately on a BD FACSCalibur (BD Biosciences, San Jose, CA, USA) and analyzed with FlowJo (Tree Star, Ashland, OR, USA).

Cellular fatty acid oxidation Cells were plated at 100,000 cells/well in a 12-well plate in DMEM + P/S with 20% FBS for MDFs and 15% for HDFs. For low-dose (4-8J/m^2) treatments, cells were exposed to UV-C and then returned to standard media for 24 hours. For high-dose UV-C (20-24J/m^2) and IR (4.6 – 100Gy) treatments, cells were either exposed, washed with PBS, then incubated for 30 minutes with DMEM 2% fatty acid-free BSA, and 5.5mM glucose or immediately given DMEM 2% fatty acid-free BSA, and 5.5mM glucose plus 40μM MMC for 30 minutes. Media was then changed to DMEM 2% fatty acid-free BSA, 5.5mM glucose (+/- genotoxin), and 2μCi ^{3}H palmitic acid and incubated for 2-10hrs. The media was then collected and hydrolyzed ^{3}H palmitic acid (as ^{3}H water) was extracted by the same technique as in tissues. After the media was removed, the cells were washed with 1x PBS and incubated for 10 minutes with 0.1M NaOH at room temperature, and total protein collected for quantitation using BSA standards. After subtracting the background cpm, the sample cpm was divided by the protein concentration for a measure of cumulative FAO.

ATP measurements MDFs and HDFs were plated at a density of 10,000 cells per 96 well. Sixteen hours later, cells were dosed with UV-C, IR or 40μM MMC. Up to 2 hrs later, 100μL fresh media was added and ATP measured upon the addition of 100μL Cell Titer Glo reagent (Promega, Madison, WI, USA). The plate was shaken for 2 minutes and then

incubated at room temperature in the dark for 10 minutes before determining the luminescence in plate reader (Biotek Synergy 2). ATP content was normalized to protein content as determined by BCA.

Mitochondrial content 18,000 MDFs were plated after 0 or 4J/m² UV-C treatment and placed at 37°C in a 5% CO_2, 3% O_2 incubator for 24hrs. Media was then changed to 80nM Mitoview Green (Biotium, Fremont, CA, USA) in standard MDF media for 30min. Cells were washed with PBS and read on a plate reader.

Quantitative real-time PCR Total RNA was isolated from cells and tissues using Qiazol (QIAGEN, Hilden, Germany) and cDNA synthesized by random hexamer priming with the Verso cDNA kit (Thermo, Cambridge, MA, USA). qRT-PCR was performed using Taq-Pro DNA polymerase (Denville, Holliston, MA, USA) and SYBR green dye (Lonza, Portsmouth, NH, USA). Fold changes were calculated by the delta delta C_t method using β-actin as a standard, and normalized to the experimental WT control. Primer sequences are as follows:

β-actin F:AGCTTCTTTGCAGCTCCTTCGTTG R:TTCTGACCCATTCCCACCATCACA
Cd36 F: GAGCAACTGGTGGATGGTTT R: GCAGAATCAAGGGAGAGCAC
Cpt1β F: TTGCCCTACAGCTGGCTCATTTCC R: GCACCCAGATGATTGGGATACTGT
Lcad F:TCTTTTCCTCGGAGCATGACA R:GACCTCTCTACTCACTTCTCCAG
Vlcad F:CTACTGTGCTTCAGGGACACC R:CAAAGGACTTCGATTCTGCCC
Pgc1α F: AGCCGTGACCACTGACAACGAG R: GCTGCATGGTTCTGAGTGCTAAG
Leptin F: TGAAGCCCAGGAATGAAGTC R: TCAAGACCATTGTCACCAGG
Pparα F: TGTTTGTGGCTGCTATAATTTGC R: GCAACTTCTCAATGTAGCCTATGTTT
Acox1 F: CCTGATTCAGCAAGGTAGGG R: TCGCAGACCCTGAAGAAATC

Histology Perigonadal white adipose tissue (WAT) depots were isolated, washed in PBS, and fixed in Bouin's solution for 24 hours. Paraffin embedded tissue was then sectioned and stained with hematoxylin and eosin for overall morphology or immunostained as previously described using the following primary antibodies: rabbit anti-mouse UCP-1 (Abcam, Cambridge MA, USA) at a dilution of 1:500 or rat anti-mouse F4/80 diluted 1:200 (eBioscience, San Diego, CA, USA). Controls were performed simultaneously.

Westerns Tissues and cells were homogenized with NP-40 buffer containing protease and phosphatase inhibitors and DTT. Samples were normalized for protein content, boiled with SDS loading buffer separated by SDS-PAGE, transferred to PVDF membrane (Whatman, Maidstone, UK) and blotted for phospho-ACC1 (S79, #3661), phospho-AMPK (T172, #2535), ACC1 (#4190), AMPK (#2532), phospho-LKB1 (#3482), LKB1 (#3050), Parp-1 (#9542), and Actin (#4967) from Cell Signaling Technologies (Danvers, MA, USA) and PAR (51-811HKC) from BD Biosciences (San Jose, CA, USA).

Lipid Profiling Sera lipidomics profiling was conducted using liquid chromatography separations coupled with mass spectrometry based analysis on a Thermo Exactive Mass Spectrometer. Detailed methods have been described[44,45].

NAD+ determination MDFs were plated at 500,000 per 10cm plate. The following day media was removed, cells treated +/- 20J/m^2 UV-C, and then media returned. Five

minutes later, cells were washed with PBS, trypsinized and NAD+ determined using the EnzyChrom NAD+/NADH Assay kit (E2ND-100, Bio-Assay systems, Hayward, CA, USA).

Immunofluorescence MDFs were plated on 18mm circular coverslips at 350,000 cells per well in a 12 well plate. Cells were treated with 40μM MMC or 20J/m² UV-C, incubated for the indicated amount of time, rinsed twice with PBS and permeabilized 5 minutes at room temperature with 0.5% Triton in PBS. Cells were then fixed in 3.7% formaldehyde in PBS for 10 minutes and washed twice in PBS. Cells were then incubated for 10 minutes in 0.5% NP-40 in PBS, washed in PBS, then blocked in PBS+0.5% BSA (PBB) for 20 minutes. Primary antibody (1:200, anti-PAR clone 10H, Enzo Life Sciences, Farmingdale, NY, USA) was incubated in PBB overnight at 4°C. Cells were then washed 3x5 minutes in PBB, incubated 1hr at 37°C in secondary (goat anti-mouse 1:1000 Alexa Fluor Thermo Fisher, Cambridge, MA, USA) in PBB. Cells were washed 3x5 minutes in PBB, rinsed in PBS, and mounted with DAPI on slides. Cells were imaged using a Zeiss LSM 700 confocal microscope, acquired using Zen Black software and analyzed using Fiji software.

Statistics The indicated statistical analyses were performed either in Excel or in GraphPad Prism.

ACKNOWLEDGEMENTS

We thank David Sinclair and Zhi-Min Yuan for insightful discussions; Gokhan Hotamisligil for use of metabolic facilities; PJ Brooks for sharing cell lines; Casimiro Gerarduzzi for assistance with IR procedures; and Brien Hopkins for graphical assistance.

Funding

This work was funded in part by grants from the Luke O'Brien Foundation, NIA AG-036712 and NIDDK DK-090629 to JRM, P30-DK040561 to BSK, Swiss National Science Foundation P1LAP3_158895 to AL, NIH training grants (Interdisciplinary Genes and Environment T32ES016645 and Radiation Biology T32CA009078), and the National Science Foundation Graduate Research Fellowship NSF-DGE1144152 to LEB.

Supplementary Information

Supplementary information accompanies this paper and consists of 6 supplementary figures.

Competing Financial Interests

BSK is the inventor on general metabolomics-related IP that has been licensed to Metabolon via Weill Medical College of Cornell University and for which he receives royalty payments via Weill Medical College of Cornell University. He also consults for and has a small equity in the company. Metabolon offers biochemical profiling services and is developing molecular diagnostic assays detecting and monitoring disease. Metabolon has

no rights or proprietary access to the research results presented and/or new IP generated under these grants/studies. BSK's interests were reviewed by the Brigham and Women's Hospital and Partners Healthcare in accordance with their institutional policy. Accordingly, upon review, the institution determined that BSK's financial interest in Metabolon does not create a significant financial conflict of interest (FCOI) with this research. The addition of this statement where appropriate was explicitly requested and approved by BWH.

Supplemental Figures

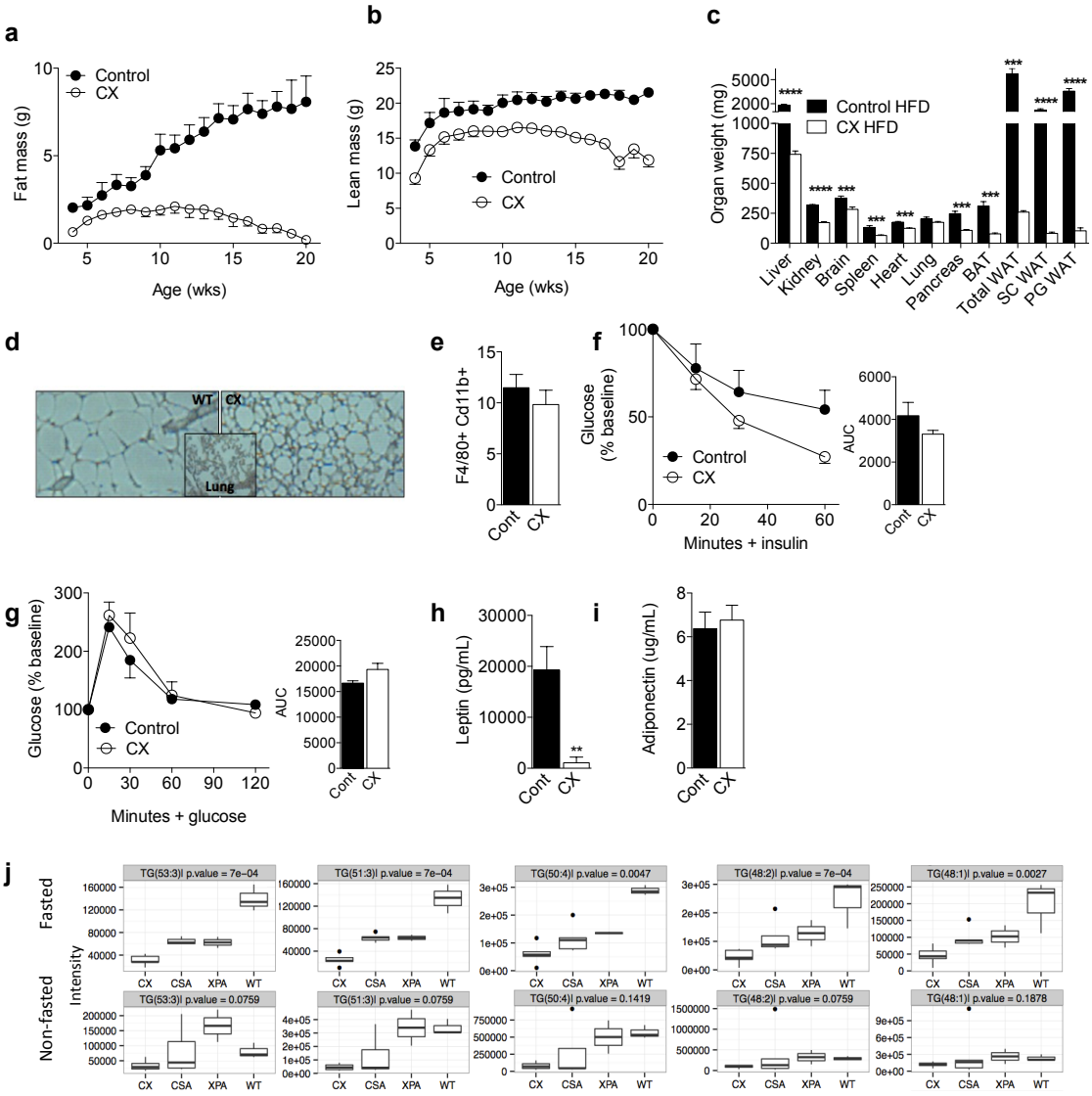

Supplemental Figure 3.1: Perturbations in energy metabolism indicative of improved metabolic fitness in CX mice. Absolute fat **(a)** and lean **(b)** mass of animals described in Figure 3.1a-c, n=14-16/group. **c.** Organ weights as described in Figure 3.1d expressed in mg absolute weight, n=4/group; Student's T test. **d.** F4/80 staining of paraffin-embedded white adipose tissue from Control (WT) and CX mice. Inset: lung tissue with F4/80 positive resident macrophages as a positive control. **e.** FACS analysis of F4/80+CD11b+ macrophages expresses as a percent of total cells in stromal vascular fraction from subcutaneous WAT from Control and CX mice as indicated, n=5-6/genotype, Student's T test. Insulin tolerance test **(f)** and glucose tolerance test **(g)** of 14wk Control and CX mice (n=3-4/group). Right: Area under the curve (AUC) of the indicated groups. **h.** Serum leptin levels in 12-16wk old Control and CX mice n=4/group; Student's T test. **i.** Serum adiponectin levels in 12-16wk old Control and CX mice n=5/group. **j.** Relative intensity of fed and fasted serum triglycerides as described in Figure 3.1i separated by genotype; 2-way ANOVA with Bonferroni post-test. **p<0.01, ***p<0.001, ****p<0.0001.

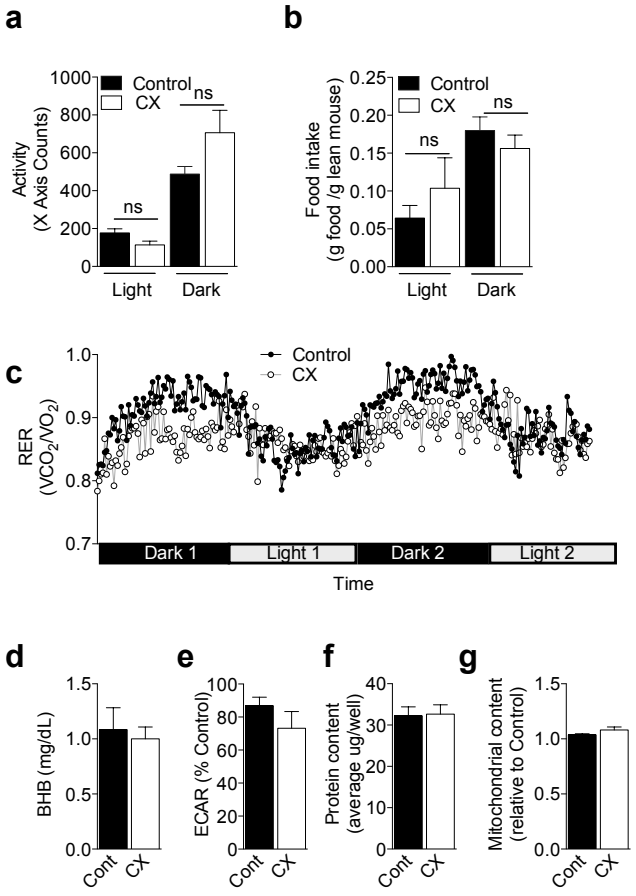

Supplemental Figure 3.2: Increased fatty acid oxidation in CX mice *in vivo* and in cells *in vitro*. Horizontal activity **(a)** and food consumption **(b)** in metabolic cages as described in Figure 3.2a-c, n=12/group. **c.** Respiratory exchange ratio in metabolic cages over 2 days in a representative experiment with 4 animals per genotype as described in Figure 3.2c. **d.** Concentration of beta-hydroxybutyrate in fasted serum from 12-16wk old control and CX mice, n=12/group. **e.** Extracellular acidification rate (ECAR) expressed as a percentage of Control MDFs from Figure 3.2g, n=3/genotype. **f.** Protein content by BCA of cells described in Figure 3.2g after Seahorse analysis, n=3/genotype. **g.** Relative mitochondrial content by Mitoview Green of cells described in Figure 3.2g, n=3/genotype.

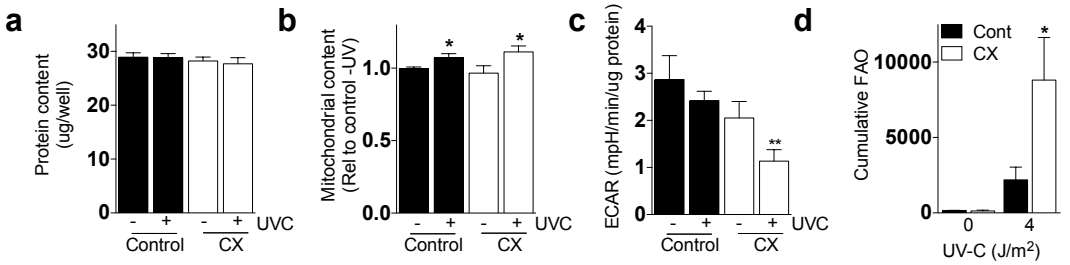

Supplemental Figure 3.3: Increased FAO is a cell-autonomous beneficial, adaptive response triggered by genotoxic stress in CX cells. a. Protein content of cells described in Figure 3.3a immediately after Seahorse analysis, n=3 independent MDF lines/genotype. **b.** Relative mitochondrial content 24hrs after 0 or 4J/m² UV-C; Student's T test within genotype between treatment groups, n=5/group. **c.** Extracellular acidification rate (ECAR) of cells described in Figure 3.3b expressed as a percentage of Control untreated cells; 1way ANOVA between genotypes within treatment group with Dunnett's post test, n=3 lines/genotype. **d.** Cultured pre-adipocytes from subcutaneous WAT SVF of control and CX mice and treated as in 3c; Student's T test within genotype between +/- UV treatment, n=3 lines/genotype. *p<0.05, **p<0.01.

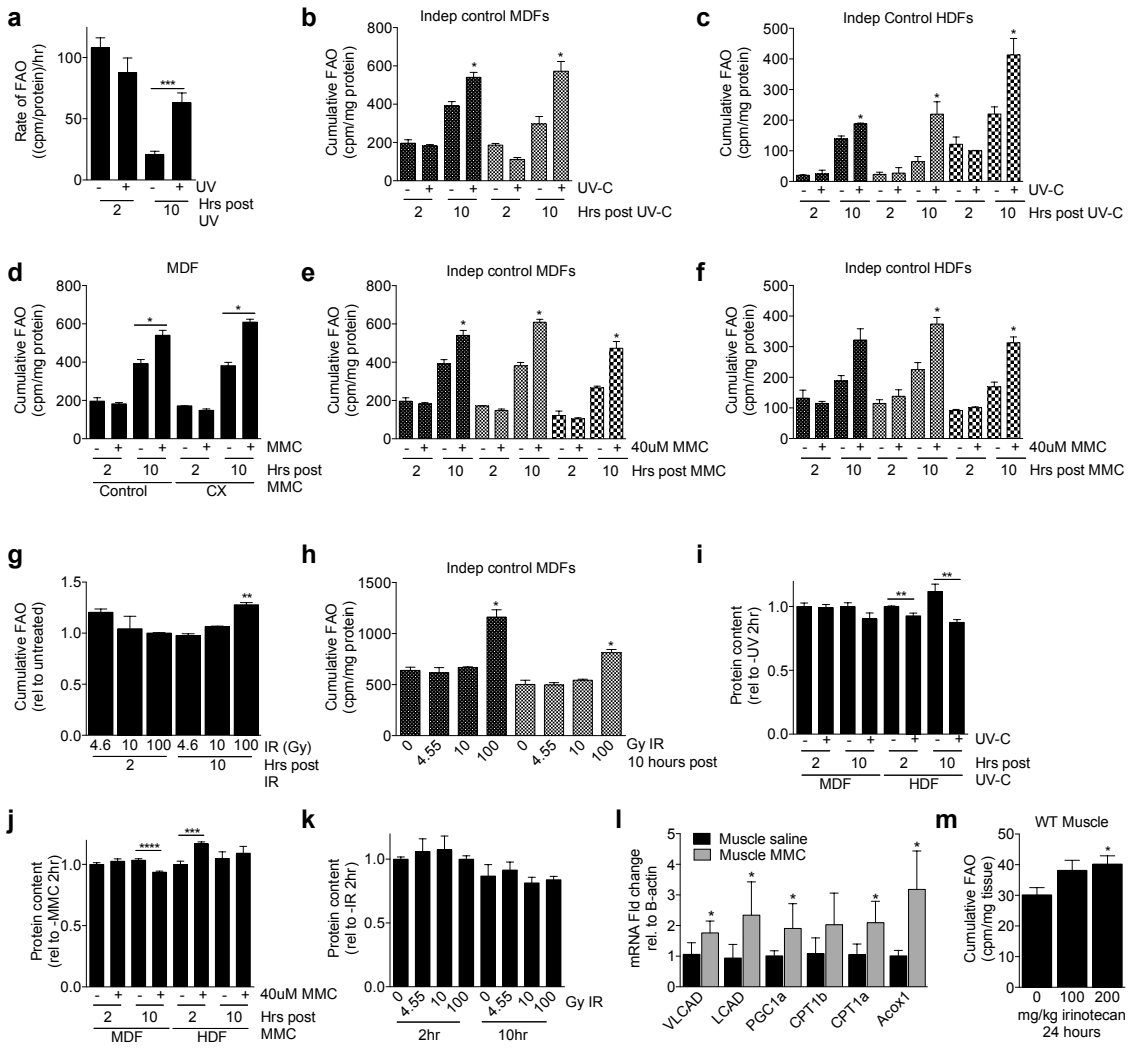

Supplemental Figure 3.4: Increased FAO is a general response to acute genotoxic stress. **a.** The rate of FAO of tritiated palmitate in WT MDFs between 2 and 10 hours after 20J/m² UV-C as described in Figure 3.4a; Student's T test. **b.** Two independent control MDF lines exposed to 20J/m² UV-C as described in Figure 3.4b; Student's T test between treatment groups within the indicated time point. **c.** Three independent WT HDF lines exposed to 24J/m² UV-C as described in Figure 3.4b, Student's T test between treatment groups within the indicated time point. **d.** Cumulative FAO of tritiated palmitate over the indicated time period of representative Control or CX MDFs exposed to 40μM MMC; Student's T test between treatment groups within time point. **e.** Three independent control MDF lines exposed to 40μM MMC as described in Figure 3.4d, Student's T test between treatment groups within the indicated time point. **f.** Three independent WT HDF lines exposed to 40μM MMC as described in Figure 3.4d, Student's T test between treatment groups within the indicated time point. **g.** Cumulative FAO of 2 independent MDF lines exposed to 4.6, 10 or 100Gy IR expressed relative to mock treated cells; Student's T test between indicted group and untreated. **h.** Two independent control MDF lines exposed to 0, 4.6, 10 or 100Gy IR as described in Supplemental Figure 3.4g. **i**. Relative protein content of cells described in Figure

3.4a,b and Supplemental Figure 3.4a-c, n=3/group, Student's T test. **j.** Relative protein content of cells described in Figure 3.4d and Supplemental Figure 3.4e,f, n=3/group, Student's T test. **k.** Relative protein content of cells described in Supplemental Figure 3.4g,h, n=3/group; Student's T test. **l.** Gene expression of FAO-related genes in muscle from 8wk WT mice injected IP with 10mg/kg MMC or saline and harvested after 24hrs as in Figure 3.4e-f, n=4/group; Student's T test. **m.** FAO capacity of muscle from 8wk WT mice injected IP with 100 or 200mg/kg irinotecan or saline and harvested after 24hrs as in Figure 3.4g, n=4/group; Student's T test. *p<0.05, **p<0.01, ***p<0.001, ****p<0.0001.

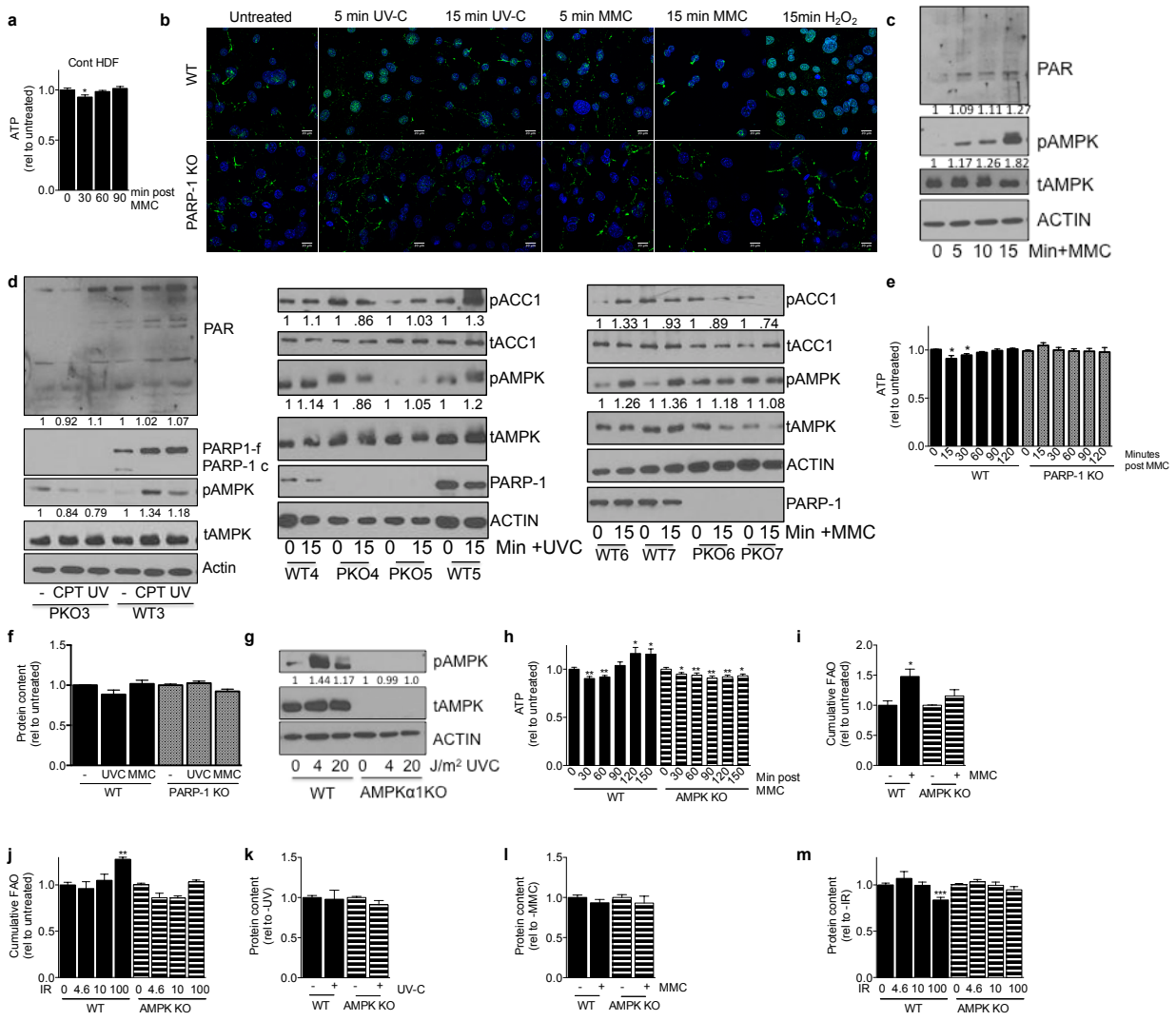

Supplemental Figure 3.5: PARP-1-dependent NAD+/ATP depletion and AMPK activation link DNA damage to increased FAO. **a.** Steady-state ATP levels of WT HDFs treated with 40μM MMC for the indicated time, n=4 lines/genotype; 1way ANOVA with Dunnett's multiple comparisons test. **b.** Immunofluorescence for PAR/DAPI in WT and PARP-1 KO MDFs 5 and 15 minutes after exposure to 20J/m^2 UV-C, 40μM MMC, or 100μM H_2O_2. **c.** Western blot of WT MDFs 0, 5, 10, and 15 minutes after exposure to 40μM MMC. **d.** Western blots of five independent WT and PARP-1 KO MDF lines after 15-minute exposure to 100μM Camptothecin, 40μM MMC, or 20J/m^2 UV-C as indicated. **e.** Steady-state ATP levels of WT and PARP-1 KO MDFs over a time course after exposure to 40μM MMC, n=3 lines/genotype; 1way ANOVA with Dunnett's multiple comparisons test. **f.** Relative protein content of WT and PARP-1 KO MDFs after exposures described in Figure 3.5e, n=3-4 lines/genotype. **g.** Western blot of WT and AMPKα1KO MDFs exposed to 1hr of 4 or 20J/m^2 UV-C. **h.** Steady-state ATP levels of WT and AMPKα1KO MDFs over a time course after exposure to 40μM MMC, n=3-4 lines/genotype; 1way ANOVA with Dunnett's multiple comparisons test. **i.** Relative cumulative FAO of tritiated palmitate in WT and AMPKα1KO MDFs 10hrs after exposure to 40μM MMC, n=2 lines/genotype in duplicate; Student's T test relative to untreated within genotype. **j.** Relative cumulative FAO of tritiated palmitate in WT and AMPKα1KO MDFs 10hrs after exposure to 4.6, 10 and 100Gy ionizing radiation, n=2-4 lines/genotype in duplicate; Student's T test relative to untreated within genotype. **k-m.** Relative protein content of WT and AMPKα1KO MDFs after exposures

described in Figure 3.5h, and Supplemental Figures 3.5i, and 3.5j, respectively, n=2-4/group, Student's T test, *p<0.05, **p<0.01, ***p<0.001.

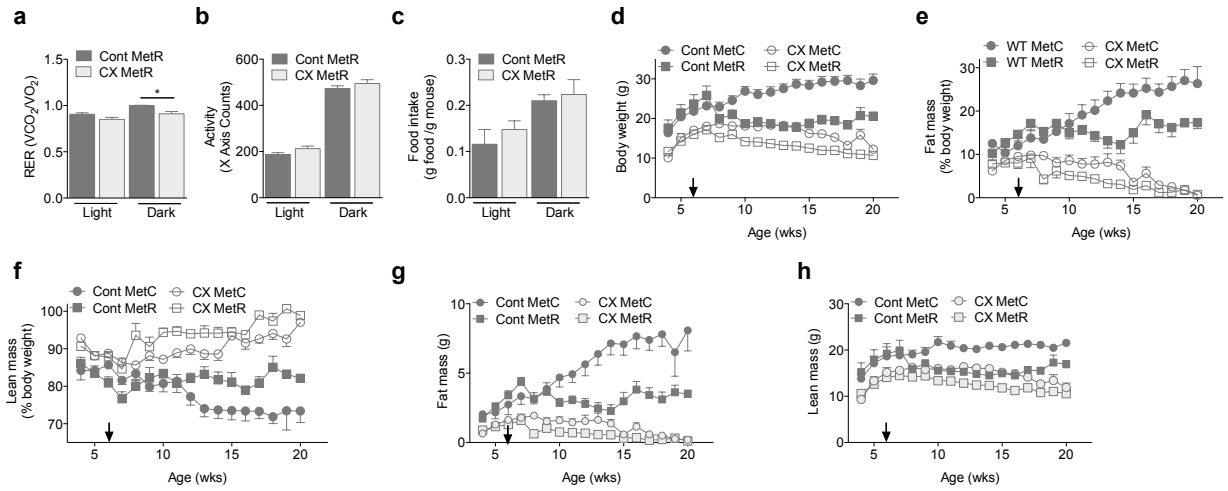

Supplemental Figure 3.6: Detrimental and beneficial adaptations of modulating fatty acid oxidation in response to genotoxic stress. RER **(a)**, horizontal activity **(b)**, and food consumption **(c)** of 10-14wk Control and CX mice fed a MetR diet for 2wks prior to indirect calorimetry, n=4/group; Student's T test. Body weight, **(d)** Percent fat **(e)** and lean **(f),** absolute fat **(g)** and lean **(h)** mass of Control and CX mice on MetC or MetR diets for 16wks, n=8-17/group, also shown in Figure 3.6c. *p<0.05.

REFERENCES

1. Marczuk-Krynicka D, Hryniewiecki T, Piatek J, Paluszak J. The effect of brief food withdrawal on the level of free radicals and other parameters of oxidative status in the liver. *Med Sci Monit.* 2003;9(3):BR131-135.

2. Taguchi K, Motohashi H, Yamamoto M. Molecular mechanisms of the Keap1–Nrf2 pathway in stress response and cancer evolution. *Genes Cells.* 2011;16(2):123-140.

3. Bhatt AN, Chauhan A, Khanna S, et al. Transient elevation of glycolysis confers radio-resistance by facilitating DNA repair in cells. *BMC Cancer.* 2015;15:335.

4. Fox CJ, Hammerman PS, Thompson CB. Fuel feeds function: energy metabolism and the T-cell response. *Nat Rev Immunol.* 2005;5(11):844-852.

5. Jacobson EL, Antol KM, Juarez-Salinas H, Jacobson MK. Poly(ADP-ribose) metabolism in ultraviolet irradiated human fibroblasts. *The Journal of biological chemistry.* 1983;258(1):103-107.

6. Oleinick NL, Evans HH. Poly(ADP-ribose) and the response of cells to ionizing radiation. *Radiat Res.* 1985;101(1):29-46.

7. Bowman KJ, Newell DR, Calvert AH, Curtin NJ. Differential effects of the poly (ADP-ribose) polymerase (PARP) inhibitor NU1025 on topoisomerase I and II inhibitor cytotoxicity in L1210 cells in vitro. *Br J Cancer.* 2001;84(1):106-112.

8. Whish WJ, Davies MI, Shall S. Stimulation of poly(ADP-ribose) polymerase activity by the anti-tumour antibiotic, streptozotocin. *Biochem Biophys Res Commun.* 1975;65(2):722-730.

9. Berger NA. Poly(ADP-ribose) in the cellular response to DNA damage. *Radiation research.* 1985;101(1):4-15.

10. Alano CC, Garnier P, Ying W, Higashi Y, Kauppinen TM, Swanson RA. NAD+ depletion is necessary and sufficient for poly(ADP-ribose) polymerase-1-mediated neuronal death. *The Journal of neuroscience : the official journal of the Society for Neuroscience.* 2010;30(8):2967-2978.

11. Sims JL, Berger SJ, Berger NA. Poly(ADP-ribose) Polymerase inhibitors preserve nicotinamide adenine dinucleotide and adenosine 5'-triphosphate pools in DNA-damaged cells: mechanism of stimulation of unscheduled DNA synthesis. *Biochemistry.* 1983;22(22):5188-5194.

12. Fouquerel E, Goellner EM, Yu Z, et al. ARTD1/PARP1 negatively regulates glycolysis by inhibiting hexokinase 1 independent of NAD+ depletion. *Cell Rep.* 2014;8(6):1819-1831.

13. Bungard D, Fuerth BJ, Zeng PY, et al. Signaling kinase AMPK activates stress-promoted transcription via histone H2B phosphorylation. *Science.* 2010;329(5996):1201-1205.

14. Kim SY, Jeong S, Jung E, et al. AMP-activated protein kinase-alpha1 as an activating kinase of TGF-beta-activated kinase 1 has a key role in inflammatory signals. *Cell death & disease.* 2012;3:e357.

15. Hardie DG, Ross FA, Hawley SA. AMPK: a nutrient and energy sensor that maintains energy homeostasis. *Nat Rev Mol Cell Biol.* 2012;13(4):251-262.

16. Budanov AV, Karin M. p53 target genes sestrin1 and sestrin2 connect genotoxic stress and mTOR signaling. *Cell.* 2008;134(3):451-460.

17. Natale V. A comprehensive description of the severity groups in Cockayne syndrome. *Am J Med Genet A.* 2011;155A(5):1081-1095.

18. Sykora P, Wilson DM, 3rd, Bohr VA. Repair of persistent strand breaks in the mitochondrial genome. *Mech Ageing Dev.* 2012;133(4):169-175.

19. Brace LE, Vose SC, Vargas DF, Zhao S, Wang XP, Mitchell JR. Lifespan extension by dietary intervention in a mouse model of Cockayne syndrome uncouples early postnatal development from segmental progeria. *Aging Cell.* 2013;12(6):1144-1147.

20. van de Ven M, Andressoo JO, Holcomb VB, et al. Extended longevity mechanisms in short-lived progeroid mice: identification of a preservative stress response associated with successful aging. *Mech Ageing Dev.* 2007;128(1):58-63.

21. Guo Y, Lu Y, Houle D, et al. Pancreatic islet-specific expression of an insulin-like growth factor-I transgene compensates islet cell growth in growth hormone receptor gene-deficient mice. *Endocrinology.* 2005;146(6):2602-2609.

22. Bruss MD, Khambatta CF, Ruby MA, Aggarwal I, Hellerstein MK. Calorie restriction increases fatty acid synthesis and whole body fat oxidation rates. *Am J Physiol Endocrinol Metab.* 2010;298(1):E108-116.

23. Susa D, Mitchell JR, Verweij M, et al. Congenital DNA repair deficiency results in protection against renal ischemia reperfusion injury in mice. *Aging Cell.* 2009;8(2):192-200.

24. van de Ven M, Andressoo JO, Holcomb VB, et al. Adaptive stress response in segmental progeria resembles long-lived dwarfism and calorie restriction in mice. *PLoS Genet.* 2006;2(12):e192.

25. Wang Y, Chakravarty P, Ranes M, et al. Dysregulation of gene expression as a cause of Cockayne syndrome neurological disease. *Proc Natl Acad Sci U S A.* 2014;111:14454-14459.

26. Hasek BE, Stewart LK, Henagan TM, et al. Dietary methionine restriction enhances metabolic flexibility and increases uncoupled respiration in both fed and fasted states. *Am J Physiol Regul Integr Comp Physiol.* 2010;299(3):R728-739.

27. Formentini L, Macchiarulo A, Cipriani G, et al. Poly(ADP-ribose) catabolism triggers AMP-dependent mitochondrial energy failure. *J Biol Chem.* 2009;284(26):17668-17676.

28. Bungard D, Fuerth BJ, Zeng PY, et al. Signaling kinase AMPK activates stress-promoted transcription via histone H2B phosphorylation. *Science.* 2010;329:1201-1205.

29. Rodier F, Coppé JP, Patil CK, et al. Persistent DNA damage signalling triggers senescence-associated inflammatory cytokine secretion. *Nat Cell Biol.* 2009;11(8):973-979.

30. Lall R, Ganapathy S, Yang M, et al. Low-dose radiation exposure induces a HIF-1-mediated adaptive and protective metabolic response. *Cell Death Differ.* 2014;21:836-844.

31. Jeong SM, Xiao C, Finley LW, et al. SIRT4 has tumor-suppressive activity and regulates the cellular metabolic response to DNA damage by inhibiting mitochondrial glutamine metabolism. *Cancer Cell.* 2013;23(4):450-463.

32. Hancock CR, Han DH, Chen M, et al. High-fat diets cause insulin resistance despite an increase in muscle mitochondria. *Proc Natl Acad Sci U S A.* 2008;105(22):7815-7820.

33. Zhang S, Hulver MW, McMillan RP, Cline MA, Gilbert ER. The pivotal role of pyruvate dehydrogenase kinases in metabolic flexibility. *Nutr Metab (Lond).* 2014;11(1):10.

34. Hue L, Taegtmeyer H. The Randle cycle revisited: a new head for an old hat. *American journal of physiology Endocrinology and metabolism.* 2009;297(3):E578-591.

35. Cao SX, Dhahbi JM, Mote PL, Spindler SR. Genomic profiling of short- and long-term caloric restriction effects in the liver of aging mice. *Proc Natl Acad Sci U S A.* 2001;98(19):10630-10635.

36. Fang EF, Scheibye-Knudsen M, Brace LE, et al. Defective mitophagy in XPA via PARP-1 hyperactivation and NAD(+)/SIRT1 reduction. *Cell.* 2014;157:882-896.

37. Scheibye-Knudsen M, Ramamoorthy M, Sykora P, et al. Cockayne syndrome group B protein prevents the accumulation of damaged mitochondria by promoting mitochondrial autophagy. *J Exp Med.* 2012;209:855-869.

38. Scheibye-Knudsen M, Mitchell SJ, Fang EF, et al. A High-Fat Diet and NAD(+) Activate Sirt1 to Rescue Premature Aging in Cockayne Syndrome. *Cell Metab.* 2014;20:840-855.

39. Hasty P, Campisi J, Hoeijmakers J, van Steeg H, Vijg J. Aging and genome maintenance: lessons from the mouse? *Science.* 2003;299(5611):1355-1359.

40. Lee C, Raffaghello L, Brandhorst S, et al. Fasting cycles retard growth of tumors and sensitize a range of cancer cell types to chemotherapy. *Science translational medicine.* 2012;4(124):124ra127.

41. Peng W, Robertson L, Gallinetti J, et al. Surgical stress resistance induced by single amino acid deprivation requires Gcn2 in mice. *Sci Transl Med.* 2012;4(118):118ra111.

42. Mitchell JR, Verweij M, Brand K, et al. Short-term dietary restriction and fasting precondition against ischemia reperfusion injury in mice. *Aging Cell.* 2010;9(1):40-53.

43. Miller RA, Buehner G, Chang Y, Harper JM, Sigler R, Smith-Wheelock M. Methionine-deficient diet extends mouse lifespan, slows immune and lens aging, alters glucose, T4, IGF-I and insulin levels, and increases hepatocyte MIF levels and stress resistance. *Aging Cell.* 2005;4(3):119-125.

44. Bird SS, Marur VR, Sniatynski MJ, Greenberg HK, Kristal BS. Serum lipidomics profiling using LC-MS and high-energy collisional dissociation fragmentation: focus on triglyceride detection and characterization. *Analytical chemistry.* 2011;83(17):6648-6657.

45. Bird SS, Marur VR, Sniatynski MJ, Greenberg HK, Kristal BS. Lipidomics profiling by high-resolution LC-MS and high-energy collisional dissociation fragmentation: focus on characterization of mitochondrial cardiolipins and monolysocardiolipins. *Analytical chemistry.* 2011;83(3):940-949.

CHAPTER 4

Neurodegeneration in Cockayne syndrome model mice: mechanisms of myelin loss and potential connection to increased fatty acid oxidation

Lear E. Brace[1], Sarah C. Vose[1], J. Humberto Trevino Villarreal[1], Sandro Santagata[2], Lior Mayo[3], Maria Ericcson[4], Roderick T. Bronson[5], Bruce S. Kristal[6], James R. Mitchell.[1]

[1] Department of Genetics and Complex Diseases, Harvard T.H. Chan School of Public Health, 655 Huntington Ave, Boston, MA 02115, USA
[2] Department of Pathology, Harvard Medical School/BWH/DFCI, 75 Francis St, Boston, MA, 02115, USA
[3] Department of Neurology, Brigham and Women's Hospital, 77 Avenue Louis Pasteur, Boston, MA, USA
[4] Cell Biology Electron Microscopy Facility, 220 Longwood Ave, Boston, MA, USA
[5] Rodent Histopathology Laboratory, Harvard Medical School, 77 Avenue Louis Pasteur, Boston, MA 02115, USA
[6] Departments of Neurosurgery, Harvard Medical School, Brigham and Women's Hospital, 221 Longwood Avenue, Boston, MA 02115, USA

Author contributions

L.E.B. S.C.V and J.R.M. designed experiments. L.E.B., S.C.V., and M.E. performed the experiments. L.E.B., S.C.V., J.H.T.dV., S.S., L.M., R.T.B, B.S.K., and J.R.M. analyzed the data.

ABSTRACT

Cockayne syndrome (CS) is a rare, segmental progeroid disorder associated with mutations in either of two genes involved in transcription-coupled DNA repair, *CSA* or *CSB*. CS is characterized by failure to thrive, cerebellar ataxia, and progressive neurodegeneration associated with patchy demyelination, loss of hearing and peripheral neuropathy. We utilized the CX mouse model of severe CS with loss of CSA and the global-genome repair protein XPA, which phenocopies critical neurodegenerative symptoms observed in human patients including cerebellar ataxia, progressive loss of peripheral motor function and loss of myelin. Characterization of the central and peripheral nervous system of CX mice revealed astrocyte activation, demyelination, and neural cell dysfunction without hypersensitivity to oxidative stress. Metabolic analysis of central and peripheral nerves revealed an increase in fatty acid oxidation capacity in CX brain and sciatic nerve subsequent to NAD+ loss and an increase in PARP-1 regulated genes. Astrocytes are known to utilize fatty acids alternatively to glucose as fuel, displayed a significantly higher basal oxygen consumption rate and a significant increase in expression of genes controlling catabolism of abundant lipid species in myelin. These results confirm that CX mice recapitulate key neurodegenerative phenotypes of CS including demyelination, which is associated with increased astrocyte fatty acid oxidation capacity.

INTRODUCTION

Cockayne syndrome is a rare and progressive autosomal recessive disorder with symptoms including growth failure, neurological dysfunction including cerebellar atrophy leading to ataxia, hearing and vision loss, and photosensitivity without cancer incidence[1]. The average lifespan of CS patients is 16 years, though three subtypes determine the severity and lifespan with the most severe type producing a lifespan of 2-7 years[2]. After a seemingly normal development, patients are often diagnosed by age 2 after a slow deterioration in mental and physical capacities. Motor, language, and cognitive development is delayed and many lose total verbal skills, yet a consistently common feature is an engaging and endearing personality.

Since the initial report in 1936[3], the key genes in the pathophysiology of CS have been determined, along with dysfunction found in numerous tissues and organ systems but no therapy has yet to prove beneficial. CS results from inborn defects in DNA repair proteins that specialize in the removal of UV-induced, helix distorting lesions and some types of oxidative DNA damage via the nucleotide excision repair pathway. Despite extensive investigation into the two major genes responsible for CS, *ERCC8 (CSA)* and *ERCC6 (CSB)*[4,5], no clear genotype:phenotype relationship exists[6] and the mechanisms by which the neuropathology progresses remain speculative.

Reduced oligodendrocyte numbers and patchy loss of myelin are observed both in the central and peripheral nervous tissue, contributing to the question of whether the neurological disease in CS is one of neurodegeneration with neuronal loss and demyelination, or that of dysmyelination due to loss of oligodendrocyte/Scwhann cell function. Case reports for both types of myelin disruption exist, as well as evidence of remyelination efforts in CS brains, but the evidence for progressive loss of peripheral and central myelin is highly convincing[7]. The patchy, often called tigroid pattern, loss of peripheral myelin is known to contribute to peripheral neuropathy of limbs and in CS patients, can be reduced by up to 50%[8]. The gradual reduction in nerve conduction velocity supports CS being a demyelinating neuropathy, eventually leading to secondary axonal degradation and cachexia[1].

Our lab recently published a mouse model of severe Cockayne syndrome that recapitulates the neurodegenerative phenotypes of CS[9]. The CX mouse model (exhibiting total loss of nucleotide excision repair proteins CSA and XPA), displays early cerebellar ataxia reported in other severe NER models, likely resulting from increased death of cerebellar granular neurons (CGNs) and reduced Purkinje cell layer arborization during postnatal development[10]. CX animals present with progressive loss of motor coordination, spasticity and dystonia particularly in the hind limbs, resulting in the inability to walk by approximately 20 weeks and death due to unknown causes[9].

CX mice also display profound alterations in cellular and organismal energy metabolism characterized by an adaptive shift to oxidative metabolism, with an increase in fatty acid oxidation *in vivo*. This increase is driven in large part by unrepaired DNA damage, which activates PARP-1, resulting in NAD+ depletion, energy crisis and activation of the energy deprivation sensing kinase, AMPK. As described in Chapter 3, this adaptive response is beneficial for maintaining energy homeostasis in CX cells, as well as in wildtype cells subject to genotoxic stress.

While the human brain only accounts for roughly 2% of body mass, it consumes 20% of the total oxygen and 25% of the total glucose in the whole body, of which 90% of the ATP generated is in brain tissue mitochondria using oxidative phosphorylation[11]. Intense controversy lies in the metabolic demands of the brain, specifically in cell type-specific utilization of fuel. Glucose is the main energy source for the brain, and the metabolic networking that exists between neurons, astrocytes and oligodendrocytes is intensely cooperative. Neurons have a low glycolytic capacity and much of the lactate used to fuel neurons is generated by astrocytes[12,13]. Liver-derived ketone bodies are also utilized as an energy substrate by neurons and glial cell types, especially during early development and fasting conditions[14]. Ketones can also be generated locally in astrocytes after oxidation of free fatty acids to fuel acetyl-CoA shuttling into neurons[15]. Fatty acids are capable of passing the blood brain barrier (BBB) and studies have highlighted increased uptake of fatty acids in rat brain by *in vivo* nuclear magnetic resonance spectroscopy and that astrocytes preferentially utilize fatty acids *in vitro*[16,17].

Here, we set out to further characterize central and peripheral demyelination in CX mice, and to determine the underlying mechanism of myelin loss. We found that CX neurons displayed no hypersensitivity to oxidative stress either *in vitro* or *in vivo*. We did, however, find evidence of increased expression of genes involved in catabolism of key fats present in myelin. Finally, we observed that astrocytes *in vitro* displayed an increase in oxidative metabolism, and that peripheral and central nerve tissue *ex vivo* displayed an increase in fatty acid oxidation capacity. Together these data suggest astrocytes in peripheral and central nerve tissues undergo metabolic adaptations to preserve energy homeostasis as observed in other tissues, which could possibly contribute to demyelination through catabolism of myelin lipids.

RESULTS

Peripheral Nervous system dysfunction and myelin loss in CX mice

We began investigating alterations in the peripheral nervous system of CX animals by interrogating white matter and neuronal health in the spinal column. H&E and luxol fast blue (LFB) staining revealed loss of white matter in the peripheral space of the spinal column (Figure 4.1a). Silver staining highlighted the increased presence of agryrophillic neurons, indicative of neuronal cell death, which progressively increased with age in CX

mice compared to controls (Figure 4.1a). It is unclear whether neuronal death is a result of loss of myelin sheath integrity or if it is the cause.

Next, we measured gene expression changes in markers of glial health, neuronal growth, and myelin-associated proteins in CX peripheral nerves compared to controls. mRNA expression of the glial fibrillary acidic protein, GFAP, was highly increased in CX sciatic nerve (Figure 4.1b), indicative of astrocytosis and activation of astrocytes. Interestingly, GFAP mutations are causative of Alexander disease in which symptoms include mental and physical retardation, dementia, and spasticity[18]. We saw no significant evidence for increased inflammation in CX peripheral nerves. Many myelin-associated proteins including myelin oligodendrocyte glycoprotein (MOG), peripheral myelin protein 22 (PMP22) and ciliary neurotrophic factor (CNTF) had a significantly decreased mRNA expression in CX tissues, supporting the loss of myelin associated proteins and depressed neuronal health in CX peripheral nerves (Figure 4.1b).

We next performed luxol fast blue staining of the sciatic nerve, which revealed digestion chambers filled with neutral lipid, indicative of degradation of myelin, that worsened with age in CX mice (Figure 4.1c). To interrogate the health of neuronal axons and myelinating Schwann cells, longitudinal sections of sciatic nerve were prepared and photographed on a transmission electron microscope (TEM). Thick slices depicted disorganized fibers and many cross-sectional axons with collapsed myelin sheaths (Figure 4.1d). TEM images of thin slices revealed degenerative alterations in the integrity of

myelin that would likely result in reduced nerve conduction velocity (Figure 4.1e), including degeneration of the myelin sheath from the inside out surrounding degenerated neutral lipids (Figure 4.1e!), myelin balloons (Figure 4.1e @), neurofilament hyperplasia (Figure 4.1e #), dense cytoplasm of degenerating lipid (Figure 4.1e $), and splitting of myelin (Figure 4.1e %).

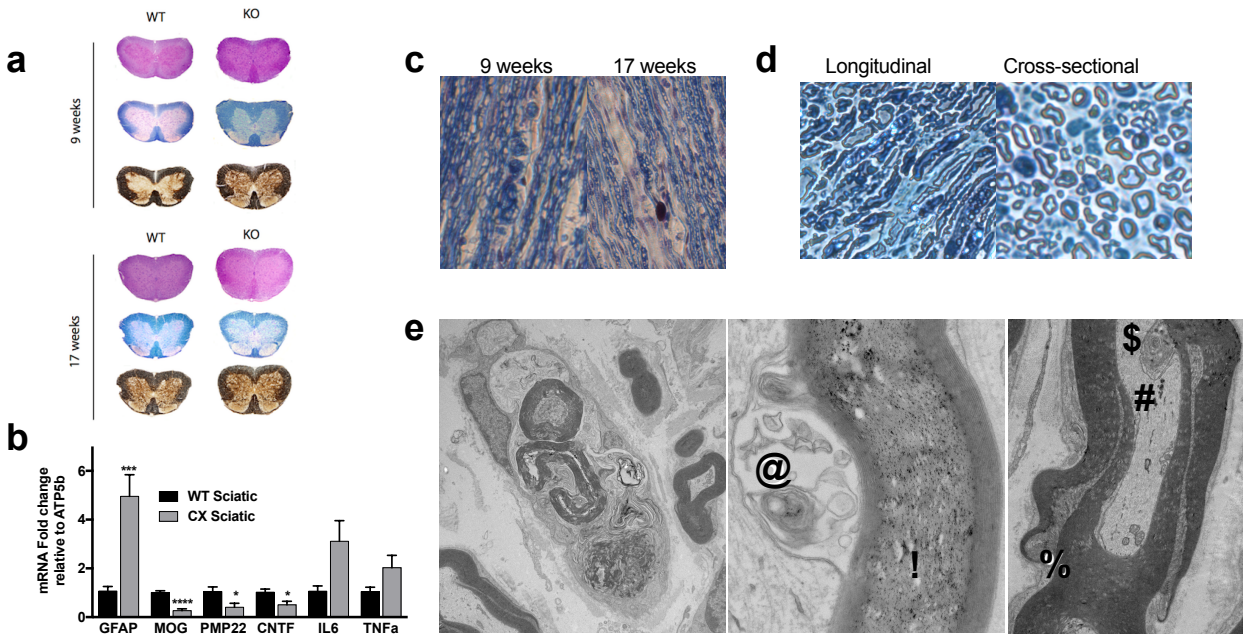

Figure 4.1. Peripheral Nervous system dysfunction and myelin loss in CX mice. a. H&E, luxol fast blue, and silver staining of spinal column of control and CX animals at the indicated ages. **b**. Gene expression of control and CX sciatic nerves, n=4-5/group, Student's t test. **c**. Luxol fast blue staining of CX sciatic nerves at the indicated ages depicting digestion chambers, mag 1500x. **d**. Longitudinal and cross sectional sections of CX sciatic nerve cut 0.5µm thick and stained with toluidine blue and imaged at 60x magnification. **e**. Ultrathin sections of sciatic nerve cut at 60nm thickness, middle panel 15000x magnification and left and right panels at 3000x magnification depicting degeneration of the myelin sheath from the inside out surrounding degenerated neutral lipids (!), myelin balloons (@), neurofilament hyperplasia (#), dense cytoplasm of degenerating lipid ($), and splitting of myelin (%).

Central nervous system dysfunction and myelin loss in CX mice

We next investigated gene expression of central nervous system tissues for markers of glial health, neuronal growth, and myelin-associated proteins. mRNA expression of the glial fibrillary acidic protein, GFAP, was highly increased in CX cortex and cerebellum, again indicative of astrocytosis and activation of astrocytes (Figure 4.2a). Expression of the main myelin-associated protein, myelin basic protein (MBP), was significantly decreased in both CX cortex and cerebellum compared to controls, as was brain-derived neurotrophic factor (BDNF), supporting the loss of myelin associated proteins and decreased neuronal health in the CX brain (Figure 4.2a).

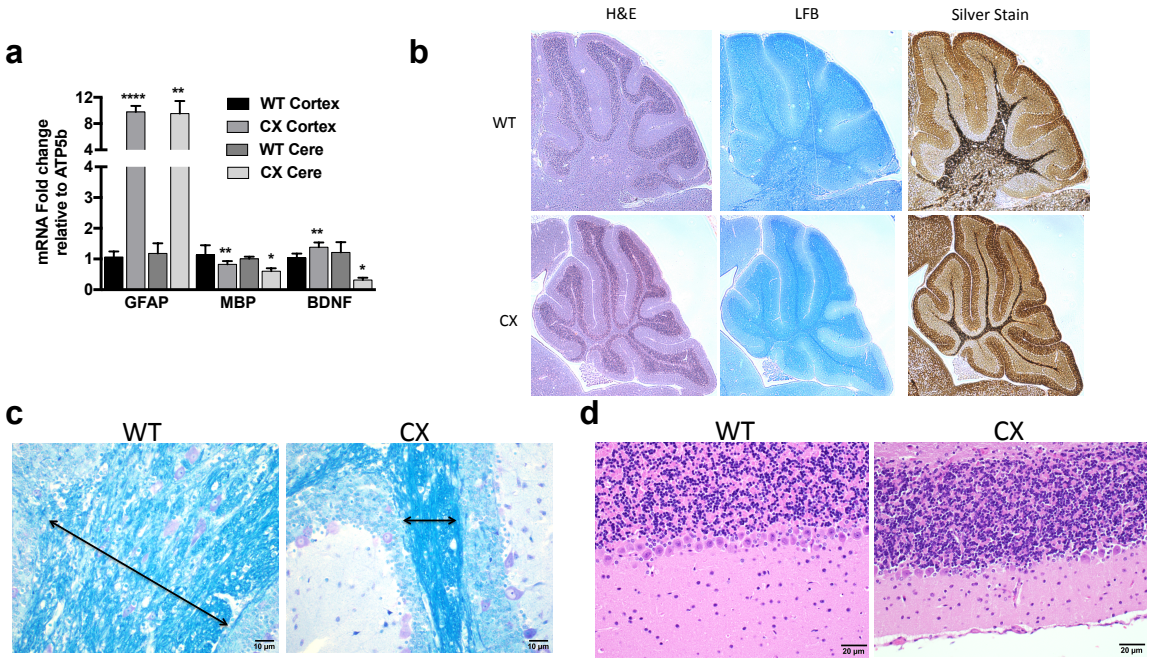

Figure 4.2. Central nervous system dysfunction and myelin loss in CX mice. a. Gene expression analysis of control and CX cortex and cerebellum, n=5/group, Student's t test. **b**. H&E, luxol fast blue, and silver staining of cerebellum of preweaning control and CX animals. **c**. Luxol fast blue staining of cerebellum from 17-week-old WT and CX animals. **d**. H&E staining of animals described in **c**.

Myelin loss was also evident in cerebellum of preweaning mice. CX cerebellum displayed reduced white matter and luxol fast blue staining of lipids, as well as increased silver staining, indicating neuronal death (Figure 4.2b). Similarly, the thickness of cerebellar white matter was significantly reduced in 17-week-old CX mice vs. littermate controls and glial cell number was increased (Figure 4.2c). As is often observed in CS patients, the Purkinje cell layer was also reduced in CX cerebellum compared to controls (Figure 4.2d). Neuronal health was clearly impaired in CX animals as in CS patients and to determine if cell loss is related to an increased susceptibility to oxidative stress.

CX neuronal response to oxidative stress

Loss of myelin can result from death of myelinating cells, or secondarily following the loss of associated neurons. Thus, we first asked whether neurons were hypersensitive to death caused by oxidative stress. Though a hallmark of the phenotype in CS is hypersensitivity to ultraviolet light, there is controversy whether CS cells are similarly hypersensitive to oxidative DNA damaging agents or ischemia-induced reactive oxygen species. Initially, we investigated if dermal fibroblasts from CS patients and next-of-kin controls exhibited hypersensitivity to certain oxidative stress-inducing agents as has been reported previously[19]. As a control, we showed that CS patient fibroblasts were hypersensitive to ultraviolet light, but not to hydrogen peroxide (Figure 4.3 a, b).

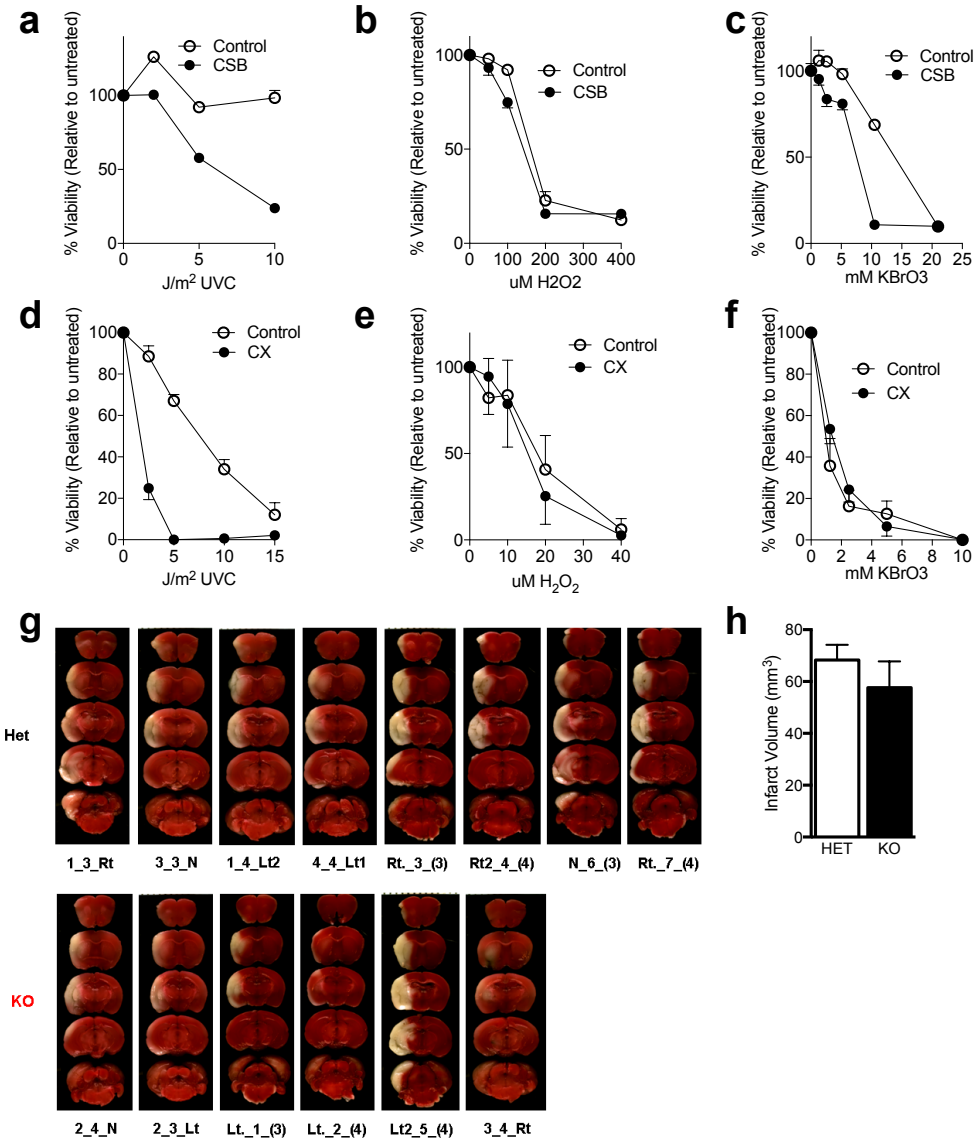

Figure 4.3. CX neuronal response to oxidative stress. a-c. Human dermal fibroblasts isolated from CS patients and next-of-kin controls exposed to increasing doses of ultraviolet C light (**a**), hydrogen peroxide (**b**), and potassium bromide (**c**) and the percent viability was determined using MTT assays, n=6/genotype. **d-f**. CGN isolated from control and CX mice were exposed to increasing doses of ultraviolet C light (**d**), hydrogen peroxide (**e**), and potassium bromide (**f**) and the percent viability was determined using MTT assays, n=6/genotype. **g**. Coronal plane images of CSA +/- and CSA -/- mice after 2 hours of MCAO injury with reperfusion measured by Laser Doppler. **h**. Quantification of infarct volume after MCAO injury as depicted in panel **g**.

There was, however, a hypersensitivity to potassium bromide compared to next-of-kin control fibroblasts (Figure 4.3c). We then cultured cerebellum granule neurons (CGNs) from control and CX animals and measured their sensitivities to these stressors. CX CGNs were indeed hypersensitive to ultraviolet light (Figure 4.3d), but not to either oxidative stress agent (Figure 4.3 e, f).

Finally, we investigated the potential of hypersensitivity to oxidative stress *in vivo* using a model of ischemia reperfusion injury. To this end, male *Csa* heterozygous and *Csa* knockout mice were subject to middle cerebral artery occlusion (MCAO) to induce transient focal brain ischemia. We did not, however, observe any significant differences in the infarct volume between the two genotypes (Figure 4.3 g, h) suggesting that oxidative damage is not mediating neuronal loss in single *Csa* knockout mice.

Myelin catabolism in CX brain

Since we did not observe any primary neuronal hypersensitivity to oxidative stress as potentially causative of secondary loss of myelin, we next looked directly at potential changes in gene expression of pathways controlling myelin generation and breakdown. The dry mass of myelin is made up of approximately 70-85% lipids and 15-30% proteins. We hypothesized that the patchy, tigroid pattern of white matter loss in the central nervous system of CS patients could result from focal areas of increased myelin catabolism. We began by investigating expression changes in enzymes regulating myelin

catabolism. Numerous leukodystrophy disorders (in red) highlight the necessity for the regulation of these enzymes to mediate lipid metabolism of nervous tissue (Figure 4.4a). Overlapping symptoms include loss of motor function, muscle rigidity, and loss of vision and hearing[20]. Although myelin is made up of mostly lipid, there is no single lipid species that is exclusively found in myelin. The lipid in the highest abundance is galactocerebroside, and the concentration of cerebroside is directly proportional to the amount of myelin present. Another component and target for breakdown into fatty acids is sphingomyelin, which serves to strengthen the myelin sheath via hydrocarbon chains.

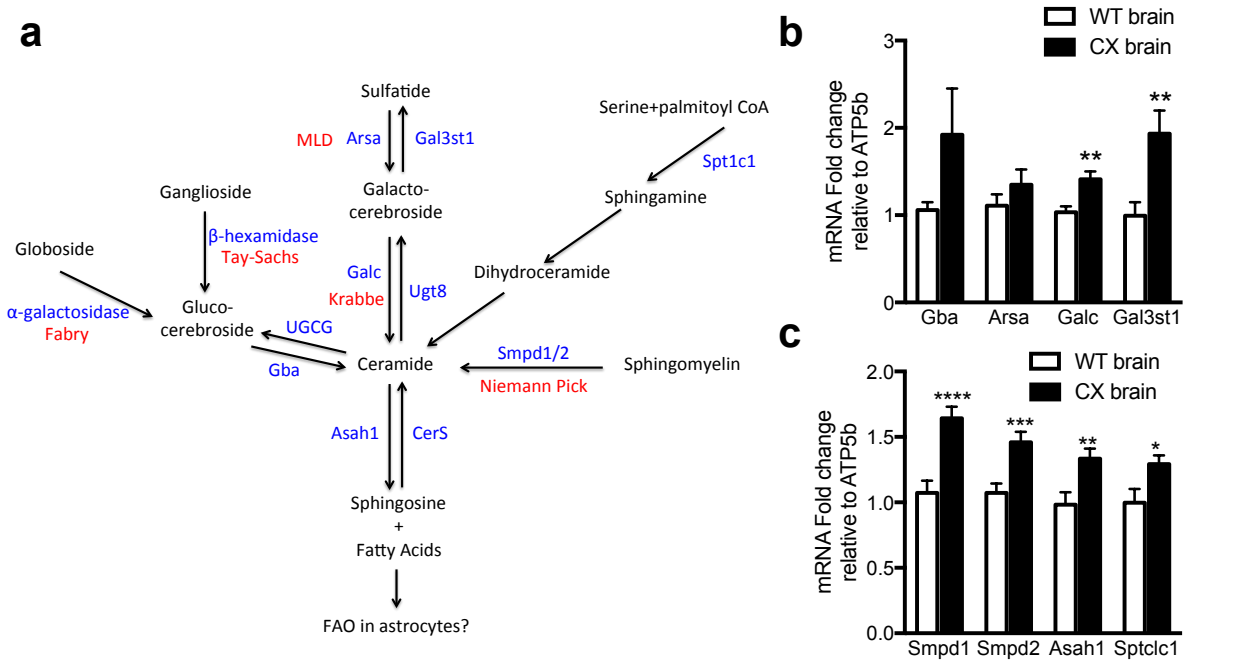

Figure 4.4. Myelin catabolism in CX brain. a. Model of key enzymes and associated disorders in myelin catabolism to fatty acids. **b**. Gene expression of control and CX brain for enzymes involved in galactosidase catabolism, n=15-17/genotype, Student's t test. **c**. Gene expression of control and CX brain for enzymes involved in sphingomyelin catabolism, n=15-17/genotype, Student's t test.

The catabolism of these lipid species converges on ceramide to ultimately breakdown to sphingosine and fatty acids (Figure 4.4a). We found an increased mRNA expression of enzymes known to catabolize galactocerebroside in CX brains compared to controls (Figure 4.4b). We also found increased expression of genes involved in sphingomyelin catabolism in CX brains compared to controls (Figure 4.4c).

Myelin loss correlates with PARP-1 activation and increased FAO in CNS and PNS of CX mice

In a previous study, we identified a PARP-1- and AMPK-dependent increase in fatty acid oxidation (FAO) in multiple CX tissues and cells including liver, muscle and fibroblasts[21]. While this response was found to be a beneficial, adaptive response to restore energy homeostasis, work from our collaborators indicates that constitutive PARP-1 activation eventually precipitates neurodegeneration in CX mice, and that this can be ameliorated by NAD+ repletion[22]. We thus sought to address whether a similar increase in PARP-1 activation and FAO occurs in the CX nervous system, and its potential to impact myelin loss. Indeed, we discovered reduced NAD+ levels in CX brains compared to control animals (Figure 4.5a) and increased PARP-1 staining in spinal columns of aged CX animals compared to controls (Figure 4.5b). mRNA expression of PARP-1-regulated genes was significantly increased in CX cortex and cerebellum (Figure 4.5 c), as well as in were wildtype but not PARP-1 knockout mouse dermal fibroblasts (MDFs) treated with an

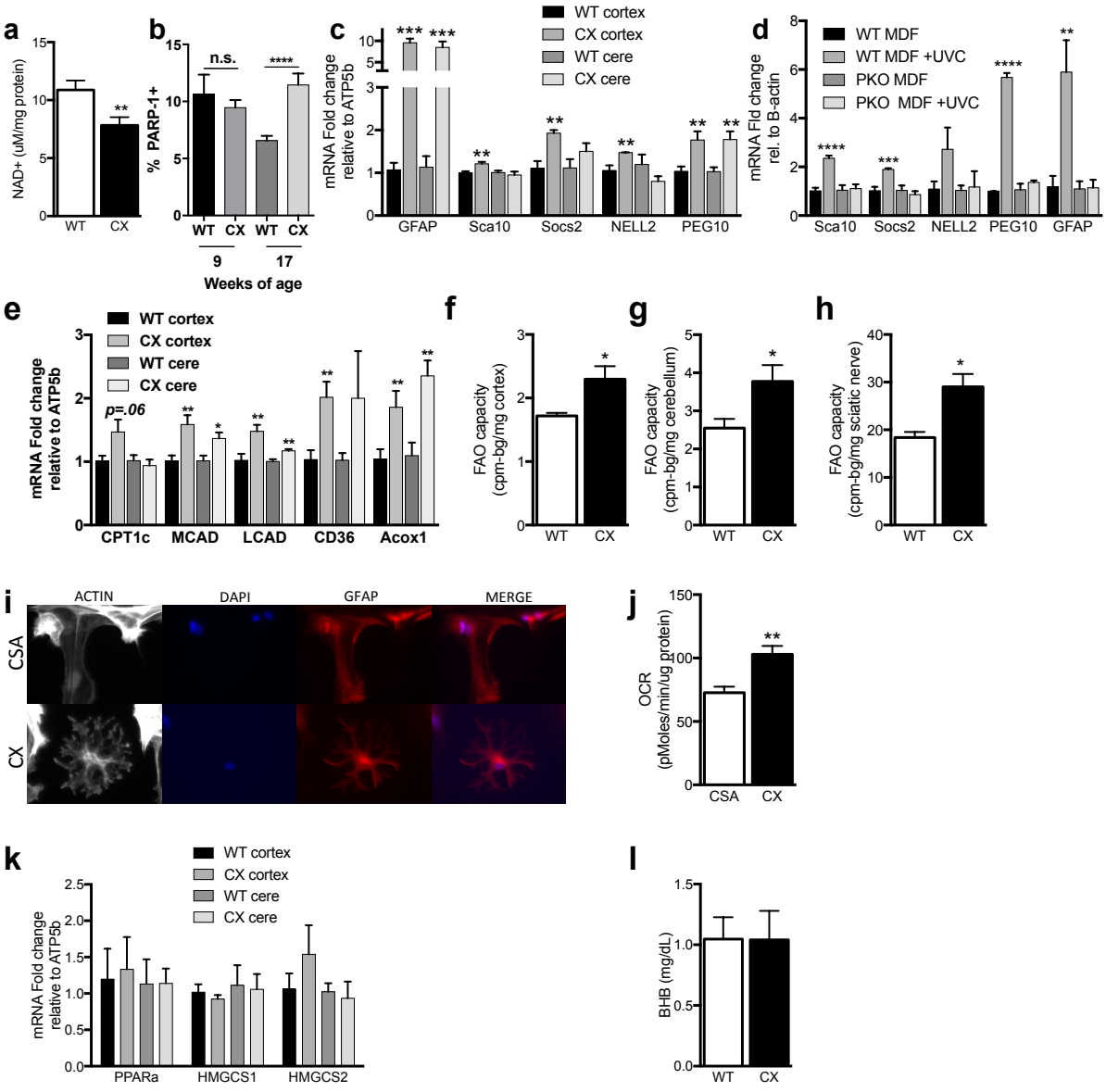

Figure 4.5. Myelin loss correlates with PARP-1 activation and increased FAO in CNS and PNS of CX mice. a. NAD+ content of whole control and CX brains normalized to protein content, n=9-10 in duplicate per genotype, Student's t test. **b**. Quantification of PARP-1 IHC staining in spinal column of control and CX mice at the indicated ages, n=1-2/group measuring 5-6 vertebrae per animal, Student's t test. **c**. Gene expression of control and CX cortex and cerebellum for PARP-1 regulated genes, n=8/group, Student's t test. **d**. Gene expression of wildtype and PARP-1 knockout mouse dermal fibroblasts +/- 20 J/m^2 ultraviolet-C radiation collected after 6 hours for PARP-1 regulated genes, n=4/group, Student's t test. **e**. Gene expression of control and CX cortex and cerebellum for FAO related transcripts, n=5/group, Student's t test. **f-h**. FAO capacity of control and CX cortex (**f**), cerebellum (**g**), and sciatic nerve (**h**), n=3/group in duplicate, Student's t test. **i**. Representative images of immunofluorescence staining for GFAP and DAPI of

Figure 4.5 legend continued:

control and CX astrocytes. **j**. Oxygen consumption rate of control and CX astrocytes by Seahorse cell metabolism analyzer normalized to protein content, n=2 cell lines per group in quadruplicate, Student's test. **k**. mRNA expression of ketogenic genes in WT and CX cortex and cerebellum, n=4/group, Student's t test. **l**. Beta-hydroxybutyrate levels of WT and CX brain lysates, n=3/genotype.

acute dose of genotoxic stress (Figure 4.5 d). Interestingly, *Gfap* expression was significantly increased in WT MDFs treated with ultraviolet-C, and this also required PARP-1 (Figure 4.5 d). GFAP is an intermediate filament protein expressed mainly in astrocytes but in many cells types, including fibroblasts. GFAP is thought to aid in astrocyte mechanical stress maintenance and mediate cell shape, but its function in other cell types is poorly understood. The role PARP-1 plays in GFAP expression and action could lead to key insights in this pathway, especially in the brain.

With growing evidence of PARP-1 activation in the central and peripheral nervous system of CX mice, we next looked for evidence of increased FAO/oxidative phosphorylation. mRNA expression of FAO-related genes was increased in both CX cerebellum and cortex (Figure 4.5e). Furthermore, isolated sciatic nerves, cerebellum, and cortex of CX mice all displayed an increased capacity for fatty acid oxidation *ex vivo* (Figure 4.5f-h). These data support our previous findings that accumulation of DNA lesions drives a PARP-1-dependent increase in FAO, and extend this finding to the nervous system.

Fatty acids can be delivered via peripheral blood supply through the blood brain barrier, which itself is covered in an almost continuous sheath of astrocytes[23], a cell type that has been shown at least *in vitro* to readily uptake and utilize fatty acids in FAO[24]. To test if the observed increase in FAO in the CX nervous system was occurring in astrocytes, we isolated astrocytes from CX and control animals before postnatal day 5. The purity of astrocyte cultures was confirmed by visualization of GFAP staining (Figure 4.5i). Using the Seahorse Cell Metabolism Analyzer, we next observed that astrocytes from CX brains had a significantly increased basal oxygen consumption rate compared to astrocytes from control animals (Figure 4.5j).

Astrocytes produce ketone bodies from free fatty acids via the same ketogenic pathway used by hepatocytes[17,25,26]. Interestingly, mRNA expression of ketogenic gene expression in cortex and cerebellar was not different between control and CX mice (Figure 4.5k). Similarly, β-hydroxybutyrate (BHB) levels were similar between control and CX mouse whole brain homogenates under fasting conditions (Figure 4.5l). Taken at face value, these data fail to support myelin degradation as fueling ketone body production in astrocytes to supplement energy metabolism in their client cells (neurons). However, flux analysis experimentation would be required to determine if ketone levels are altered in CX brains. Future experiments would also be required to determine if myelin itself is a substrate for FAO in CX nervous system, as well as the fate of carbons derived from oxidation.

DISCUSSION

CX mice closely model the range of neurological features observed in human patients with Cockayne syndrome. Histological and gene expression analyses of both the CX central and peripheral nervous system revealed extensive dysfunction including cerebellar atrophy, neuronal cell death, astroglial activation, myelin degeneration, increased PARP-1 levels, and increased expression of PARP-1-regulated genes. Stemming from our previous work linking the chronic DNA damage that accumulates with loss of NER to increased oxidative phosphorylation and progressive loss of adiposity, we were interested to determine if the myelin loss could also be driven by this adaptation. We confirmed that the increased PARP-1 activation in CX nervous tissue resulted in loss of NAD+, increased FAO-related gene expression, and increased FAO capacity. Moreover, we determined that astrocytes from CX mice have a higher basal oxygen consumption rate compared to controls, indicating that this cell type, which is known to preferentially consume fatty acids as fuel[17], is potentially driving fat oxidation in the nervous system. Lastly, we investigated the potential for increased fatty acid oxidation to be causative of the patchy, focal loss of myelin sheaths around neurons and determined an increased gene expression profile for catabolism of major myelin lipid components. Further investigation is required to determine if fat oxidation is increased in these focal areas of myelin loss and if the substrate truly is myelin-derived lipids.

Dysmyelination vs. Demyelination in Cockayne syndrome pathology

Due to the wide range of mouse models of Cockayne syndrome generated that model mild to severe CS, the neurological phenotypes are widespread and the cause of white matter loss has been reported to be due to either dysmyelination and demyelination. Dysmyelination would be a consequence of delayed or unstable myelin formation whereas demyelination would be due to the loss of previously normal myelin. The CX mouse is the first model that allows for the investigation of progressive neurodegeneration due to severe Cockayne syndrome. Other mouse models of DNA repair deficiency have shown promising results, but fall short either due to a preweaning lifespan or model a less significant defect. Reports from $Csb^{m/m}/Xpc^{-/-}$ mice with a lifespan of under 28 days similarly depict loss of myelin-associated proteins and reduced myelination but conclude that the latter is a result of dysmyelination and not demyelination[27]. Since these animals succumb to death before postnatal day 28, it is likely difficult to deconstruct neurological alterations resulting from death versus early development with loss of DNA repair. The argument that dysmyelination is occurring due to a *developmental* defect in the $Csb^{m/m}/Xpc^{-/-}$ mice that do not survive weaning[27] only further supports the likelihood that the abnormality is degenerative and a result of demyelination. Models such as the $Ercc1^{\Delta/-}$ mice more closely mimic severe XP/CS or COFS (cerebro-oculo-facio-skeletal syndrome) but have the same relative lifespan as CX mice, also show abnormal myelin structures due to demyelination[28]. As is seen in the

Ercc1$^{\Delta/-}$ and CX mice, human CS patients present myelin loss in both the central and peripheral nervous system, meaning that two distinct cell types, oligodendrocytes in the central and Schwann cells in the peripheral nervous system, are implicated in the disorder. Formation of onion bulb structures also supports attempts to repair demyelinated nerve segments and indicate active remyelination efforts[1]. The myelin structures visualized in sciatic nerve TEM from CX mice show areas of appropriate myelin formation nearby areas of complete axonal loss and evidence supporting remyelination efforts. To conclusively remark on these processes in CX mice, sciatic nerves would need to be visualized across the lifespan and compared to wildtype mice at the same age, or utilize noninvasive methods for measuring peripheral neuropathy.

Nerve conduction velocity as a marker of neurodegenerative progression

Secondary to the progressive demyelination occurring in CS patients and in the CX mouse model is axonal loss, which ultimately affects both motor and sensory function, presenting as impaired balance and coordination. A powerful tool in gauging the demyelination process in CS patients is measuring peripheral nerve conduction velocity over time. Numerous reports outlined that nerve conduction velocity is negatively correlated with clinical CS severity, often reduced by up to 50%[8,29]. Further supporting our data that DNA damage can impact myelin, it has been shown that acute treatment with genotoxic chemotherapeutic agents also demonstrate a dose-dependent slowdown of sensory nerve conduction velocity in mice as well as in human patients[30,31]. Since we

previously showed that acute doses of genotoxic agents increase FAO, this adaptation could also be facilitating the segmental demyelination contributing to the peripheral neuropathy seen in patients treated with repeated chemotherapeutic agents.

Changes in nerve function and pathology are also observed in humans and rodents during normal aging. In humans, nerve conduction velocity decreases with advancing age,[32,33] with progressive loss of both large and small myelinated fiber density[34]. Similarly, in mice, nerve conduction velocity declines in the last third of life[35]. The average lifespan of CX mice is approximately 20 weeks, though we have demonstrated extension of maximum lifespan to 27 weeks if fed a methionine restricted diet (Figure 3.6c) and 21.5 weeks upon NAD+ supplementation in the drinking water (Figure 5.3f). The ultimate cause of death in CX animals is malnutrition/dehydration due to the loss of sensory and motor control with severe peripheral neuropathy and the inability to properly intake food and water. One possible mechanism of how both methionine restriction and NAD+ supplementation extend lifespan in CX mice could be due to a slowing myelin loss and therefore of peripheral neuropathy that allows for the maintenance of proper nutrition. If future interventions of NAD+ supplementation, PARP-1 inhibition, methionine restriction, or dietary restriction are tested in CX mice and CS patients, the measure of nerve conduction velocity changes over time would be a highly suitable and easily performed cross sectional endpoint.

Misconceptions in nervous system metabolism

To this day, the energy needs of the brain is an extremely topic for many researchers. Consensus does agree that glucose is the key blood-borne substrate utilized by the adult central nervous system to support metabolic demands[36]. Other considerations are for the neuronal uptake of lactate generated from astrocytes as a part of the "astrocyte-neuron lactate shuttle hypothesis" and liver-derived ketone body uptake[13,37-39]. The role that alternative fuels, such as fatty acids, and supporting glial cells play in energy metabolism has received considerably less attention. Astrocytes are the first cell type encountered by nutrients entering the brain through the blood brain barrier, making them a prime site for uptake, storage, and processing of nutrients[40]. They play critical roles in maintaining neuronal transmission, glycogen storage, and lactate production to support neuronal metabolism[13,41]. If the minor glycogen stores in astrocytes are depleted and blood glucose levels decline under fasting conditions, ketone bodies can be utilized as key substrates for energy production. Ketone bodies are commonly thought be derived from fatty acids in the liver and permeate the blood brain barrier for uptake in neurons and glial cells[14] but the ketogenic pathway used by hepatocytes is almost identical in astrocytes and has been shown that both cell types prefer fatty acids to glucose as the primary fuel source for ketone body production[24-26].

Under conditions of hypoxia in the brain, the electron transport chain slows and ATP is depleted, increasing AMP levels and activating AMPK to maintain astroglial fatty

acid oxidation and ketogenesis[42,43]. Under severe hypoxia, such as during ischemic stroke, the stimulation of astrocytic fatty acid oxidation is protective against damage[44]. Raising ketone body levels by starvation also protects the brain against hypoxia/ischemia-induced damage in animal models[45-47], which is supported by enhanced neurogenesis and neuron survival under conditions of caloric restriction[48]. We determined that CX mice have an increased gene expression profile and capacity for fatty acid oxidation both in the central and peripheral nervous system and CX astrocytes have a higher basal oxygen consumption compared to controls. Increased PARP-1 activity has been previously shown in CX cerebellar mitochondria[22] and we measured decreased NAD+ in whole brain homogenates. Therefore, these data support the cell-autonomous PARP-1 and AMPK dependent mechanism linking DNA damage to increased fatty acid oxidation that was presented in Chapter 3[21].

The majority of fatty acids that are oxidized in nervous tissue most likely derive from the circulation, however, the fact that focal areas of lipid-rich myelin loss increases with age suggested that fatty acids derived from this source could also serve as metabolic fuel for astrocytes. Age-related myelin breakdown has been shown under conditions of normal aging and in neurodegenerative diseases[49-57]. Furthermore, the expression of MCT1, the monocarboxylic acid transporter that allows ketone bodies through the blood-brain barrier (BBB), decreases with age[58]. The compensatory response of deriving ketone bodies in the brain would therefore intensify in astrocytes. Other groups have shown increased myelin degeneration coinciding with activation of the sphingomyelinase

pathway, accumulation of lipid droplets and increased fatty acid oxidation and ketone body synthesis during aging in normal mice[15]. Future investigation is needed to determine if FAO is increased in the focal areas of myelin loss, possibly by using immunohistochemistry, and if the source fatty acids are derived from myelin or from the periphery. It is commonly thought that only short chain fatty acids are able to pass the BBB through MCT1 so the presence of long-chain fatty acids in the CNS may point to catabolism of myelin versus influx from the blood supply[59]. However, other proteins are involved in fatty acid intake through the BBB including FABP5[60], but as this protein is also expressed in astrocytes, its depletion would not allow distinguishing between fatty acids derived from the periphery. Radiolabeling assays may also be able to comment on the contribution myelin-derived fatty acids play in the overall increased FAO in nervous tissue or by measuring expression of myelin-catabolizing proteins at sites of focal damage, such as sphingomyelinase and cereobrosidases. Being able to distinguish between the sources of a fatty acid species will be a difficult task, possibly being accomplished by infusing fatty acids labeled with stable isotopes and following the incorporation into tissues, but the availability of a mouse that closely models the human disease will allow us to better answer this question.

MATERIALS & METHODS

Mice and Histology Animals were utilized as described in Chapters 2 and 3. Mice were perfused with Bouin's fixative and the Harvard Rodent Histopathology Core performed whole body necropsies. Slides of the central and peripheral nervous system were prepared and stained with hematoxylin and eosin, luxol fast blue, and silver stain. Blinded slides were investigated by Sandro Santagata.

TEM Animals were perfused with fixative (2.5% glutaraldehyde, 1.25% paraformaldehyde, and 0.03% picric acid in 0.1M sodium cacodylate buffer pH 7.4). Sciatic nerves were isolated and postfixed for 2 hours at room temperature in the same fixative, washed in 0.1M sodium cacodylate buffer and postfixed with 1% osmium tetroxide/1.5% potassium ferrocyanide for 1 hour, washed 3x with water and incubated in 1% aqueous uranyl acetate for 1 hour followed by 2x wash in water and dehydration in grades of alcohol (10min each; 50%, 70%, 90%, 2x10 100%). Samples then put in propyleneoxide for 1hr and infiltrated ON in a 1:1 mixture of propyleneoxide and TAAB Epon (Marivac Canada). The following day samples were embedded in TAAB Epon and polymerized at 60oC for 48hrs. Thick 0.5µm sections were cut and stained with toluidine blue for assessment and ultrathin sections (60nm) were cut on a Reichert Ultracut-S microtome, pick up on to copper grids stained with lead citrate and examined in a JEOL 1200EX Transmission electron microscope or a TechnaiG^2 and images were recorded with an AMT 2k CCD camera.

Astrocyte isolation Astrocytes were isolated using methods previously described [61]. Briefly, the cortexes of P1-P4 pups were isolated and dissociated into HBSS with 0.5% trypsin after removal of the cerebellum, olfactory bulbs and meningeal artery system. The pelleted cortex was washed and the single cell suspension was grown in poly-d-lysine treated flasks in 10% FBS DMEM +P/S for 1.5 weeks with media changes every three days. When confluency was reached, flasks first shook at 180rpm for 30 minutes on an orbital shaker to remove microglia. Next fresh media was added and flask shook at 240rpm for 6 hours to remove oligodendrocytes precursor cells. The remaining culture of "pure" astrocytes was then grown and utilized in experiments.

Cerebellum Granule Neuron isolation and oxidative damage assays Brains were dissected from postnatal day 7 pups and the cerebellum washed in Hank's Buffered Salt Solution with the removal of meninges and blood vessels. The cerebellums were then rinsed in HBSS and minced before the addition of 0.5% trypsin for 20minutes at 370C. DNaseI in FBS was added with gentle tapping for 5-10minutes. Pieces were mixed and spun down in HBSS. Cells were then resuspended, counted, and plated in BME media with 10% FBS and KCl. Cells were then treated with hydrogen peroxide, ultraviolet-C light, and potassium bromide to measure the sensitivity between genotypes. Human dermal fibroblasts (described in Chapter 3 methods, gift from PJ Brooks) were also utilized to measure the sensitivity to UVC light and oxidative stress with a readout of MTT. Briefly, after 24-hour exposure to oxidative damage, 5mg/ml MTT in PBS was diluted to 0.5mg/ml in serum-containing media. 100µL was added to each 96 well and

incubated for 4 hours at 37˚C. Media was removed and 100µl acidified isopropanol was added and plate was read at 570nm in a plate reader.

Real time quantitative Polymerase Chain Reaction Total RNA was isolated from tissues using Qiazol (QIAGEN, Hilden, Germany) and cDNA synthesized by random hexamer priming with the Verso cDNA kit (Thermo, Cambridge, MA, USA). qRT-PCR was performed using Taq-Pro DNA polymerase (Denville, Holliston, MA, USA) and SYBR green dye (Lonza, Portsmouth, NH, USA). Fold changes were calculated by the DDC_t method using B-actin as a standard, and normalized to the experimental WT control. Primer sequences are as follows:

β-actin F:AGCTTCTTTGCAGCTCCTTCGTTG R:TTCTGACCCATTCCCACCATCACA, *Atp5b* F:GGGTCAGTCAGGTCATCAGC R:CACAATGCAGGAAAGGATCA,
Cd36 F: GAGCAACTGGTGGATGGTTT R: GCAGAATCAAGGGAGAGCAC,
Cpt1c F:CAAACTCTTCCCACCAGTCG R:GCAAATGACTTCCTGAGGTTG,
Lcad F:TCTTTTCCTCGGAGCATGACA R:GACCTCTCTACTCACTTCTCCAG,
Vlcad F:CTACTGTGCTTCAGGGACACC R:CAAAGGACTTCGATTCTGCCC,
Acox1 F: CCTGATTCAGCAAGGTAGGG R: TCGCAGACCCTGAAGAAATC,
Pparα F: TGTTTGTGGCTGCTATAATTTGC R:GCAACTTCTCAATGTAGCCTATGTTT,
Gfap F:TTTCTCGGATCTGGAGGTTG R:AGATCGCCACCTACAGGAAA,
Mbp F:TCTGCTGTGTGCTTGGAGTC R:GGCCTCAGAGGACAGTGATG,
Mog F:GACCTGCAGGAGGATCGTAG R:ACCAAGAAGAGGCAGCAATG,
Pmp22 F:GAACAGGAACAGAGCCAGGA R:AGCCGTCCAACACTGCTACT,
Cntf F:CCATCCACTGAGTCAAGGCT R:TGGCTAGCAAGGAAGATTCG,
Il6 F: ACCAGAGGAAATTTTCAATAGGC R: TGATGCACTTGCAGAAAACA,
Tnfα F:AGGGTCTGGGCCATAGAACT R:CCACCACGCTCTTCTGTCTAC,
Bdnf F:GCCTTCATGCAACCGAAGTA R:TGAGTCTCCAGGACAGCAAA,
Sca1o F:CATCTCATCCGTCTGATTGG R:GCTGTCCAGGATCAGAGGAA,
Sosc2 F:CGCGAGCTCAGTCAAACAG R:AAGAAAGTTCCTTCTGGAGCC,
Nell2 F:GATGGCTGTAGAAACGGAGG R:CCCTCAGAGCACTCGTCAAT,
Peg1o F:CAGAACGAATAAGGTCCCCA R:CATAGCTCGGACAAACAGGG,
Hmgcs1 F:AACTGGTGCAGAAATCTCTAGC R:GGTTGAATAGCTCAGAACTAGCC,
Hmgcs2 F:GAAGAGAGCGATGCAGGAAAC R:GTCCACATATTGGGCTGGAAA,
Smpd1 F:TCTCACGGGAACAAAAATTCA R:GTTACCAGCTGATGCCCTTC,
Smpd2 F:TATGTTTGCTCAGGTAGGGA R:GAAGCACTCCAGCCATGAAG,
Asah1 F:TGGTCCAGAAGGAGGATACG R:TCTCACCTGGGTCCTAGCC,
Spt1c1 F:GGTGGAGAAGCCATACGAGT R:CGAGGGTTCTATGGCACATT,

Gba F: GATGGAGAAGTCACAACTGGC R:GCTTTGTCCCCACCTACTCA,
Arsa F:CCATGGATCTCGTCTGGGTA R:ACGTCACCTTGGATGGTGTT,
Galc F:CCCTGACATCTTTGCATTCC R:CGATTTCCTCTTCCTTGCTG,
Gal3st1 F:TGGCAGCAGAGTCATCTCAG R:AGAGAAGACACAGCGGGATG

NAD+ Approximately 20mg size pieces of tissue were prepared and used in the EnzyChrom NAD+ Assay Kit from BioAssays (Hayward, CA). Samples were normalized to protein content.

FAO capacity Sciatic nerve and whole brain was removed and split half for 2x cortex and 2x cerebellum pieces. Tissues were then weighed and placed in KH buffer containing 25mM $NaHCO_3$, 118mM NaCl, 4.7mM KCl, 1.2mM $MgSO_4$, 1.2mM NaH_2PO_4, 1.2mM $CaCl_2$ and glucose (2.5mM). Tissues were kept in buffer on ice until all dissections were completed. Each tissue then transferred to KH buffer plus 2% Fatty acid free BSA and 2.5mM glucose, with 2μCi ^3H palmitic acid (Perkin Elmer, Waltham, MA, USA) and incubated at 37ºC for 1hr. The buffer was collected and hydrolyzed ^3H palmitic acid (as ^3H water) was extracted. 100μL of buffer was added to 100μL of 10% trichloroacetic acid (TCA), vortexed, incubated at RT for 15 min, spun at 16,000rpm for 10min, and the supernatant collected into a new tube. TCA (5%; 100μL) and 40μL BSA (10%) was added to the supernatant, vortexed, incubated at RT for 15min, spun at 16,000 rpm for 10min, and the supernatant transferred to a new tube. Chloroform:methanol (2:1, 750μL) was added to the supernatant, along with KCl: HCl (2 M each, 300μL), vortexed and spun at 16,000 rpm for 10min. The upper layer (~600μL) was collected into 5ml EcoLume, mixed,

and counted in a liquid scintillation counter. After subtracting background cpm, the sample cpm was divided by the tissue weight to determine FAO capacity.

Seahorse OCR was determined in astrocytes using the Seahorse Cell Metabolism Analyzer XF24. Cells were plated at 50,000 per well in poly-d-lysine coated XF24 plates and 24hours later switched to unbuffered XF assay media with 11mM glucose, 2mM glutamine and pyruvate at pH7.4. Measurements were taken after 2 minutes mixing and 5 minutes measuring. Plates were normalized to protein content by BCA.

Ketone bodies β-hydroxybutyrate levels were measured in serum and homogenized tissue (Pointe Scientific, Canton, MI, USA). Tissue was normalized to protein content by BCA.

Middle Cerebral Artery Occlusion MCAO was performed on *Csa*$^{+/-}$ and *Csa*$^{-/-}$ mice as described [62,63]. Briefly, mice were anesthetized with 2% isoflurane and maintained on 1.5% isoflurane in 70% nitrous oxide and 30% oxygen and a silicone-coated 8-0 monofilament was introduced in the internal carotid artery and advanced to occlude the middle cerebral artery for 0.5, 1, or 2h. After 2h MCAO, the animals were briefly reanesthetized and the filament was withdrawn for reperfusion studies. Regional cerebral blood flow was measured by laser-Doppler (PF2B; Perimed, Stockholm, Sweden) using a flexible probe, placed over the temporal bone after removal of part of the temporalis muscle, to confirm

occlusion and reperfusion. Rectal temperature was maintained between 36.5°C and 37.5°C with a homeothermic blanket (Frederick Haer and Co., Brunswick, ME, USA).

Statistics The indicated statistical analyses were performed either in Excel or in GraphPad Prism.

ACKNOWLEDGEMENTS

We thank Dottie Vargas for assistance in mouse colony maintenance, Michael Moskowitz' lab for MCAO studies, and David Sinclair, Zhi-min Yuan, and Ed Nielan for helpful discussions

REFERENCES

1. Weidenheim KM, Dickson DW, Rapin I. Neuropathology of Cockayne syndrome: Evidence for impaired development, premature aging, and neurodegeneration. *Mech Ageing Dev.* 2009;130(9):619-636.

2. Natale V. A comprehensive description of the severity groups in Cockayne syndrome. *Am J Med Genet A.* 2011;155A(5):1081-1095.

3. Cockayne EA. Dwarfism with retinal atrophy and deafness. *Arch Dis Child.* 1936;11(61):1-8.

4. Troelstra C, van Gool A, de Wit J, Vermeulen W, Bootsma D, Hoeijmakers JH. ERCC6, a member of a subfamily of putative helicases, is involved in Cockayne's syndrome and preferential repair of active genes. *Cell.* 1992;71(6):939-953.

5. Henning KA, Li L, Iyer N, et al. The Cockayne syndrome group A gene encodes a WD repeat protein that interacts with CSB protein and a subunit of RNA polymerase II TFIIH. *Cell.* 1995;82(4):555-564.

6. Bailey AD, Gray LT, Pavelitz T, et al. The conserved Cockayne syndrome B-piggyBac fusion protein (CSB-PGBD3) affects DNA repair and induces both interferon-like and innate antiviral responses in CSB-null cells. *DNA Repair (Amst).* 2012;11(5):488-501.

7. Vos A, Gabreëls-Festen A, Joosten E, Gabreëls F, Renier W, Mullaart R. The neuropathy of Cockayne syndrome. *Acta Neuropathol.* 1983;61(2):153-156.

8. Moosa A, Dubowitz V. Peripheral neuropathy in Cockayne's syndrome. *Arch Dis Child.* 1970;45(243):674-677.

9. Brace LE, Vose SC, Vargas DF, Zhao S, Wang XP, Mitchell JR. Lifespan extension by dietary intervention in a mouse model of Cockayne Syndrome uncouples early postnatal development from segmental progeria. *Aging Cell.* 2013.

10. Murai M, Enokido Y, Inamura N, et al. Early postnatal ataxia and abnormal cerebellar development in mice lacking Xeroderma pigmentosum Group A and

Cockayne syndrome Group B DNA repair genes. *Proc Natl Acad Sci U S A.* 2001;98(23):13379-13384.

11. Schönfeld P, Reiser G. Why does brain metabolism not favor burning of fatty acids to provide energy? Reflections on disadvantages of the use of free fatty acids as fuel for brain. *J Cereb Blood Flow Metab.* 2013;33(10):1493-1499.

12. Bélanger M, Allaman I, Magistretti PJ. Brain energy metabolism: focus on astrocyte-neuron metabolic cooperation. *Cell Metab.* 2011;14(6):724-738.

13. Pellerin L, Magistretti PJ. Sweet sixteen for ANLS. *J Cereb Blood Flow Metab.* 2012;32(7):1152-1166.

14. Morris AA. Cerebral ketone body metabolism. *J Inherit Metab Dis.* 2005;28(2):109-121.

15. Klosinski LP, Yao J, Yin F, et al. White Matter Lipids as a Ketogenic Fuel Supply in Aging Female Brain: Implications for Alzheimer's Disease. *EBioMedicine.* 2015;2(12):1888-1904.

16. Ebert D, Haller RG, Walton ME. Energy contribution of octanoate to intact rat brain metabolism measured by 13C nuclear magnetic resonance spectroscopy. *J Neurosci.* 2003;23(13):5928-5935.

17. Edmond J. Energy metabolism in developing brain cells. *Can J Physiol Pharmacol.* 1992;70 Suppl:S118-129.

18. Rodriguez D. Leukodystrophies with astrocytic dysfunction. *Handb Clin Neurol.* 2013;113:1619-1628.

19. Cleaver JE, Brennan-Minnella AM, Swanson RA, et al. Mitochondrial reactive oxygen species are scavenged by Cockayne syndrome B protein in human fibroblasts without nuclear DNA damage. *Proc Natl Acad Sci U S A.* 2014;111(37):13487-13492.

20. Duncan ID, Radcliff AB. Inherited and acquired disorders of myelin: The underlying myelin pathology. *Exp Neurol.* 2016;283(Pt B):452-475.

21. Brace LE, Vose SC, Stanya K, et al. Increased oxidative phosphorylation in response to acute and chronic DNA damage. *Aging and Mechanisms of Disease.* 2016.

22. Fang EF, Scheibye-Knudsen M, Brace LE, et al. Defective mitophagy in XPA via PARP-1 hyperactivation and NAD(+)/SIRT1 reduction. *Cell.* 2014;157:882-896.

23. Virgintino D, Monaghan P, Robertson D, et al. An immunohistochemical and morphometric study on astrocytes and microvasculature in the human cerebral cortex. *Histochem J.* 1997;29(9):655-660.

24. Edmond J, Robbins RA, Bergstrom JD, Cole RA, de Vellis J. Capacity for substrate utilization in oxidative metabolism by neurons, astrocytes, and oligodendrocytes from developing brain in primary culture. *J Neurosci Res.* 1987;18(4):551-561.

25. Guzmán M, Blázquez C. Ketone body synthesis in the brain: possible neuroprotective effects. *Prostaglandins Leukot Essent Fatty Acids.* 2004;70(3):287-292.

26. McGarry JD, Foster DW. Regulation of hepatic fatty acid oxidation and ketone body production. *Annu Rev Biochem.* 1980;49:395-420.

27. Revet I, Feeney L, Tang AA, Huang EJ, Cleaver JE. Dysmyelination not demyelination causes neurological symptoms in preweaned mice in a murine model of Cockayne syndrome. *Proc Natl Acad Sci U S A.* 2012;109(12):4627-4632.

28. Goss JR, Stolz DB, Robinson AR, et al. Premature aging-related peripheral neuropathy in a mouse model of progeria. *Mech Ageing Dev.* 2011;132(8-9):437-442.

29. Gitiaux C, Blin-Rochemaure N, Hully M, et al. Progressive demyelinating neuropathy correlates with clinical severity in Cockayne syndrome. *Clin Neurophysiol.* 2015;126(7):1435-1439.

30. Dzagnidze A, Katsarava Z, Makhalova J, et al. Repair capacity for platinum-DNA adducts determines the severity of cisplatin-induced peripheral neuropathy. *J Neurosci.* 2007;27(35):9451-9457.

31. Grisold W, Cavaletti G, Windebank AJ. Peripheral neuropathies from chemotherapeutics and targeted agents: diagnosis, treatment, and prevention. *Neuro Oncol.* 2012;14 Suppl 4:iv45-54.

32. Taylor PK. Non-linear effects of age on nerve conduction in adults. *J Neurol Sci.* 1984;66(2-3):223-234.

33. Suzuki M. Peripheral neuropathy in the elderly. *Handb Clin Neurol.* 2013;115:803-813.

34. Tohgi H, Tsukagoshi H, Toyokura Y. Quantitative changes with age in normal sural nerves. *Acta Neuropathol.* 1977;38(3):213-220.

35. Verdú E, Ceballos D, Vilches JJ, Navarro X. Influence of aging on peripheral nerve function and regeneration. *J Peripher Nerv Syst.* 2000;5(4):191-208.

36. Dienel GA, Hertz L. Glucose and lactate metabolism during brain activation. *J Neurosci Res.* 2001;66(5):824-838.

37. Bouzier-Sore AK, Pellerin L. Unraveling the complex metabolic nature of astrocytes. *Front Cell Neurosci.* 2013;7:179.

38. Pellerin L. How astrocytes feed hungry neurons. *Mol Neurobiol.* 2005;32(1):59-72.

39. Schousboe A, Bak LK, Waagepetersen HS. Astrocytic Control of Biosynthesis and Turnover of the Neurotransmitters Glutamate and GABA. *Front Endocrinol (Lausanne).* 2013;4:102.

40. Tsacopoulos M, Magistretti PJ. Metabolic coupling between glia and neurons. *J Neurosci.* 1996;16(3):877-885.

41. Pellerin L, Pellegri G, Bittar PG, et al. Evidence supporting the existence of an activity-dependent astrocyte-neuron lactate shuttle. *Dev Neurosci.* 1998;20(4-5):291-299.

42. Blázquez C, Woods A, de Ceballos ML, Carling D, Guzmán M. The AMP-activated protein kinase is involved in the regulation of ketone body production by astrocytes. *J Neurochem.* 1999;73(4):1674-1682.

43. Hardie DG, Hawley SA. AMP-activated protein kinase: the energy charge hypothesis revisited. *Bioessays.* 2001;23(12):1112-1119.

44. Sayre NL, Sifuentes M, Holstein D, Cheng SY, Zhu X, Lechleiter JD. Stimulation of astrocyte fatty acid oxidation by thyroid hormone is protective against ischemic stroke-induced damage. *J Cereb Blood Flow Metab.* 2016.

45. Go KG, Prenen GH, Korf J. Protective effect of fasting upon cerebral hypoxic-ischemic injury. *Metab Brain Dis.* 1988;3(4):257-263.

46. Marie C, Bralet AM, Gueldry S, Bralet J. Fasting prior to transient cerebral ischemia reduces delayed neuronal necrosis. *Metab Brain Dis.* 1990;5(2):65-75.

47. Yager JY, Heitjan DF, Towfighi J, Vannucci RC. Effect of insulin-induced and fasting hypoglycemia on perinatal hypoxic-ischemic brain damage. *Pediatr Res.* 1992;31(2):138-142.

48. Mattson MP, Chan SL, Duan W. Modification of brain aging and neurodegenerative disorders by genes, diet, and behavior. *Physiol Rev.* 2002;82(3):637-672.

49. Bartzokis G, Lu PH, Mintz J. Quantifying age-related myelin breakdown with MRI: novel therapeutic targets for preventing cognitive decline and Alzheimer's disease. *J Alzheimers Dis.* 2004;6(6 Suppl):S53-59.

50. DeCarli C, Murphy DG, Tranh M, et al. The effect of white matter hyperintensity volume on brain structure, cognitive performance, and cerebral metabolism of glucose in 51 healthy adults. *Neurology.* 1995;45(11):2077-2084.

51. Erten-Lyons D, Woltjer R, Kaye J, et al. Neuropathologic basis of white matter hyperintensity accumulation with advanced age. *Neurology.* 2013;81(11):977-983.

52. Ge Y, Grossman RI, Babb JS, Rabin ML, Mannon LJ, Kolson DL. Age-related total gray matter and white matter changes in normal adult brain. Part I: volumetric MR imaging analysis. *AJNR Am J Neuroradiol.* 2002;23(8):1327-1333.

53. Ge Y, Grossman RI, Babb JS, Rabin ML, Mannon LJ, Kolson DL. Age-related total gray matter and white matter changes in normal adult brain. Part II: quantitative magnetization transfer ratio histogram analysis. *AJNR Am J Neuroradiol.* 2002;23(8):1334-1341.

54. Lu PH, Lee GJ, Tishler TA, Meghpara M, Thompson PM, Bartzokis G. Myelin breakdown mediates age-related slowing in cognitive processing speed in healthy elderly men. *Brain Cogn.* 2013;81(1):131-138.

55. Lebel C, Gee M, Camicioli R, Wieler M, Martin W, Beaulieu C. Diffusion tensor imaging of white matter tract evolution over the lifespan. *Neuroimage.* 2012;60(1):340-352.

56. Zhang L, Dean D, Liu JZ, Sahgal V, Wang X, Yue GH. Quantifying degeneration of white matter in normal aging using fractal dimension. *Neurobiol Aging.* 2007;28(10):1543-1555.

57. Tang Y, Nyengaard JR, Pakkenberg B, Gundersen HJ. Age-induced white matter changes in the human brain: a stereological investigation. *Neurobiol Aging.* 1997;18(6):609-615.

58. Ding F, Yao J, Rettberg JR, Chen S, Brinton RD. Early decline in glucose transport and metabolism precedes shift to ketogenic system in female aging and Alzheimer's mouse brain: implication for bioenergetic intervention. *PLoS One.* 2013;8(11):e79977.

59. Omidi Y, Barar J. Impacts of blood-brain barrier in drug delivery and targeting of brain tumors. *Bioimpacts.* 2012;2(1):5-22.

60. Pan Y, Scanlon MJ, Owada Y, Yamamoto Y, Porter CJ, Nicolazzo JA. Fatty Acid-Binding Protein 5 Facilitates the Blood-Brain Barrier Transport of Docosahexaenoic Acid. *Mol Pharm.* 2015;12(12):4375-4385.

61. Schildge S, Bohrer C, Beck K, Schachtrup C. Isolation and culture of mouse cortical astrocytes. *J Vis Exp.* 2013(71).

62. Qiu J, Nishimura M, Wang Y, et al. Early release of HMGB-1 from neurons after the onset of brain ischemia. *J Cereb Blood Flow Metab.* 2008;28(5):927-938.

63. Endres M, Laufs U, Huang Z, et al. Stroke protection by 3-hydroxy-3-methylglutaryl (HMG)-CoA reductase inhibitors mediated by endothelial nitric oxide synthase. *Proc Natl Acad Sci U S A.* 1998;95(15):8880-8885.

CHAPTER 5

Interventional approaches to Cockayne syndrome treatment using a mouse model

Lear E. Brace[1], Sarah C. Vose[1], Alban Longchamp[1], Chris Hine[1], Evandro Fang[2], Sachin Thakur[3], David Sinclair[3], Roderick T. Bronson[4], Chih-Hao Lee[1], Bruce S. Kristal[5], James R. Mitchell.[1]

[1] Department of Genetics and Complex Diseases, Harvard T.H. Chan School of Public Health, 655 Huntington Ave, Boston, MA 02115, USA
[2] Laboratory of Molecular Gerontology, National Institute on Aging (NIA), National Institutes of Health (NIH), Baltimore, MD 21224, USA
[3]Department of Genetics, Harvard Medical School, 77 Louis Pasteur, Boston, MA, 02115, USA
[4]Rodent Histopathology Laboratory, Harvard Medical School, 77 Avenue Louis Pasteur, Boston, MA 02115, USA
[5] Departments of Neurosurgery, Harvard Medical School, Brigham and Women's Hospital, 221 Longwood Avenue, Boston, MA 02115, USA

Author contributions
L.E.B., S.C.V., and J.R.M. designed experiments. L.E.B., S.C.V., A.L., and E.F. performed the experiments. L.E.B., S.C.V., A.L., C.H., R.T.B., C.H.L., B.S.K., and J.R.M. analyzed the data.

ABSTRACT

Cockayne syndrome (CS) is a rare autosomal recessive disease caused by defects in key proteins of the nucleotide excision DNA repair pathway. Major CS symptoms include a severe growth defect, progressive peripheral and central demyelination and neurodegeneration, and a shortened lifespan of approximately 16 years. No treatment currently exists. The *Csa*$^{-/-}$/*Xpa*$^{-/-}$ mouse (CX), described by our group phenocopies all of these major aspects of the human disease, including a shortened lifespan of approximately 5 months, and thus represents a potential model in which to test novel interventional approaches. Here, we identified new markers of dysfunction in the CX mouse model, including defects in adipogenesis, hematopoiesis, hydrogen sulfide (H_2S) production, and increased serum markers of liver damage that could potentially be used in addition to lifespan to assess the efficacy of interventional approaches. We also tested novel approaches including adipogenic activators, H_2S supplementation and NAD+ precursor supplementation. One such intervention, the NAD+ precursor NMN, resulted in significant longevity extension, and improved outcome in other measures including preservation of hematopoietic potential.

INTRODUCTION

Cockayne syndrome is a rare congenital disorder caused by inborn defects in DNA repair with wide-ranging defects found in almost all organ systems including neurodegeneration, growth failure, and photosensitivity without cancer incidence. Many

of the commons symptoms of CS progressively worsen with age, even though the average lifespan is 16 years but can be as short as 2-5 years in the most severe forms[1]. The CX model developed by our lab phenocopies many symptoms observed in CS patients, including failure to thrive, progressive loss of adiposity, demyelination and neurodegeneration leading to premature death at approximately 5 months of age[2,3].

However, lifespan and progressive neurodegeneration are not the most convenient or necessarily the most useful markers with which to measure potential therapeutics. In this chapter, we thus evaluated a number of different cell/organ systems for the potential to serve as markers of disease progression, including adipose tissue, bone marrow stem cell populations, H_2S production capacity and serum markers of liver damage. Furthermore, we tested interventional approaches including fat transplant, NAD+ or H_2S supplementation to modulate phenotypes in these systems.

Previously we described the progressive loss of adiposity in CX mice and the contribution of a beneficial increase in fatty acid oxidation (FAO) to this process. However, there are other non-mutually exclusive mechanisms that could contribute to loss of adiposity which are unlikely to be beneficial, including defective adipogenesis and increased preadipocyte cellular senescence. Adipocyte differentiation is a tightly regulated process driven by the expression of several key genes that lead to conversion of resident mesenchymal progenitors to lipid-filled, mature adipocytes[4,5]. Differentiation is initiated by the inhibition of Pref-1, a negative regulator of adipocyte and osteoblast

differentiation, and the activation of CREB. This in turn activates C/EBPβ, inducing the expression of the transcription factors C/EBPα and PPARγ, which then bind to promoter regions of genes controlling adipocyte differentiation[6,7]. If adipogenesis were indeed defective in CX mice, contributing to adiposity loss, a potentially beneficial therapy could be activators of adipogenesis, or fat transplants from wildtype animals and could also provide increased substrate for fat oxidation upon damage. Furthermore, in several diverse progeroid models with various defects in NER (*Ercc1*[8], Pol Eta[9]), premature cellular senescence of preadipocytes in white adipose tissue has been demonstrated.

Observations in similar progeroid models depict fatty replacement and reduced hematopoiesis in bone marrow (BM), referred to as marrow adipose tissue (MAT), and support inquiry of the marrow populations in CX mice[10]. MAT has been shown to act as a negative regulator of hematopoiesis[11] and in a similar lipodystrophic model, *Ercc1*$^{-/-}$, fatty replacement of BM, along with reduced hematopoietic proliferation was observed[10]. BM consists of hematopoietic and mesenchymal stromal cell (HSC and MSC) lineages[12]. The former gives rise to all mature blood cell types through long-term reconstituting hematopoietic stem cells (LT-HSC)[13], and the latter able to differentiate into osteoblasts, chondrocytes, and adipocytes among other cell types[5]. Body fat stores are inversely correlated with MAT[14], and is often inversely correlated both to corporal fat and bone mineral density[15]. MAT cell density is known to increase upon ageing, during starvation, osteoporosis, and during normal pubertal bone development, making it unclear if the adipocytes are deleterious to bone mass and/or HSC populations, if they are just filling

space left by lost bone, or represent a compensatory mechanism to tackle bone loss[16]. Wild-type animals on 30% dietary restriction (DR) for at least 3 weeks have significantly elevated MAT with the decrease in body fat[17]. Similarly, individuals with Anorexia Nervosa (AN) have significantly less body fat, leading to increased MAT and elevated circulating levels of Pref-1; both of which can be reversed with increased weight gain[18,19].

Another potentially influential endpoint is the production of H_2S, which has emerged recently as a biologically relevant gas that has toxic effects at high doses but beneficial effects on health at low doses. Our group showed that dietary restriction (DR) or methionine restriction (MetR) increases the production of H_2S in the liver and kidney of wildtype animals and its production is essential for DR-mediated stress resistance[20]. H_2S has also been shown to increase with diet-induced lifespan extension[20] and with data showing MetR increases lifespan of CX mice[3], probing the production of H_2S in this mouse model might prove to be a powerful endpoint.

Finally, enzymes such as aspartate transaminase (AST) and alanine transaminase (ALT) are commonly elevated in CS patients, indicative of mild liver damage[21] and would be easily accessible serum markers that would be measurable throughout the lifespan of CX mice to mark any reductions due to effective therapy.

RESULTS

Endpoints to measure adipose loss in CX mice

Throughout their short lifespan, CX mice progressively lose body weight, specifically body fat[2,3]. While we were aware of at least one mechanism of lipodystrophy via increased FAO[3], other pathways may also contribute to the overall adipose loss. We previously suspected that adipocyte size was reduced in CX mice from H&E staining of adipose tissue throughout the lifespan[3]. Subcutaneous WAT was then excised from CX mice and non-mutant littermates and cell number was counted per milligram of tissue. We determined that CX mice have an average of two fold more cells per mg of subcutaneous WAT (Figure 5.1 a). This experiment does not correct for cell size or lipid content and thus these limitations must be considered. However, it does show there are significant differences in adipose tissue of CX animals vs. non-mutant littermates supporting further inquiry. The reduced size of adipocytes urged us to next investigate if there exists a failure in adipogenesis, which should differentiate pre-adipocytes into mature adipocytes with a single, large lipid droplet. We isolated subcutaneous fat from month-old CX and non-mutant littermates and processed and plated pre-adipocytes from the stromal vascular fraction. The cells were then differentiated over 2 weeks using a cocktail of dexamethasone, IBMX, indomethacin, and insulin, and mature adipocytes stained with Oil Red O. Pre-adipocytes from WT and $Csa^{-/-}$ mice consistently differentiated into large lipid filled droplets while $Xpa^{-/-}$ cells displayed a lower efficiency (Figure 5.1 b). However,

the adipogenesis was severely impaired in CX cells and any lipid-filled cells were significantly smaller (Figure 5.1 b). Furthermore, mRNA gene expression of adipogenesis-related genes reflected significant impairment in differentiated CX adipocytes, while supporting a gene expression profile of increased FAO (Figure 5.1 c). Whether this defect stems from the inability to terminally differentiate or if these cells are simply not accumulating fat due to increased FAO or both, remains to be determined. Impaired adipogenesis could also result from aging-induced cellular senescence[22]. Indeed, when subcutaneous fat was isolated from young and old WT and CX mice, we found a significant increase in SA-β-galactosidase staining in CX fat compared to WT at a young age, with a further increase over the lifespan (Figure 5.1 d). CX fat thus far is simultaneously being rapidly burned for fuel, undergoing senescence, and showing impaired adipogenesis.

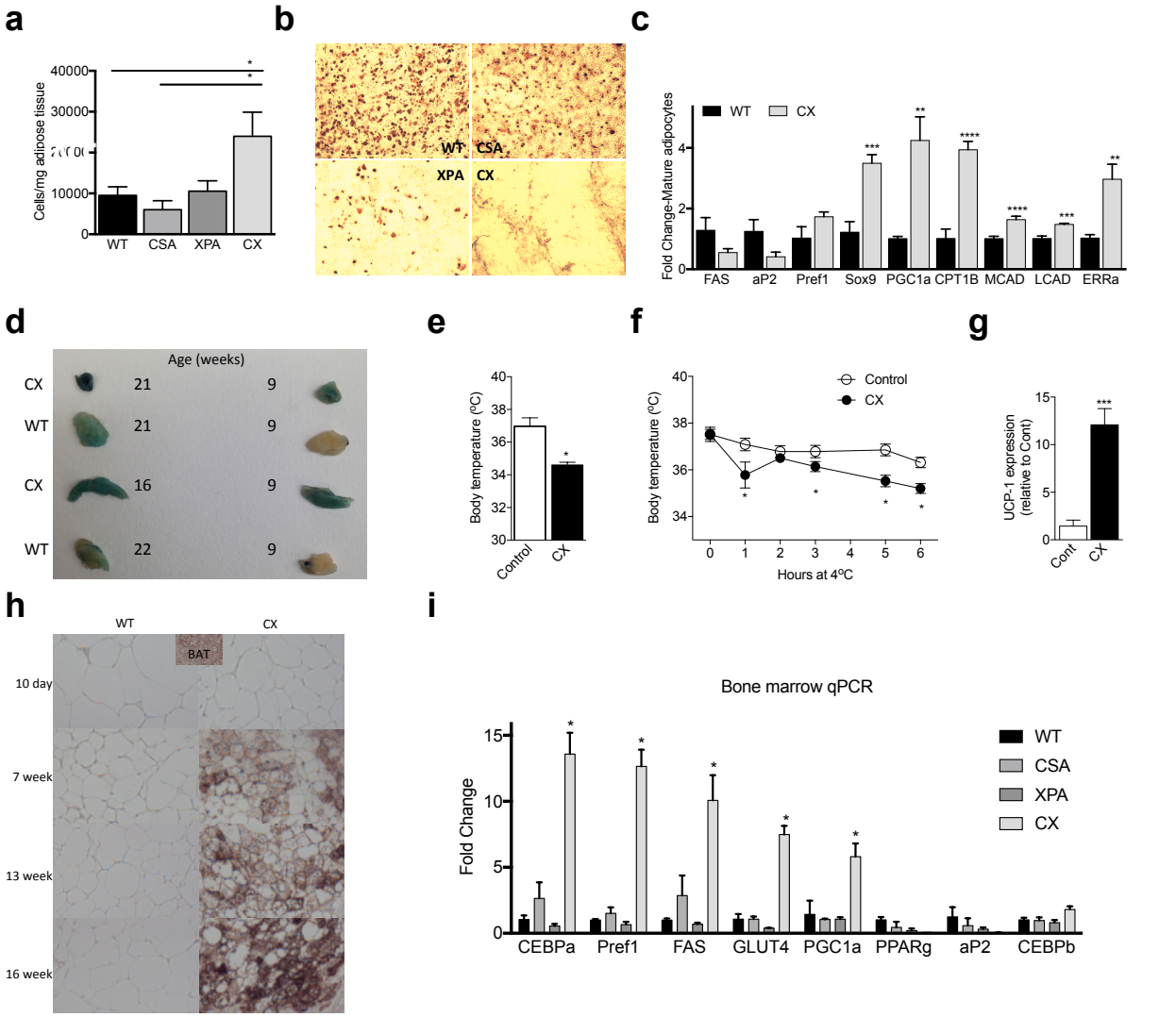

Figure 5.1 Endpoints to measure adipose loss in CX mice. a. Number of cells per mg tissue isolated after collagenase II digestion of subcutaneous WAT from the indicated genotypes, n=5-9/genotype at 4 weeks of age, Student's t test. **b**. Oil red O staining of differentiated adipocytes isolated from the stromal vascular fraction of subcutaneous WAT from the indicated genotypes, representative image of n=4/genotype, age 12-16 weeks. **c**. mRNA expression of mature adipocytes differentiated from the stromal vascular fraction of subcutaneous WAT from WT and CX mice, n=4/genotype, Student's t test. **d**. SA-β galactosidase staining of subcutaneous WAT isolated from WT and CX mice at the indicated ages. **e**. Basal body temperature of WT and CX mice by anal probe n=3/genotype, Student's t test. **f**. Body temperature over time of WT and CX mice after being placed at 4°C for six hours, n=5-6/genotype, Student's t test. **g**. mRNA expression of WT and CX WAT n=4, Student's t test. **h**. Immunohistochemistry for UCP-1 expression in subcutaneous white adipose tissue slides from WT and CX mice at the indicated ages. **i**. Gene expression of flushed bone marrow from mice of the indicated genotype between ages 13-17 weeks, n=3/genotype, Student's t test. *p<0.05, **p<0.01, ***p<0.001, ****p<0.0001.

A side effect of losing body fat is loss of insulation, and we had known for years that CX animals must be housed with control animals to provide warmth. We then measured body temperature and determined that CX animals have a lower baseline body temperature (Figure 5.1 e) are unable to regulate their body temperature when placed in a cold environment (Figure 5.1 f). Subsequently, we investigated alterations in brown fat, as its primary function is thermoregulation. *Ucp-1* expression levels were indeed increased in CX adipose tissue compared to controls (Figure 5.1 g). We then measured UCP-1 expression in subcutaneous fat depots by immunohistochemistry and saw increased browning in CX mice from middle (7 weeks) to old age (16 weeks) (Figure 5.1 h). The fact that brown fat contains numerous, small lipid droplets and an increased number of mitochondria led us to hypothesize that at the same time CX animals are burning fatty acids isolated from the lipid droplets of potentially immature white fat, the process of browning to produce heat could occur simultaneously.

A prominent phenotypic overlap exists between short-lived progeria models such as CX mice, long-lived dwarf mice, and caloric restriction including a reduced size and body temperature, hypoglycemia and alterations in the growth hormone/insulin-like growth factor-1 (GH/IGF-1) axis[23]. Since wildtype animals on DR rapidly lose body fat while simultaneously increasing MAT[17], we next sought to determine if the lack of adipogenesis occurring in CX fat depots paralleled with increased adipogenesis in MAT. Bone marrow was flushed from control littermates and CX animals and significant

elevations in mRNA expression of many genes regulating adipogenesis were observed in CX BM (Figure 5.1 i).

We determined several mechanisms of loss of peripheral adiposity in the CX model including increased FAO, dysfunctional adipogenesis, cellular senescence, and browning. Interventions, such as adipogenic activators could be utilized and the efficacy established using the endpoints described here. We also observed a potential relationship between peripheral adiposity and adiposity of the bone marrow niche, which merits further investigation.

Defective hematopoietic cell growth in CX mice with amelioration upon NAD+ repletion

Considering the frequently inverse relationship between WAT and MAT[14,17,24,25] and the severe lack of body fat in CX mice, CX BM should be primed for formation of MAT compared to BM of WT mice. We first investigated the bone marrow niche of femurs for signs of alterations in adiposity. We determined a significant increase in marrow adiposity in CX long bones compared to control littermates (Figure 5.2 a). In this niche, hematopoietic stem cells differentiate into adipocytes, among other cell types[5]. Flushed bone marrow was then plated in a methylcellulose media and the hematopoietic cell growth was measured over one week. A 2.5-fold reduction in hematopoietic cell proliferation was measured in CX BM cells compared to BM of non-mutant littermates

(Figure 5.2 b). It is unclear if this cell population is exhausted due to increased differentiation into marrow fat, however it does serve to be an effective marker of dysfunction. Co-transplantation of CX BM into irradiated wild-type mice could determine if stem cell progenitors are able to self-renew. As a potential therapy, WT BM transplants could normalize HSC and MSC populations within CX mice and potentially aid in body fat maintenance and/or development.

Another potential therapy that could utilize HSC proliferation as a measurable endpoint is NAD+ supplementation. We also measured HSC proliferation in cohort of WT and CX animals treated for two weeks with 500mg/kg/day NR compared to vehicle treated[26]. CX animals treated with vehicle again have significantly reduced hematopoietic growth compared to WT mice, however with 2 weeks of NR treatment, CX HSC proliferation is significantly increased compared to even WT animals that received NR (Figure 5.2 c). Interestingly, NR treatment did slightly but significantly reduce HSC proliferation in WT animals (Figure 5.2 c). Performing daily injections is not only laborious for the investigator, but also detrimental for an animal to receive a regular prick.

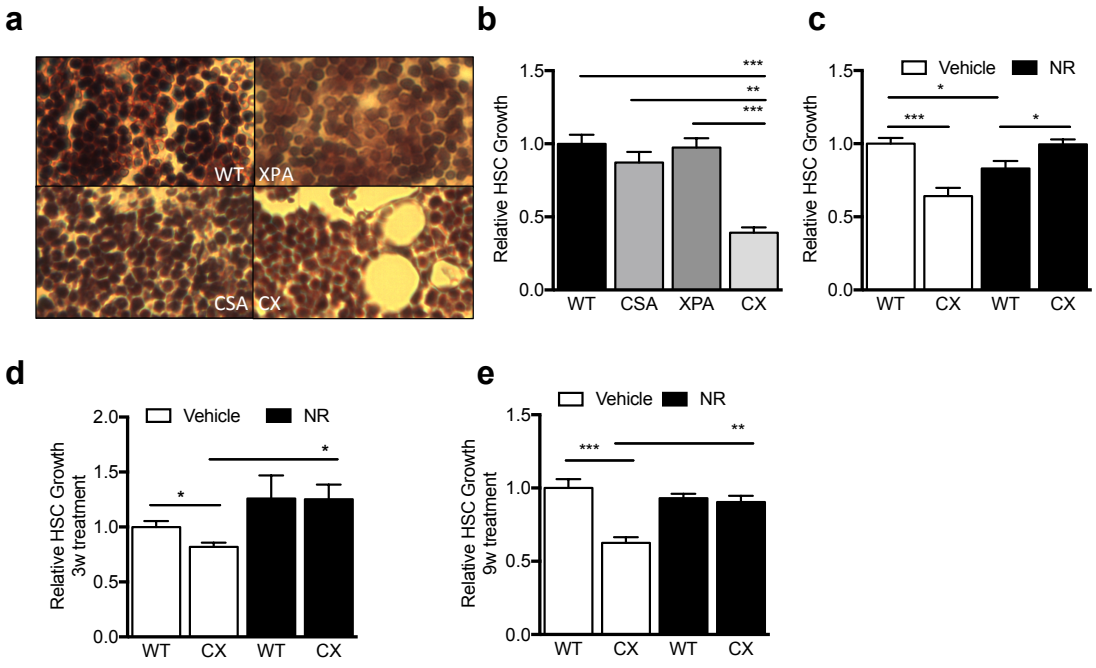

Figure 5.2 Defective hematopoietic cell growth in CX mice with amelioration upon NAD+ repletion. a. H&E staining of long bones isolated from 5-6 week old mice of indicated genotypes. **b**. Hematopoietic cell growth from flushed bone marrow of indicated genotypes over 1 week in methylcellulose media, n=7-8/genotype, Student's t test. **c**. Hematopoietic cell growth in methylcellulose media from flushed bone marrow of indicated genotype with either 2 week daily intramuscular injection of saline or 500mg/kg NR, n=4/group, Student's t test. **d**. & **e**. Hematopoietic cell growth in methylcellulose media from flushed bone marrow of indicated genotypes that either drank regular water of NR-treated water (500mg/kg/mouse) for 3 weeks (**d**, n=3/group), or 9 (**e**, n=4-6/group) weeks, Student's t test. *p<0.05, **p<0.01, ***p<0.001.

For this reason, we then resuspended NR in the drinking water of CX and WT animals. After 3 weeks of drinking NR water, CX animals significantly increased HSC proliferation (Figure 5.2 d), and to an even greater expanse after 9 weeks (Figure 5.2 e). Undoubtedly, fatty replacement and/or defects in hematopoietic progenitor cell proliferation can lead to critical abnormalities in mature blood cells, and these endpoints merit further investigation in the CX mouse model for interventional approaches such as NAD+ supplementation.

Beneficial responses to NAD+ precursors in healthspan and lifespan of CX mice

Following positive results from the use of short-term NR to increase NAD+ levels in CX mice, we then explored using NMN, which is the metabolized product of NR and is thought to be a more stable NAD+ precursor (David Sinclair, personal communication). A cohort of 24 CX mice were split between a vehicle normal water group or NMN-treated water and metabolic parameters were measured throughout their lifespan. CX animals treated with NMN showed no significant alterations in body weight or composition (Figure 5.3 a-e), however they did maintain adiposity late in life (Figure 5.3 b,c) while consuming similar amounts of food and water compared to untreated, though more food water consumed for longer in life (Figure 5.3 f, g). There were also no significant changes in fasted blood glucose levels or serum β-hydroxybutyrate (BHB) (Figure 5.3 h, i). However, CX animals that drank NMN-treated water had a significantly increased median and maximum lifespan compared to CX mice that drank normal water (mean 18.4wks water vs. 19.9wks NMN water, maximum 20.3wks water vs. 21.6wks NMN water; log-rank test p=0.039) (Figure 5.3 j). Clearly the metabolic endpoints described above are not useful for this intervention, however lifespan extension was achieved in CX animals and NMN treatment continues to be an attractive therapy for use in human CS patients.

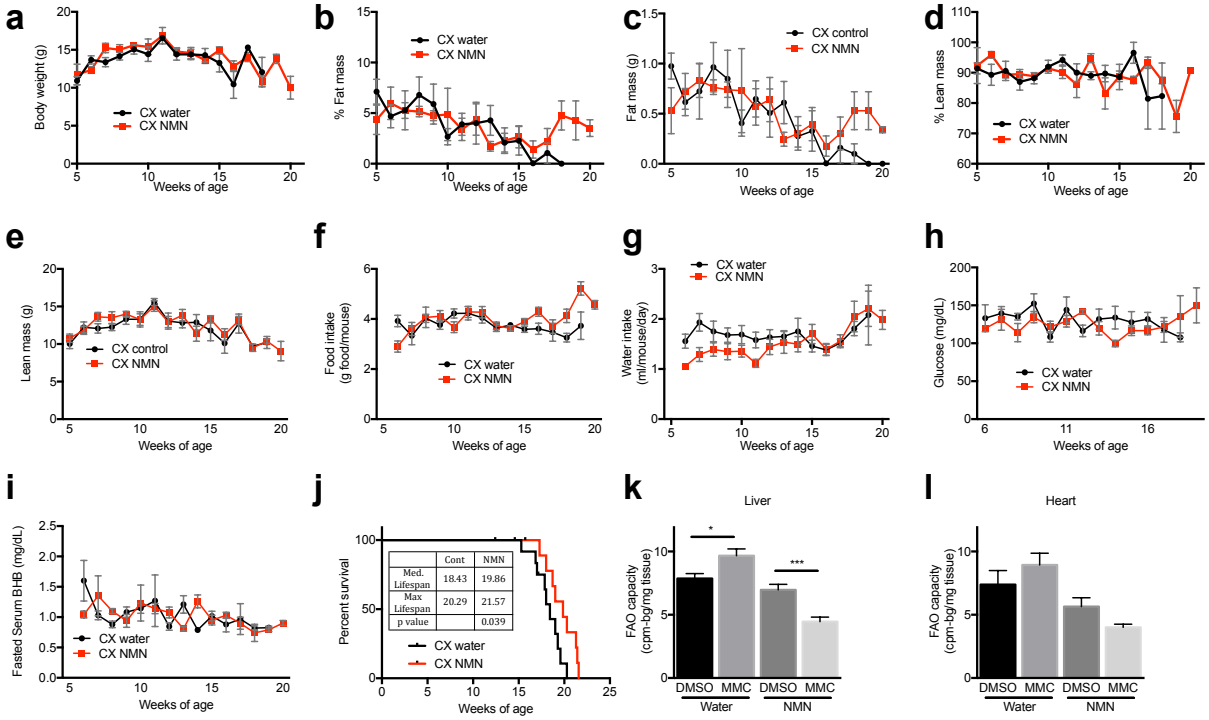

Figure 5.3. Beneficial responses to NAD+ precursors in healthspan and lifespan of CX mice. a.-f. Body weight **(a)**, percent fat **(b)**, absolute fat **(c)**, percent lean **(d)**, absolute lean **(e)**, food intake **(f)**, water intake **(g)**, blood glucose **(h)**, β-hydroxybutyrate levels in fasted serum **(i)** and lifespan **(j)** of CX mice that drank regular water or NMN-treated water beginning at 6 weeks of age, n= 10-12/group. **k-l**. Cumulative FAO capacity of Liver (**k**) and Heart (**l**) from Control mice 24hours after a single injection of 10mg/kg MMC or saline that drank either regular water or NMN-treated water from 6 weeks of age, n=3-4/group, Student's t test. *p<0.05, ***p<0.001.

As stated previously, CX animals must be housed with WT animals for warmth as well as for assistance in creating a nest from bedding. As a result, WT animals were also treated with NMN in the drinking water for 20+ weeks. Though NR treated WT displayed no significant improvement in hematopoietic cell growth (Figure 5.2 c), we questioned whether long term NMN treatment would modulate the acute DNA damage response of increased FAO described previously [3]. We then injected WT animals that drank normal water and NMN water with an acute dose of mitomycin C, MMC, an intrastrand crosslinking agent. Twenty-four hours later, mice were harvested and the capacity to burn

exogenous tritiated palmitate was measured *ex vivo* for one hour. In each tissue, NMN treatment reduced the DMSO injected FAO capacity, however, the response of increased capacity in response to MMC was blunted significantly in the liver and with a trend in the heart (Figure 5.3 k, l). We previously concluded that increased FAO is in fact a beneficial response to increased DNA damage in order to increase levels of ATP. NMN treatment could then ease the energy demand on the cell by providing more substrate for PARP-1, which would then require less ATP utilization via salvage/recycling of NAD+.

Hydrogen sulfide in Cockayne syndrome

The metabolic alterations seen in short-lived progeria models have long been compared to DR[23]. Our lab recently determined that DR induces the production of hydrogen sulfide, which has protective effects for stress resistance[20]. Furthermore, H_2S levels are thought to decline with age[27]. We thus began by measuring H_2S in young and old control vs. CX mice using the lead acetate method whereby homogenized liver was mixed with a substrate and cofactor and exposed to lead acetate soaked filter paper. The amount of H_2S produced in a certain timeframe is determined by the amount of black precipitate in the form of lead sulfide. There was no observable difference in H_2S produced by CX livers by ten days of age compared to controls, but by 15 weeks CX livers had a significantly increased capacity for H_2S production that could be further increased with a short fast (Figure 5.4 a). Next, we measured H_2S production in liver and brain from WT and CX animals throughout the lifespan and after long-term MetR. In WT liver, H_2S

production peaked around 10 weeks of age and showed an increase upon MetR whereas production may be at maximum capacity by "middle age" in CX liver (Figure 5.4 b). However, in WT brain, no observable changes in H_2S production were seen with age though a slight increase upon MetR and capacity was lower in CX brain, especially upon MetR (Figure 5.4 b).

Since H_2S production appeared to increase with methionine restriction that also is known to intensify FAO, we then measured serum H_2S production in response to acute DNA damage, which we have shown to increase FAO *in vitro* and *in vivo* (Figure 3.4). WT animals injected with a single acute dose of MMC produced a significant increase in H_2S production compared to saline injected controls (Figure 5.4 c). Another chemotherapeutic agent, cyclophosphamide also increased H_2S production though to a lesser degree (Figure 5.4 d). The regulation of H_2S production in specific tissues is being readily investigated, and if and how metabolism alters production is yet to be determined.

Next, we asked whether increasing H_2S in CX mice via a prodrug could potentially improve healthspan and increase lifespan. We utilized the Sulfagenix, sodium polysulthionate, a H_2S prodrug, and fed it to 12 CX mice at 80mg/kg/day in a final 1% agar-based casein diet with a control group of 12 CX mice that ate the casein diet without drug. We found no significant differences between groups in all metabolic parameters, including weight, fat and lean percentage and mass, fasted blood glucose and BHB, or food and water intake (Figure 5.4 e-m). Unfortunately, we also failed to observe any

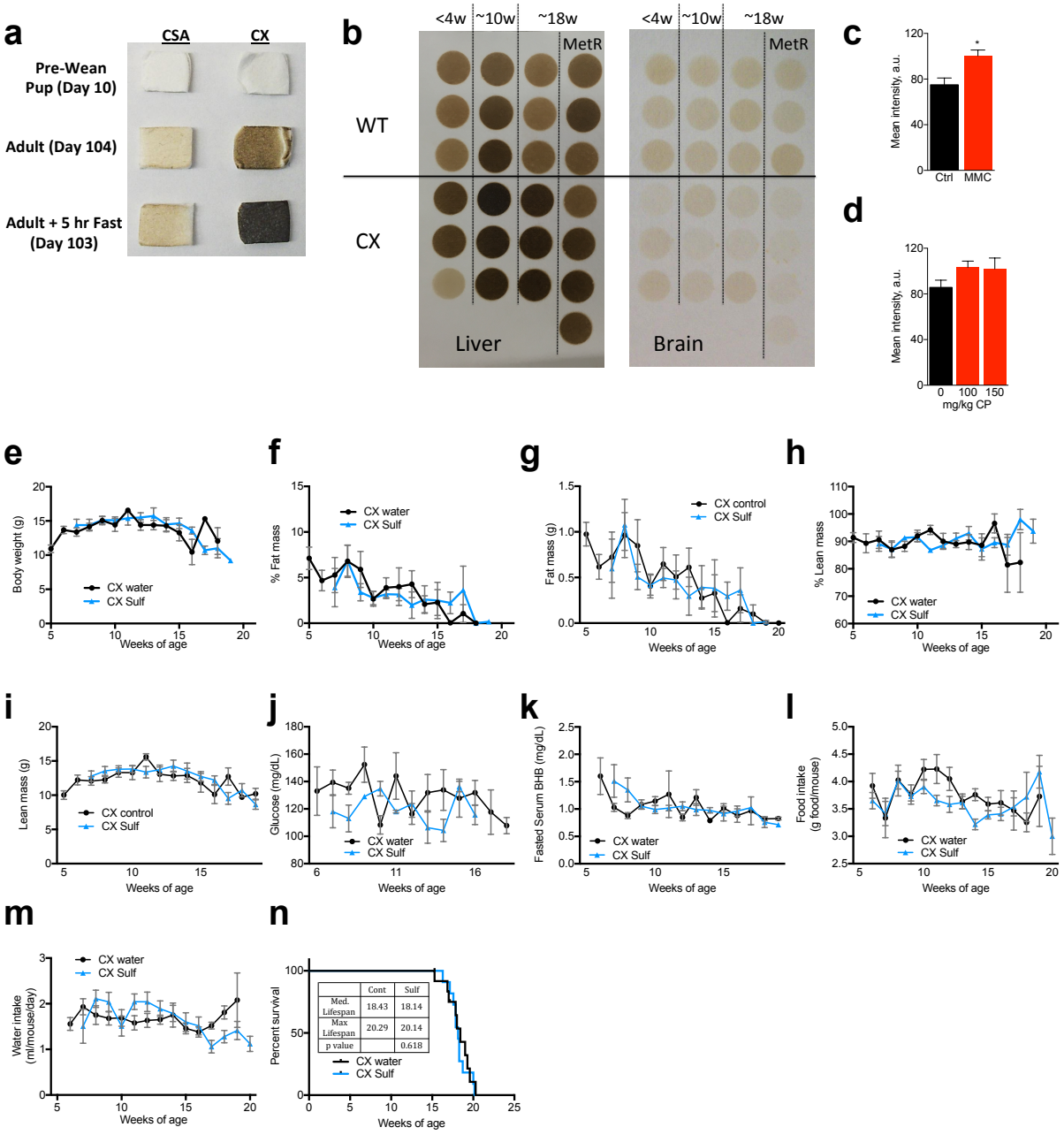

Figure 5.4. Hydrogen sulfide in Cockayne syndrome. a. Hydrogen sulfide (H_2S) production visualized by lead sulfide production on lead acetate-treated filter paper by liver homogenates from the indicated genotypes at the indicated ages. **b**. H_2S production visualized by lead sulfide production on lead acetate-treated filter paper covering a 96 well plate by liver and brain homogenates from the indicated genotypes fed the indicated diets at the indicated ages. **c.-d**. H_2S production visualized by lead sulfide production on lead acetate-treated filter paper and quantified using ImageJ of liver homogenates from WT mice injected with a single dose of either saline or MMC (**c**) or cyclophosphamide (**d**) after 24 hours, n=3-4/group, Student's t test. **e.-n**. Body weight, **(e)** Percent fat **(f)**, absolute fat mass (**g**), percent lean **(h)**, absolute lean mass (**i**), blood glucose **(j)**,

Figure 5.4 Legend continued:
β-hydroxybutyrate levels in fasted serum **(k),** food intake **(l),** water intake **(m)**, and lifespan **(n)** of CX mice that ate casein 1% agar based diet with or without 80mg/kg sulfagenix H_2S prodrug beginning at 6 weeks of age, n= 10-12/group.

benefit of the prodrug on lifespan in CX mice (Figure 5.4 n) as was observed with lifetime NMN supplementation (Figure 5.3 j). Though at this dose, we failed to see an improvement in CX lifespan, higher doses could prove efficacious.

Serum markers as cross-sectional endpoints in CX mice

The most effective endpoints for measuring the value of an intervention are often ones that can be performed longitudinally with minimally invasive procedures. We showed previously that serum triglyceride (TG) levels are significantly reduced in CX mice, especially under fasted conditions (Figure 3.1 i, j). MetR thus far has been the most successful intervention, increasing lifespan of CX mice to a maximum of 27 weeks (Figure 3.6 c), whereas NMN has provided positive but lesser improvements (Figure 5.3 j). We then measured fasted serum TG levels in CX mice vs. controls during these interventions. Surprisingly, while a long-term MetR diet decreased serum TG levels in wildtype mice, CX mice produced increased serum TG levels up to wildtype levels (aged 16-20 weeks, Figure 5.5 a). However, no improvements in serum TG levels were seen in CX mice treated with two-week daily injections of NR (Figure 5.5 b) or during NMN provided in drinking water or Sulfagenix in the food (Figure 5.5 c).

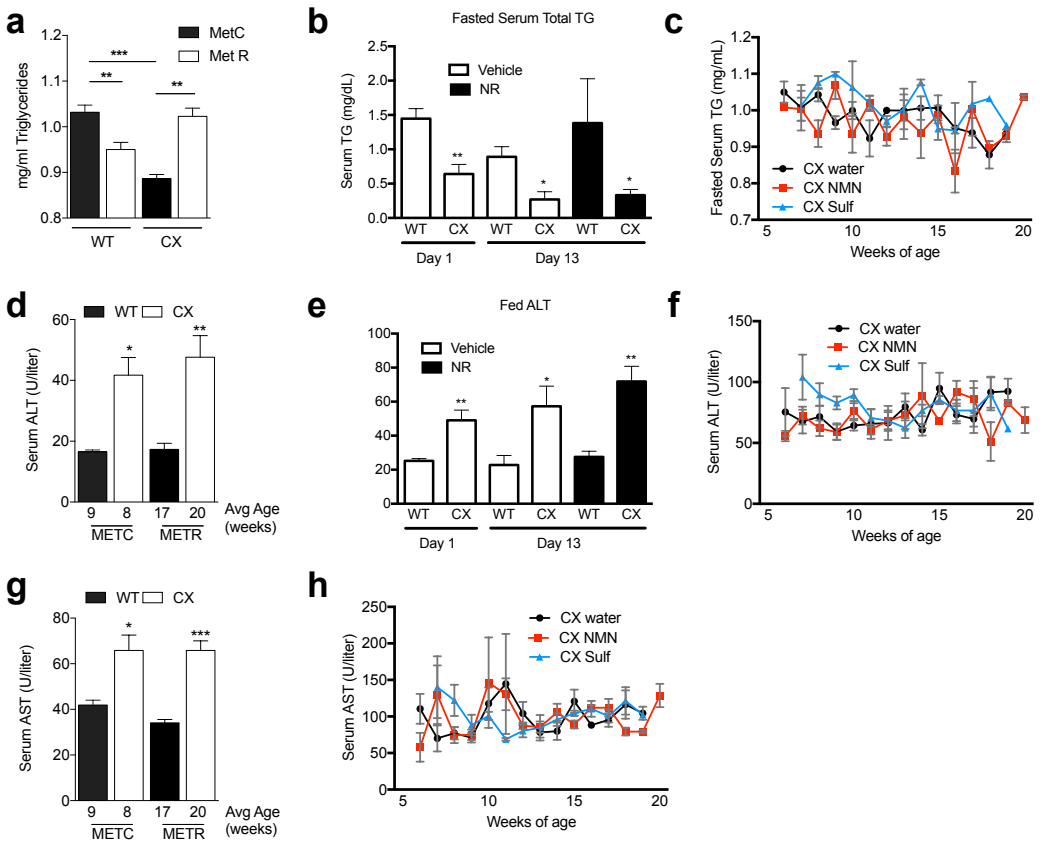

Figure 5.5. Serum markers as cross-sectional endpoints in CX mice. **a**. Triglyceride levels in fasted serum obtained from the tail vein of WT and CX mice on a methionine sufficient or methionine restricted diet, n=3/group, aged 16-20 weeks, Student's t test. **b**. Triglyceride levels in fasted serum obtained from the tail vein of WT and CX mice before and after daily 2 week intramuscular injections with 500mg/kg/day NR or saline, n=4/group, aged 10-15 weeks, Student's t test **c**. Triglyceride levels in fasted serum obtained from the tail vein of CX mice throughout the lifespan consuming either regular water and food, NMN-treated water and regular food, or regular water and Sulfagenix treated food, n=12/group. **d**. ALT levels from fed serum obtained from the tail vein of WT and CX mice on a methionine sufficient or methionine restricted diet, n=3-4/group. **e**. ALT levels in fed serum obtained from the tail vein of WT and CX mice before and after daily 2 week intramuscular injections with 500mg/kg/day NR or saline, n=4/group, aged 10-15 weeks, Student's t test. **f**. ALT levels in fed serum obtained from the tail vein of CX mice throughout the lifespan consuming either regular water and food, NMN-treated water and regular food, or regular water and Sulfagenix treated food, n=12/group, Student's t test. **g**. AST levels from fed serum obtained from the tail vein of WT and CX mice on a methionine sufficient or methionine restricted diet, n=3-4/group. **h**. AST levels in fed serum obtained from the tail vein of CX mice throughout the lifespan consuming either regular water and food, NMN-treated water and regular food, or regular water and Sulfagenix treated food, n=12/group, Student's t test. *p<0.05, **p<0.01, ***p<0.001, ****p<0.0001.

We next asked whether these interventions mediated alterations in AST and ALT, liver enzymes that measure inflammation and damage. Liver enzymes are continuously significantly increased compared to wildtype controls. The increased ALT and AST levels obtained in CX mice compared to controls failed to be lowered upon treatment with MetR, NR, NMN, or Sulfagenix treatment (Figure 5.5 d-h). Both TG and liver enzymes are easily measured in the serum of mice as in human patients. Though not all interventions attempted here proved efficacious using these endpoints, they remain attractive methods for quick and relatively painless measures of improvement for new therapies.

DISCUSSION

Because the CX mouse presents with the major symptoms of CS, including neurodegeneration, failure to thrive and short lifespan, it has considerable potential as a useful tool in which to test interventional approaches. Nonetheless, lifespan and progressive neurodegeneration are not the most convenient or necessarily the most useful markers with which to measure potential therapies. The data presented here represent an attempt to further define perturbations in the CX model that could both improve our understanding of the etiology of pleiotropic disease symptoms, while at the same time provide better markers that can be measured over time to determine if a therapy is successful and worth testing in CS patients.

We found evidence of defective adipogenesis and increased cellular senescence, both of which could contribute to loss of adiposity, in addition to the previously described increase in fatty acid oxidation. Increased browning and reduced thermogenesis was also observed in CX mice, which could serve to further compromise WAT function. As is typical in many settings in which general adiposity is reduced, we also observed an inverse increase in adipogenesis in the bone marrow niche, which could compromise hematopoietic cell growth. This was accompanied by defects in HSC growth *ex vivo*, suggestive that in addition to increased marrow adiposity, cell autonomous defects in CX HSCs could contribute to reduced stem cell function.

Two pharmacological interventions, NAD+ supplementation in the form of NMN or NR, and H_2S supplementation in the form of a pro-drug, were tested in CX mice. Neither significantly altered lean or fat body mass or altered blood glucose or fasted ketone body production, but NMN did significantly increase lifespan in a small cohort. Though the H_2S pro-drug did not improve overall lifespan or alter markers of healthspan, we do have evidence of an already increased production of H_2S in CX mice compared to controls. This response may tie in to the metabolic adaptation of DNA damage driving increased oxidative phosphorylation as we did see increased H_2S production in serum from animals treated with a single acute dose of genotoxic agents.

Lastly, we explored the use of serum markers that can be measured weekly with little to no disruption to the animal. While we did observe improvement in fasted serum

TG in CX mice fed a MetR diet, no improvement was made with NAD+ supplementation in the form of NMN or NR. Furthermore, we showed that CX mice have increased liver enzymes and although NAD+ supplementation did not reduce AST or ALT levels, they serve as valuable markers of dysfunction.

The endpoints described here that would be the most ideally measured in CS patients include serum and blood markers, either under fasted or fed conditions, including hydrogen sulfide production, liver enzymes, ketone bodies, glucose, and triglycerides. Fat transplants and/or activators of adipogenesis could be utilized as an interventional therapy for CS patients and may aid in fat production to fuel the beneficial metabolic adaptation of increased FAO. There are currently no treatments for patients with Cockayne syndrome. Most therapies are palliative such as cataract surgery, drugs for tremors and seizures, and physical therapy. The use of mouse models of CS, especially the most severe types as modeled using CX mice, could progress on this front using endpoints and potential interventions such as those described here.

MATERIALS & METHODS

Mice All mouse experiments were performed with the approval of the Harvard Medical Area institutional animal care and use committee. Mice carrying *Xpa* and/or *Csa* knockout alleles in a C57BL/6 background and AMPKα1 knockout mice in a C57BL/6

background were maintained under standard laboratory conditions (temperature 20–24 °C, relative humidity 50–60%, 12hr light/12hr dark) and allowed free access to food (Research Diets D12450B with 10% calories from fat, 18% from casein and 72% from carbohydrate) and water unless otherwise indicated as described previously[3]. Other diets utilized include facility chow pellets (PicoLab 5058, Purina, St. Louis, MO, USA), high fat diet (Research diets, 60% calories from fat), and a 1% agar-based diet using D12450BSpx (Research Diets, New Brunswick, NJ, USA) and individual crystalline amino acids (Ajinomoto, Tokyo, Japan) in proportions to those in casein. MetR diets contained 1.5g Met/kg food and lacking Cys[28] compared to MetC diet with the same amino acid composition except for 4.5g Met/kg food. Cohorts of WT and CX mice were treated intramuscularly with saline or 500mg/kg/day NR as published [26]. A cohort of WT +/- NMN treated mice was IP injected with 10mg/kg mitomycin C, 100-200mg/kg cyclophosphamide or saline and organs harvested 24 hours later.

Lifespan mouse study A cohort of 36 CX mutants were split into 3 arms, first ate a casein diet in 1% agar and drank normal water, the second ate the casein diet in 1% agar with NMN-treated water for a dose of 500mg/kg/day/mouse, and the third ate casein diet in 1% agar with 80 mg/kg/day/mouse Sulfagenix (SG1002, Australia) and regular water. In addition, 8 WT mice per group were utilized as supportive littermates to CX mice. Mice were weighed and MRI'd weekly, as well as biweekly blood draws. Water and food intake was measured daily. Fed serum was isolated to measure ALT, AST, and LDH (Infinity, Thermo, Cambridge, MA, USA), and 6hr fasted serum for triglycerides (Sigma, St. Louis,

MO, USA) and ketone bodies (Pointe Scientific, Canton, MI, USA). Fasted blood glucose was also determined biweekly (EasyStep OneTouch, Lifescan, USA).

H_2S The lead acetate method of H_2S measurement was performed as in [20] but briefly, snap-frozen liver was homogenized in passive lysis buffer, freeze thawed twice and cleared by centrifugation. Samples were normalized to protein content and 10mM L-cysteine and 10mM pyridoxal-phosphate (PLP) was added as substrate and cofactor, respectively. Lead acetate paper was prepared by soaking filter paper in 20mM lead acetate and drying by vacuum. H_2S reaction mixes were then placed in closed containers with the paper sitting above the liquid phase to capture gas produced at 370C. Reactions were stopped when brown colored lead sulfide precipitate was visible. The mean intensity can also be determined using ImageJ.

Cellular experiments MDFs were isolated as in Chapter 3 and passaged in 20% FBS in DMEM + Penicillin/Streptomycin (P/S). All cell lines were incubated in 5% CO_2 and 3% O_2. The chemical P3 H_2S probe [29] was a gift by the Kyo Han Ahn from the Center for Electro-Photo Behaviors in Advanced Molecular Systems in South Korea. P3 probe (10μM) was added to cells 1 hour before detection by plate reader (excitation 360nm, emission 528nm) with or without 1hr serum deprivation.

Bone marrow The hind legs of mice were removed and cleaned of muscle and adipose tissue. The femur and tibia bones were then isolated and flushed with PBS by inserting an

18½ gauge needle. RNA was isolated from these cells and prepared for qRT-PCR as described below. Cells were also counted and 80,000 were plated in 24 well plates in 1ml of Methocult media (StemCell Technologies, Vancouver, Canada). After one week, the numbers of cells were counted. Whole long bones were also prepared and sectioned, embedded, and stained for H&E by the Harvard Rodent Histopathology lab.

Pre-adipocyte isolation and Adipogenesis Subcutaneous fat pads from WT, *Csa*$^{-/-}$, *Xpa*$^{-/-}$, and CX mice at 14-16wks of age were isolated, washed in PBS and minced. Tissue was digested for 60 minutes with 1mg/ml Collagenase II in HBSS with 7.5% FBS then passed through a 70μM filter and spun at 400g for 10 minutes. The floating adipocytes were removed and the pelleted stromal vascular fraction (SVF) was resuspended in erythrocyte lysis buffer (154mM NH_4Cl, 5.7mM K_2HPO_4, 0.1mM EDTA) for 10 minutes. The cells were then pelleted again, washed in PBS, and resuspended in 1:1 DMEM:Ham's F12 + P/S and 10% FBS. Media was changed every 2-3 days until 90% confluency was reached in about 7 days. Cells were plated to confluency in 12 well plates and differentiated using 1 μM dexamethasone, 200 μM indomethacin, 0.5 mM IMBX, and 1 μM insulin with every other day induction over the course of 2 weeks. When terminal differentiation is achieved, media is removed and wells rinsed with PBS. Wells incubated in 10% formalin for 30-60 minutes at room temperature. A stock solution of 300mg Oil Red O powder in 100ml 99% isopropanol is prepared and mixed 3 parts stock solution to 2 parts DI water and filtered. Wells are then rinsed with DI water and 60% isopropanol added for 5 minutes. Filtered Oil Red O solution is then added for 5 minutes at room

temperature. Wells are then rinsed with tap water until water runs clear. Cells can then be imaged.

SA-β galactosidase assay for senescence Subcutaneous abdominal wall adipose tissue was dissected from mice and fixed in 24 well plates in 2.5% formaldehyde and 0.25% glutaraldehyde in 1x PBS at 40C for 2-4 hours. Tissues are then washed 3x with PBS and incubated with lacZ staining solution for 370C for several hours (10ml lacZ solution: 8.55ml Solution I (2mM $MgCl_2$, 0.02% NP-40, 0.01% deoxycholic acid, 4mg/ml spermidine, in PBS pH 8), 0.45ml Solution II (210mg/ml $KFe^{2+}(CN)_6$ in DI water), 0.5ml Solution III (165mg/ml $KFe^{3+}CN$ in DI water), 0.5ml X-gal (20mg/ml in 1:1 DMSO:EtOH). Tissue then washed three times in PBS and kept in 50% EtOH in PBS.

Real time quantitative Polymerase Chain Reaction Total RNA was isolated from tissues using Qiazol (QIAGEN, Hilden, Germany) and cDNA synthesized by random hexamer priming with the Verso cDNA kit (Thermo, Cambridge, MA, USA). qRT-PCR was performed using Taq-Pro DNA polymerase (Denville, Holliston, MA, USA) and SYBR green dye (Lonza, Portsmouth, NH, USA). Fold changes were calculated by the DDC_t method using β-actin as a standard, and normalized to the experimental WT control. Primer sequences are as follows:

β-actin F:AGCTTCTTTGCAGCTCCTTCGTTG R:TTCTGACCCATTCCCACCATCACA
Cd36 F: GAGCAACTGGTGGATGGTTT R: GCAGAATCAAGGGAGAGCAC
Cpt1β F: TTGCCCTACAGCTGGCTCATTTCC R: GCACCCAGATGATTGGGATACTGT
Lcad F:TCTTTTCCTCGGAGCATGACA R:GACCTCTCTACTCACTTCTCCAG
VLCAD F:CTACTGTGCTTCAGGGACACC R:CAAAGGACTTCGATTCTGCCC
Acox1 F: CCTGATTCAGCAAGGTAGGG R: TCGCAGACCCTGAAGAAATC

Pparα F: TGTTTGTGGCTGCTATAATTTGC
R: GCAACTTCTCAATGTAGCCTATGTTT
Errα F:ACTGCCACTGCAGGATGAG R:CACAGCCTCAGCATCTTCAA
aP2 F:AAGGTGAAGAGCATCATAACCCT R:TCACGCCTTTCATAACACATTCC
Pref-1 F:AGTGCGAAACCTGGGTGTC R:GCCTCCTTGTTGAAAGTGGTCA
Sox9 F:TCCACGAAGGGTCTCTTCTC R:AGGAAGCTGGCAGACCAGTA
Pgc1α F: AGCCGTGACCACTGACAACGAG R: GCTGCATGGTTCTGAGTGCTAAG
Cebpα F:CAAGAACAGCAACGAGTACCG R:GTCACTGGTCAACTCCAGCAC
Fas F:TCCGTGAGTTCACCAACCAAA R:GGGGGTTCCCTGTTAAATGGG
Glut4 F:AAGATGGCCACGGAGAGAG R:GTGGGTTGTGGCAGTGAGTC
Pparγ F:TCGCTGATGCACTGCCTATG R:GAGAGGTCCACAGAGCTGATT
Cebpβ F:GTGTGGACACGGGACTGAC R:CGCAGGAACATCTTTAAGTGA
Mcad F:ATGCCCTGGATAGGAAGACA R:GAGCCTAGCGAGTTCAACCT
Ucp1 F:GTGAACCCGACAACTTCCGAA R: TGAAACTCCGGCTGAGAACAT

Browning Sections of subcutaneous abdominal wall fat (prepared by the Harvard Histopathology Lab) were deparaffinized and rehydrated in water, quenched in 1% hydrogen peroxide in DI water for 10 minutes. Slides were washed with PBST for 2x5min at room temperature then incubated with blocking buffer (5% normal goat serum in PBS) for 30 minutes. Primary antibody (UCP-1 polyclonal ab10983 1:500, Abcam, Cambridge, UK) in PBS and 2.5% normal goat serum was added to slides and incubated overnight at 40°C. Slides were then washed in PBST for 3x5 minutes at room temperature. Secondary antibody (biotinylated goat anti-rabbit IgG, 1:200, Vector Labs, Burlingame, CA, USA) in PBS with 2.5% normal goat serum was incubated for 1hr at room temperature then washed in PBST for 3x5minutes. ABC complex (Vecta stain elite kit, Vector Labs, Burlingame, CA, USA) added to slides and incubated for 30 minutes at room temperature then washed 3x5min in PBST. Substrate reagent was incubated for 2-8 minutes (Vector NovaRED substrate kid for peroxidase, SK-4800, Vector Labs, Burlingame, CA, USA).

Slides checked for adequate chromagen development. When sufficiently stained, slides rinsed in DI water for 5 minutes. Slides then dehydrated and mounted.

Statistics The indicated statistical analyses were performed either in Excel or in GraphPad Prism.

ACKNOWLEDGEMENTS

We thank Shirley Liao for assistance in lifespan studies, and Justin Reynolds for assistance with H_2S assays.

REFERENCES

1. Natale V. A comprehensive description of the severity groups in Cockayne syndrome. *Am J Med Genet A.* 2011;155A(5):1081-1095.

2. Brace LE, Vose SC, Vargas DF, Zhao S, Wang XP, Mitchell JR. Lifespan extension by dietary intervention in a mouse model of Cockayne Syndrome uncouples early postnatal development from segmental progeria. *Aging Cell.* 2013.

3. Brace LE, Vose SC, Stanya K, et al. Increased oxidative phosphorylation in response to acute and chronic DNA damage. *Aging and Mechanisms of Disease.* 2016.

4. Cristancho AG, Lazar MA. Forming functional fat: a growing understanding of adipocyte differentiation. *Nat Rev Mol Cell Biol.* 2011;12(11):722-734.

5. Tang QQ, Lane MD. Adipogenesis: from stem cell to adipocyte. *Annu Rev Biochem.* 2012;81:715-736.

6. Niemela S, Miettnen, S., Sarkanen, J.R., and Ashammakhi, N. *Adipose Tissue and Adipocyte Differentiation: Molecular and Cellular Aspects and Tissue Engineering Applications.* Vol 42008.

7. Rosen ED, MacDougald OA. Adipocyte differentiation from the inside out. *Nat Rev Mol Cell Biol.* 2006;7(12):885-896.

8. Karakasilioti I, Kamileri I, Chatzinikolaou G, et al. DNA damage triggers a chronic autoinflammatory response, leading to fat depletion in NER progeria. *Cell Metab.* 2013;18:403-415.

9. Chen YW, Harris RA, Hatahet Z, Chou KM. Ablation of XP-V gene causes adipose tissue senescence and metabolic abnormalities. *Proc Natl Acad Sci U S A.* 2015;112(33):E4556-4564.

10. Prasher JM, Lalai AS, Heijmans-Antonissen C, et al. Reduced hematopoietic reserves in DNA interstrand crosslink repair-deficient Ercc1-/- mice. *EMBO J.* 2005;24(4):861-871.

11. Naveiras O, Nardi V, Wenzel PL, Hauschka PV, Fahey F, Daley GQ. Bone-marrow adipocytes as negative regulators of the haematopoietic microenvironment. *Nature.* 2009;460(7252):259-263.

12. Nadri S, Soleimani M, Hosseni RH, Massumi M, Atashi A, Izadpanah R. An efficient method for isolation of murine bone marrow mesenchymal stem cells. *Int J Dev Biol.* 2007;51(8):723-729.

13. Rossi DJ, Bryder D, Seita J, Nussenzweig A, Hoeijmakers J, Weissman IL. Deficiencies in DNA damage repair limit the function of haematopoietic stem cells with age. *Nature.* 2007;447(7145):725-729.

14. Fazeli PK, Horowitz MC, Macdougald OA, et al. Marrow Fat and Bone--New Perspectives. *J Clin Endocrinol Metab.* 2013.

15. Lecka-Czernik B. Marrow fat metabolism is linked to the systemic energy metabolism. *Bone.* 2012;50(2):534-539.

16. Rosen CJ. Bone remodeling, energy metabolism, and the molecular clock. *Cell Metab.* 2008;7(1):7-10.

17. Devlin MJ, Cloutier AM, Thomas NA, et al. Caloric restriction leads to high marrow adiposity and low bone mass in growing mice. *J Bone Miner Res.* 2010;25(9):2078-2088.

18. Fazeli PK, Bredella MA, Misra M, et al. Preadipocyte factor-1 is associated with marrow adiposity and bone mineral density in women with anorexia nervosa. *J Clin Endocrinol Metab.* 2010;95(1):407-413.

19. Fazeli PK, Bredella MA, Freedman L, et al. Marrow fat and preadipocyte factor-1 levels decrease with recovery in women with anorexia nervosa. *J Bone Miner Res.* 2012;27(9):1864-1871.

20. Hine C, Harputlugil E, Zhang Y, et al. Endogenous Hydrogen Sulfide Production Is Essential for Dietary Restriction Benefits. *Cell.* 2014.

21. Nance MA, Berry SA. Cockayne syndrome: review of 140 cases. *Am J Med Genet.* 1992;42(1):68-84.

22. Tchkonia T, Morbeck DE, Von Zglinicki T, et al. Fat tissue, aging, and cellular senescence. *Aging Cell.* 2010;9(5):667-684.

23. van de Ven M, Andressoo JO, Holcomb VB, et al. Adaptive stress response in segmental progeria resembles long-lived dwarfism and calorie restriction in mice. *PLoS Genet.* 2006;2:e192.

24. Charania RS, Kern WF, Charkrabarty S, Holter J. Successful management of gelatinous transformation of the bone marrow in anorexia nervosa with hematopoietic growth factors. *Int J Eat Disord.* 2011;44(5):469-472.

25. Kawahara H, Mitani Y, Nose K, et al. Should fundoplication be added at the time of gastrostomy placement in patients who are neurologically impaired? *J Pediatr Surg.* 2010;45(12):2373-2376.

26. Fang EF, Scheibye-Knudsen M, Brace LE, et al. Defective mitophagy in XPA via PARP-1 hyperactivation and NAD(+)/SIRT1 reduction. *Cell.* 2014;157:882-896.

27. Chen YH, Yao WZ, Geng B, et al. Endogenous hydrogen sulfide in patients with COPD. *Chest*. 2005;128(5):3205-3211.

28. Miller RA, Buehner G, Chang Y, Harper JM, Sigler R, Smith-Wheelock M. Methionine-deficient diet extends mouse lifespan, slows immune and lens aging, alters glucose, T4, IGF-I and insulin levels, and increases hepatocyte MIF levels and stress resistance. *Aging Cell*. 2005;4(3):119-125.

29. Singha S, Kim D, Moon H, et al. Toward a selective, sensitive, fast-responsive, and biocompatible two-photon probe for hydrogen sulfide in live cells. *Anal Chem*. 2015;87(2):1188-1195.

CHAPTER 6

Discussion and Future Directions

Summary and Conclusions

Cockayne syndrome (CS) is a rare disorder characterized by dwarfism, photosensitivity, ataxia and early death for which only palliative care currently exists. Because some of the symptoms of CS, including loss of subcutaneous adipose tissue, premature hearing loss and neurodegeneration resemble signs or "segments" of normal aging, CS is classified as a segmental progeroid disorder. Each of the five genes associated with CS encodes a protein belonging to the nucleotide excision DNA repair pathway (NER) responsible for the removal of bulky DNA lesions, including those induced by UV light. The fact that many such segmental progeroid disorders are associated with inborn defects in DNA damage repair and signaling has been interpreted as evidence in favor of DNA damage as a major cause of the normal aging process. However, as neither the molecular etiology of aging, nor how specific defects in proteins involved in NER function underlie symptoms of CS are known, the causal molecular link between DNA damage and aging or CS remains to be rigorously tested.

Here, we established and characterized a new mouse model of severe CS, the CX model, with the goal of gaining insight into disease etiology. CX mice survive weaning with high penetrance, but have a reduced lifespan of approximately 5 months with a myriad of symptoms mimicking the human disease. In Chapter 2, we performed the initial characterization of this model and

gained insight into a developmental bottleneck during the transition from mother's milk to solid food. We determined that perinatal lethality was linked to starvation, most likely due to a lack of coordination in chewing and swallowing, as is often observed in CS patients (E. Nielan, personal communication), and that survival past the weaning period could be accomplished with high penetrance simply by providing mice with food of a soft consistency by postnatal day 14. In Chapter 3, while investigating the mechanism underlying the progressive loss of adiposity in adult CX mice, we revealed an adaptive metabolic response to DNA damage involving a general increase in oxidative phosphorylation, with a specific increase in fatty acid oxidation (FAO) *in vivo*. The increase in oxidative phosphorylation upon DNA damage was dependent on activation of PARP-1, driving NAD+ and ATP depletion and subsequent activation of AMPK, increasing FAO-related gene expression. This response represents a beneficial adaptation to energy depletion upon DNA damage, as preventing the increase in FAO, either by inhibiting mitochondrial entry of fatty acids or genetic loss of AMPK, reduced cell viability upon damage. Additionally, increasing FAO via dietary methionine restriction reduced adiposity but extended lifespan to a maximum of 27 weeks. In Chapter 4, we investigated the role of demyelination in the progressive neurodegeneration observed in CX mice, and possible links to altered energy metabolism observed in Chapter 3. We found age-dependent patchy loss of myelin with secondary axonal loss, astrogliosis and increased gene expression of key enzymes involved in the catabolism of the major myelin lipid components. Further

investigation is required to test whether myelin-derived fatty acids are being used for supplemental energy production, and the potential contribution of this to demyelination and subsequent neurodegeneration. Lastly, in Chapter 5, we used the CX mouse as a discovery platform to identify potential therapeutic interventions, such as H2S or NAD+ supplementation, combined with disease-related endpoints that could be used as markers of therapeutic interventional efficacy, including adipose tissue senescence, bone marrow cellularity or liver enzymes panels.

Utility of mild and severe mouse models of CS

The symptoms in CS patients range in severity from mild, surviving upwards of 40 years, to very severe, with average lifespan of 3-4 years[1,2]. A similar range of severities also exists in diverse mouse models of CS. Mice engineered with null alleles of *Csa* or *Csb* have very mild disease manifestations such as premature hearing loss and progressive loss of subcutaneous fat, but possess a normal lifespan[3,4]. Crossing these animals with the NER-deficient *Xpa* or *Xpc* knockout mice results in a much more severe phenotype characterized by a postnatal developmental bottleneck around two weeks of age at the time when mice switch from milk to solid food. This culminates in death likely due to starvation unless adequate nutrition in the form of food with a soft consistency is provided. Importantly, postnatal death before weaning is not characteristic of even severe CS in humans, suggesting that early death in CX mice is not a valid CS-related

endpoint (nor likely one related to normal aging). Nonetheless, CX mice that survive weaning go on to display a progressive loss of adiposity and neurodegeneration resembling severe Type II CS[5-7]. A similar developmental bottleneck is observed upon loss of other genes implicated in CS, including *Xpg* or combined $Xpd^{XPCS/XPCS}/Xpa$ or $Xpd^{TTD/TTD}/Xpa$[8,9], but also in models of NER progeria not typically associated with CS, including *Ercc1* and *Xpf*. Presumably, the soft diet intervention that disrupts the developmental bottleneck in CX mice and allows emergence of phenotypes that actually resemble CS would be similarly effective in other NER deficient models such as *Csb*/*Xpc*, although this remains to be tested.

There are several advantages to having models of both mild and severe CS in which to study disease etiology and interventional approaches. For example, interventional longevity studies including those utilizing MetR diets or NMN supplementation can be performed more rapidly in a short-lived severe model. In addition, the severe model offers a platform in which to understand and intervene in the neurodegenerative phenotype that appears to be the primary driver behind disease pathogenesis in humans. However, the use of such a severe model may prevent the elucidation of interventions that may be effective only in the context of milder disease symptoms. High-fat diet feeding may be an example of this, as it was efficacious at forestalling hearing loss in the mild $Csb^{m/m}$ model[10], but had no beneficial effects on longevity in the CX model (Figure 2.4 a).

Utility of CX mice as models of normal aging

The suitability of progeroid mice as models to study physiological aging has been, and continues to be, a topic of considerable debate[11]. Aging is a complex process and constitutes a major risk factor for pathology developments such as cardiovascular disorders, neurodegeneration, and neoplastic and metabolic syndromes, but the underlying causes remain poorly defined. The fact that a number of "segmental progeroid syndromes" that mimic some aspects, or segments, of normal aging are caused by inborn errors in genes encoding DNA damage repair and signaling proteins has been interpreted as evidence in favor of DNA damage as causative of, or at least contributing to, the normal aging process. For example, Werner and Bloom syndromes are segmental progerias with defects in ReqQ family DNA helicases, while Hutchinson Gilford progeria is caused by defects in lamin A/C that give rise to increased nuclear DNA damage signaling.

CS, caused by congenital defects in TC-NER, is similarly classified as a segmental progeroid disorder, and mouse models of such "NER progerias" are currently used as tools in which to study the role of DNA damage in the aging process. Here, we focused on two particular segments of the normal aging process evident in the CX model: progressive loss of adiposity and neurodegeneration.

Loss of subcutaneous fat in both the face and extremities is one of the most easily recognizable signs of aging in humans[12]. The progressive loss or redistribution of adipose tissue deposits, termed age-related lipodystrophy[13], consists of both loss of subcutaneous adipose and increased visceral adiposity, and is conserved across mammals including mice. Two related processes, geriatric failure to thrive in humans and terminal senescent weight loss in rodents, may also be related to age-related lipodystrophy[14]. Because the CX mouse recapitulates progressive age-related loss of adiposity, we used it as a model to understand underlying mechanisms of aging-related lipodystrophy. While previous studies in a related mouse model proposed adipose inflammation and adipocyte cell death as a mechanism underlying fat loss[15], our studies failed to uncover any increase in adipose tissue inflammation. Instead, our studies revealed numerous other mechanisms, some adaptive and others likely maladaptive, that contribute to fat loss in CX mice. So far, the best characterized of these is the adaptive increase in FAO as described in Chapter 3. Potentially, the fat loss that occurs during the normal aging process could share a similar etiology to that of CX fat loss as PARP-1 activation, reduced NAD+ and accumulation of DNA damage are all known to increase with age in rodents[16,17] and humans[18]. As outlined in Figure 5.1, our studies revealed reduced adipogenic potential, increased pre-adipocyte cellular senescence, and activation of UCP-1 and browning of white fat as mechanisms that also appear to contribute to adipose loss in the CX model. Future studies will be required to determine the relative contribution of these different mechanisms to

progressive loss of adiposity in the CX model, as well as normal aging. Such studies are important because they will reveal whether this feature of CX (or aging) results primarily from adaptive (FAO, browning) or maladaptive (reduced adipogenic potential, cellular senescence) changes in the adipose tissue. It will also be interesting to determine if these mechanisms play a role in terminal senescent weight loss/geriatric failure to thrive syndrome, for which there are currently no accepted models for research into causative mechanism.

Neurodegeneration is another segment of normal aging with likely various underlying causes, most of which are currently unknown. Similarly, CS patients as well as CX mice undergo a form of neurodegeneration that, while still poorly characterized, appears to involve primary demyelination followed by secondary axonal loss as measured in patients by a gradual reduction in nerve conduction velocity[19,20]. These velocity shifts also occur in "normal aging" in humans[21-23] and in rodents[24] though whether or not the mechanism functions in the same context as in CS remains to be seen. DNA damage is known to increase with age, but its contribution to neurodegeneration remains unclear, in part due to lack of good model systems in which to interrogate this potential relationship. The CX model provides an appropriate platform to model this relationship; however, the mechanism underlying myelin loss in CS/CX, and the potential contribution of adaptive changes in energy metabolism (Chapter 4), also remain to be determined.

In conclusion, the CX mouse has clear utility as a model with which to elucidate complex underlying mechanisms of disease pathology, but also with the potential to provide insight into some aspects of normal aging. With this potential come opportunities to examine interventions for health and lifespan improvements, ideally leading towards new therapeutic avenues for progeroid syndromes and also to better define pathways that control physiological aging.

Future interventional approaches for Cockayne syndrome patients

The lack of treatments available for CS patients is extremely disheartening. All the genes implicated in CS were cloned decades ago, and the disease, although rare, is easily recognized and diagnosed with unambiguous cell-based assays. Yet, to date there has been no effective therapy. Indeed, the only proposed clinical trial of an antioxidant mixture that extended the life of *Csb*/*Xpa* mice for several days was abruptly stopped due to funding issues. In Chapter 5, we discuss several experimental endpoints that could be used in preclinical trials in the CX model that, in addition to longevity, could be used as potential markers of efficacy of an experimental therapy. In this section, we outline both dietary and pharmacological interventional approaches with the potential to treat CS. Dietary and supplemental interventions can be easily accomplished in CS patients, as most are fed via a gastrojejunostomy feeding tube.

The use of a high fat diet (HFD) for treatment in Cockayne Syndrome has been widely discussed due to work of Scheibye-Knudsen and colleagues using these interventions in a mild mouse model of CS, *Csb*$^{m/m}$ mice. A HFD was efficacious in protection from aging-related hearing loss via a mechanism involving SIRT1 activation[10]. HFD aids in ketone body production, a key alternative fuel source in nervous tissue, as glycogen storage in astrocytes is minor and limited fats are stored besides those in myelin. *In vitro* studies have shown increased lifespan of CSB and WT worms upon treatment with ketone bodies[10,25]. In our own experiments, HFD feeding of CX animals slightly extended mean but not maximum lifespan (Figure 2.4 a). The increase in adiposity was roughly 5%, but did not persist at the end of life (Figure 2.4 d). Unfortunately, we did not measure potential changes in the spiral ganglion related to hearing loss to be able to remark on improvement upon HFD feeding, though it may have ensued. Similarly, other forms of neurological dysfunction may have been delayed, but did not affect overall lifespan. Future studies are thus required to determine the potential efficacy of increased ketone bodies via ketogenic or high fat diet with regard to multiple other CX progeroid phenotypes.

Two other dietary interventions with efficacy at extending longevity in severe NER progeria include our own study here on MetR in CX mice (Chapter 3), and another recently published work on dietary restriction in the *Ercc1*$^{\Delta/-}$ and *Xpg* models[26]. A diet low in methionine (MetR) can be procured using readily available

protein-free shakes (Mead-Johnson PFD 2) with addition of crystalline amino acid mixes; similarly, dietary restriction can be accomplished by feeding a normal diet at reduced levels. An advantage of MetR over DR is that it can be fed on an *ad libitum* basis; potentially averting the issues of hunger and poor subjective well-being that impact compliance with any regimen involving enforced food restriction. However, a major drawback shared by both MetR and DR interventions is the expectation that both will lead to a significant overall loss of body weight, predominantly of fat but also some lean body mass. While this is by no means predicted to be mutually exclusive with the benefits, it does present a practical problem with parents who typically associate improved "health" of CS children with increased growth or body weight. Thus, providing a diet that is expected to reduce body weight may not be readily accepted by parents and reduce compliance.

Our findings also bring to light pharmacological interventions with the potential to improve CS symptoms. As described below, these include NAD+ supplementation, PARP-1 inhibition, and AMPK activation. In a small cohort of CX mice, treatment with the NAD+ precursor NMN extended maximum lifespan (Figure 5.3 j). Interestingly, in the same study, a different group treated with an H2S donor had no effect. Supplementation with NAD+ precursors would ideally boost the reduced levels of NAD+ in CS patients, reducing the energy stress caused by the accumulation of unrepaired DNA damage. NMN or NR, two precursors of

NAD+ via the NAD+ salvage pathway, could be easily administered via food, water, or as a daily oral medication. Indeed, we are aware of at least one ongoing effort to test the efficacy of NAD+ supplementation in CS patients. While future studies are required to determine the complete mechanism by which NAD+ supplementation extends lifespan in CX mice, current data suggest preservation of a regulatory network involving SIRT1-mediated control of mitochondrial turnover[27]. However, several questions remain. First, how NMN or NR supplementation modulates individual NAD+ pools (not just mitochondrial) and PARP-1/SIRT1 function over the lifespan is thus of great interest. Additionally, the regulation of how supplementing NAD+ into a system in which PARP-1 is already hyperactive due to the DNA repair deficiency and SIRT1 activity therefore reduced, does not further fuel PARP-1 activity and worsen rather than improve outcome remains not well understood. Clearly, the network that regulates the activities of these two NAD+ consuming proteins (not even considering another NAD+ consumer, CD38) is still not completely understood, though their actions are intricately linked. Finally, how NAD+ depletion leads to ATP depletion and AMPK activation remains unclear. Our data point to PARP-1 acting upstream of AMPK and ATP/NAD+ depletion though it is known that AMPK interacts with both PARP-1 and SIRT1 post-translationally. Another mechanism by which AMPK alters ATP-consuming pathways is through phosphorylation of PARP-1 to enhance activity[28] or of SIRT1, to inhibit the deacetylation of p53[29]. PARP-1 mediated ATP loss is often linked to

NAD+ depletion, however the contribution of ATP to NAD+ biosynthesis is contested and remains to be tested in our system[30].

Another putative pharmacological approach to reduce energy stress is to prevent the initial NAD+ depletion by inhibiting PARP-1 activity. At least one inhibitor, Olaparib (Lynparza), is currently FDA approved for use in ovarian cancer and could be tested in the CX model for effects on NAD+ levels and disease pathogenesis. Currently, proof of principle genetic studies are underway by breeding the PARP-1 null allele into CX mice. Interestingly, preliminary results show a small tendency for PARP-1 heterozygous CX mice to do better than PAPR1 WT or KO CX mice, consistent with the notion that some PARP-1 activity may be beneficial, but not enough to deplete NAD+ levels. If this turns out to be the case, then a very careful titration of PARP-1 inhibitor may be required to reduce enzyme activity to the target level.

Finally, activators of AMPK such as metformin or AICAR could extend CX lifespan by increasing fatty acid oxidation and promoting energy homeostasis. However, without addressing the underlying PARP-1 driven NAD+ depletion, it is also possible that promoting these adaptive changes in energy metabolism may only delay rather than prevent the onset of disease symptoms. Furthermore, it remains a possibility that increased FAO observed in astrocytes could drive myelin loss and contribute to neuropathogenesis. It is essential to note though that in

studies from collaborators, PARP-1 hyperactivation and NAD+ depletion eventually drive mitochondrial dysfunction and defective SIRT1-dependent mitophagy in XPA and CX mice[27] as well as age-related accumulation of defective mitochondria in the mild CSB mouse model[4]. The adaptive changes in energy metabolism we observe may in fact precede these defects in mitochondrial function, yet fail to prevent their onset, as the central issue of DNA repair deficiency cannot be resolved. While distinguishing the difference between beneficial physiological adaptations and end-of-life decline will prove to be challenging, the CX model offers a platform in which to undertake this task.

Future Directions

The scope of this thesis ranged from DNA damage to cellular energy metabolism to neurodegeneration with translational implications for Cockayne syndrome patients as well as the aging field. The CX mouse, modeling DNA damage accumulation, allowed for connections to be made between these broad fields and opened numerous avenues of future investigations.

This work uncovered the general, beneficial, and cell-autonomous adaptation of increased fatty acid oxidation in response to DNA damage, but an improved understanding of the mechanism is essential. PARP-1 was shown to be activated by multiple types of DNA lesions, converging on AMPK activation,

however the specific progression is not completely clear and deserves further investigation. PARP-1 depletes NAD+ levels but how and why ATP levels also drop is less defined. Great controversy exists in whether PARP-1-dependent NAD+ loss alters energy levels due to NAD+ recycling. Our *in vitro* system is well suited to test these claims using specific inhibitors of the salvage pathway, such as FK866, and measuring NAD+ and ATP levels upon damage. Simultaneous measurement of AMP levels, though more difficult, will also strengthen the connection of PARP-1 activation to AMPK activation. If NAD+ depletion does not directly cause ATP loss, it could then result from either free PAR chains, cleaved by PAR glycohydrolase, PARG, bound to and inhibiting hexokinase I and blocking ATP production from glycolysis[30], or increased AMP pools upon PAR catabolism, via NUDIX hydrolases, competing for the adenine nucleotide transporter and diminishing ATP pools[31]. To determine if either or both possibilities are occurring under our conditions, the first course of action is to measure the activity of PAR catabolic enzymes, PARG and NUDIX hydrolases, in response to damage and then inhibit each enzyme alone or concurrently and determine AMP levels and AMPK activation in a time-course after DNA damage. Hexokinase activity will also be measured in response to damage with or without the addition of PAR catabolism inhibitors. These approaches will strengthen the pathway of how energy crisis upon DNA damage mediates the activation of AMPK to drive metabolic alterations.

We determined *in vitro* that loss of AMPK or blocking FAO was detrimental to cell viability and that increasing FAO via dietary methionine restriction increased CX lifespan, supporting the conclusion that the metabolic shift to FAO is a beneficial and adaptive mechanism. Our work also established many potential therapeutic interventions for CS patients by manipulating this adaptation, for example through NAD+ supplementation, partial loss of PARP-1, or a diet low in methionine. Combination therapies such as NAD+ supplementation with a methionine restricted diet should also be tested and we would assume further benefits to result. Another exciting possibility is the combination of NAD+ supplementation with a hydrogen sulfide prodrug. Microvascular dysfunction is suggested to be a driver of CS pathology[32] and H2S has been shown to stimulate endothelial cell proliferation and migration and increase vascular density (Longchamp et. al., under review) and the potential for a synergistic response of NAD+ and H2S in promoting vascular health (Das et. al., under review). The CX mouse is an excellent model to test the potential benefits of co-supplementation of NAD+ and H2S with the ability to examine vascular function, alterations in neurovasculature potentially promoting neurodegeneration, and ideally further extending lifespan.

Another conceivable method of manipulating the adaptive mechanism for a further beneficial outcome in lifespan/healthspan would be to increase fatty acid oxidation directly through the inhibition of Acetyl-CoA carboxylase 2 (ACC2).

ACC1/2 function to regulate fatty acid metabolism by producing malonyl-CoA which inhibits the transfer of the fatty acyl group from acyl CoA to carnitine with carnitine acyltransferase, thus inhibiting fatty acid oxidation. ACC1 regulates fatty acid synthesis whereas ACC2 mainly regulates FAO. Genetic loss of ACC2 has been shown to increase whole body FAO in wildtype mice with conflicting results on either maintenance or loss of overall adiposity[33,34], and inhibition of ACC1/2 with small molecules similarly increases FAO *in vivo* with slight to moderate reductions in body weight in obese mice or rats[35,36]. Similarly, use of a specific ACC2 inhibitor, soraphen A, increased FAO while inhibiting adipocyte differentiation *in vitro*[37]. These drugs can be first tested *in vitro* to determine if pretreatment with ACC2 inhibitors can protect cells against DNA damaging agents. They also hold the potential to be utilized in the future as a therapeutic intervention for CS and could be tested for *in vivo* use in the protection of normal cells against and/or sensitize tumors to chemotherapy.

An enhanced comprehension of the mechanism connecting energy stress to metabolic modifications will also allow one to exploit this adaptation under conditions of extreme energy crisis such as chemotherapy. If the energetic cost of DNA damage is what drives this beneficial adaptation, one could assume that, in the case of chemotherapy for cancer treatment, a preconditioning period that increases fatty acid oxidation may improve treatment outcome. This concept was similarly tested by short-term fasting preconditioning before chemotherapy, which

increases fat burning, and was observed to sensitize tumors to radio- or chemotherapy while protecting normal cells from damage[38-40]. Diets low in methionine have also shown to suppress metastatic cancers[41] and inhibit tumor growth[42]. We can test this *in vitro* using soft agar assays with transformed cell lines by pretreating for a few days with ACC2 inhibitors, metformin or AICAR with or without addition of a chemotherapeutic drug to investigate a synergistic effect, and analyze colony formation. If successful, subcutaneous cancer mouse models can be generated and animals pretreated with activators of FAO with or without addition of chemotherapies and measure body weight and tumor volume over time. If activating FAO prior to genotoxic slows tumor progression in mice *in vivo*, the translational implications are substantial. Short-term fasting or liquid meal replacements prior to chemotherapy or surgical stress are not difficult changes to make in one's daily life, especially if those days are surrounding major medical interventions, but if similar protection can be met by medication, the compliance would be significantly increased.

Finally, we are interested in determining if fatty acids are a well utilized fuel for the CX brain, with the potential for myelin to be a source of fatty acids via catabolism. To first determine baseline levels of metabolites in CX and control brains throughout the lifespan, focused microwave irradiation can be utilized for rapid fixation to halt metabolic flow in the brain, combined with matrix assisted laser desorption ionization mass spectrometry MALDI/MS and capillary

electrophoresis/electrospray ionization (CE/ESI)/MS[43]. This allows for visualizing multiple metabolites in discrete areas of the brain with concise quantification[44]. Using this technique, specific brain sections can be probed for ATP, ADP, AMP, NAD/NADH and ADP-ribose content. Baseline levels of these metabolites can be measured in control and CX mice across the lifespan and upon acute injection with DNA damaging agents. Imaging MS (IMS) combined with metabolomics after rapid fixation can also be used to quantify and visualize metabolic flux in the mouse brain *in vivo*. MALDI/IMS can also determine alterations in white matter lipid profiles between genotypes and over time[45]. Stable isotope labeled or gold labelled fatty acids can be injected into the circulation of a mouse and uptake and incorporation of FA measured in whole brain and in the myelin/white matter fraction using this method as was previously performed for glucose metabolism flux analysis[46]. Probing the metabolic flux in CX brains versus control mice versus control mice upon genotoxic stress from preweaning to peak CX fitness around 8-12 weeks of age, to "aged" CX between 16-22 weeks would allow us to better understand alterations in substrate utilization in response to DNA damage. To determine if myelin is a source of fatty acids for oxidation in the brain, initial steps would be to section CX and control brains over the lifespan and perform immunohistochemistry for key enzymes involved in both FAO and sphingomyelin or cerebroside breakdown and determine patterns of colocalization. Distinguishing between fatty acids derived from the circulation versus those

potentially catabolized from myelin proves to be an extremely challenging distinction and further investigation will undeniably be required.

The above avenues of investigation are in no way exhaustive as this work opened multiple fields for prospective focus. Future work will only benefit from a more well-defined mechanism connecting genotoxic stress to metabolic adaptations and will allow us to manipulate this pathway to potentially further beneficial outcome, whether in the delay of neurodegeneration in CX mice leading to lifespan extension or in protection from chemotherapy.

REFERENCES

1. Natale V. A comprehensive description of the severity groups in Cockayne syndrome. *Am J Med Genet A.* 2011;155A(5):1081-1095.

2. Nance MA, Berry SA. Cockayne syndrome: review of 140 cases. *Am J Med Genet.* 1992;42(1):68-84.

3. Kamenisch Y, Fousteri M, Knoch J, et al. Proteins of nucleotide and base excision repair pathways interact in mitochondria to protect from loss of subcutaneous fat, a hallmark of aging. *J Exp Med.* 2010;207(2):379-390.

4. Scheibye-Knudsen M, Ramamoorthy M, Sykora P, et al. Cockayne syndrome group B protein prevents the accumulation of damaged mitochondria by promoting mitochondrial autophagy. *J Exp Med.* 2012;209:855-869.

5. Murai M, Enokido Y, Inamura N, et al. Early postnatal ataxia and abnormal cerebellar development in mice lacking Xeroderma pigmentosum Group A and Cockayne syndrome Group B DNA repair genes. *Proc Natl Acad Sci U S A.* 2001;98(23):13379-13384.

6. van der Pluijm I, Garinis GA, Brandt RM, et al. Impaired genome maintenance suppresses the growth hormone--insulin-like growth factor 1 axis in mice with Cockayne syndrome. *PLoS Biol.* 2007;5(1):e2.

7. Laposa RR, Huang EJ, Cleaver JE. Increased apoptosis, p53 up-regulation, and cerebellar neuronal degeneration in repair-deficient Cockayne syndrome mice. *Proc Natl Acad Sci U S A.* 2007;104(4):1389-1394.

8. Harada YN, Shiomi N, Koike M, et al. Postnatal growth failure, short life span, and early onset of cellular senescence and subsequent immortalization in mice lacking the xeroderma pigmentosum group G gene. *Mol Cell Biol.* 1999;19(3):2366-2372.

9. Andressoo JO, Mitchell JR, de Wit J, et al. An Xpd mouse model for the combined xeroderma pigmentosum/Cockayne syndrome exhibiting both cancer predisposition and segmental progeria. *Cancer Cell.* 2006;10(2):121-132.

10. Scheibye-Knudsen M, Mitchell SJ, Fang EF, et al. A High-Fat Diet and NAD(+) Activate Sirt1 to Rescue Premature Aging in Cockayne Syndrome. *Cell Metab.* 2014;20:840-855.

11. Miller RA. 'Accelerated aging': a primrose path to insight? *Aging Cell.* 2004;3(2):47-51.

12. Tchkonia T, Morbeck DE, Von Zglinicki T, et al. Fat tissue, aging, and cellular senescence. *Aging Cell.* 2010;9(5):667-684.

13. Cartwright MJ, Tchkonia T, Kirkland JL. Aging in adipocytes: potential impact of inherent, depot-specific mechanisms. *Exp Gerontol.* 2007;42(6):463-471.

14. Black BJ, Jr., McMahan CA, Masoro EJ, Ikeno Y, Katz MS. Senescent terminal weight loss in the male F344 rat. *Am J Physiol Regul Integr Comp Physiol.* 2002;284:R336-342.

15. Karakasilioti I, Kamileri I, Chatzinikolaou G, et al. DNA damage triggers a chronic autoinflammatory response, leading to fat depletion in NER progeria. *Cell Metab.* 2013;18:403-415.

16. Yoshino J, Mills KF, Yoon MJ, Imai S. Nicotinamide mononucleotide, a key NAD(+) intermediate, treats the pathophysiology of diet- and age-induced diabetes in mice. *Cell Metab.* 2011;14(4):528-536.

17. Gomes AP, Price NL, Ling AJ, et al. Declining NAD(+) induces a pseudohypoxic state disrupting nuclear-mitochondrial communication during aging. *Cell.* 2013;155(7):1624-1638.

18. Massudi H, Grant R, Braidy N, Guest J, Farnsworth B, Guillemin GJ. Age-associated changes in oxidative stress and NAD+ metabolism in human tissue. *PLoS One.* 2012;7(7):e42357.

19. Gitiaux C, Blin-Rochemaure N, Hully M, et al. Progressive demyelinating neuropathy correlates with clinical severity in Cockayne syndrome. *Clin Neurophysiol.* 2015;126(7):1435-1439.

20. Moosa A, Dubowitz V. Peripheral neuropathy in Cockayne's syndrome. *Arch Dis Child.* 1970;45(243):674-677.

21. Taylor PK. Non-linear effects of age on nerve conduction in adults. *J Neurol Sci.* 1984;66(2-3):223-234.

22. Suzuki M. Peripheral neuropathy in the elderly. *Handb Clin Neurol.* 2013;115:803-813.

23. Tohgi H, Tsukagoshi H, Toyokura Y. Quantitative changes of sural nerves in various neurological diseases. *Acta Neuropathol.* 1977;38(2):95-101.

24. Verdú E, Ceballos D, Vilches JJ, Navarro X. Influence of aging on peripheral nerve function and regeneration. *J Peripher Nerv Syst.* 2000;5(4):191-208.

25. Edwards C, Canfield J, Copes N, Rehan M, Lipps D, Bradshaw PC. D-beta-hydroxybutyrate extends lifespan in C. elegans. *Aging (Albany NY).* 2014;6(8):621-644.

26. Vermeij WP, Dollé ME, Reiling E, et al. Restricted diet delays accelerated ageing and genomic stress in DNA-repair-deficient mice. *Nature.* 2016;537(7620):427-431.

27. Fang EF, Scheibye-Knudsen M, Brace LE, et al. Defective mitophagy in XPA via PARP-1 hyperactivation and NAD(+)/SIRT1 reduction. *Cell.* 2014;157:882-896.

28. Walker JW, Jijon HB, Madsen KL. AMP-activated protein kinase is a positive regulator of poly(ADP-ribose) polymerase. *Biochem Biophys Res Commun.* 2006;342(1):336-341.

29. Lee CW, Wong LL, Tse EY, et al. AMPK promotes p53 acetylation via phosphorylation and inactivation of SIRT1 in liver cancer cells. *Cancer Res.* 2012;72(17):4394-4404.

30. Fouquerel E, Goellner EM, Yu Z, et al. ARTD1/PARP1 negatively regulates glycolysis by inhibiting hexokinase 1 independent of NAD+ depletion. *Cell Rep.* 2014;8(6):1819-1831.

31. Formentini L, Macchiarulo A, Cipriani G, et al. Poly(ADP-ribose) catabolism triggers AMP-dependent mitochondrial energy failure. *J Biol Chem.* 2009;284(26):17668-17676.

32. Brooks PJ, Cheng TF, Cooper L. Do all of the neurologic diseases in patients with DNA repair gene mutations result from the accumulation of DNA damage? *DNA Repair (Amst).* 2008;7(6):834-848.

33. Hoehn KL, Turner N, Swarbrick MM, et al. Acute or chronic upregulation of mitochondrial fatty acid oxidation has no net effect on whole-body energy expenditure or adiposity. *Cell Metab.* 2010;11(1):70-76.

34. Abu-Elheiga L, Matzuk MM, Abo-Hashema KA, Wakil SJ. Continuous fatty acid oxidation and reduced fat storage in mice lacking acetyl-CoA carboxylase 2. *Science.* 2001;291(5513):2613-2616.

35. Glien M, Haschke G, Schroeter K, et al. Stimulation of fat oxidation, but no sustained reduction of hepatic lipids by prolonged pharmacological inhibition of acetyl CoA carboxylase. *Horm Metab Res.* 2011;43(9):601-606.

36. Harriman G, Greenwood J, Bhat S, et al. Acetyl-CoA carboxylase inhibition by ND-630 reduces hepatic steatosis, improves insulin sensitivity, and modulates dyslipidemia in rats. *Proc Natl Acad Sci U S A.* 2016;113(13):E1796-1805.

37. Cordonier EL, Jarecke SK, Hollinger FE, Zempleni J. Inhibition of acetyl-CoA carboxylases by soraphen A prevents lipid accumulation and adipocyte differentiation in 3T3-L1 cells. *Eur J Pharmacol.* 2016;780:202-208.

38. Raffaghello L, Lee C, Safdie FM, et al. Starvation-dependent differential stress resistance protects normal but not cancer cells against high-dose chemotherapy. *Proc Natl Acad Sci U S A.* 2008;105(24):8215-8220.

39. Lee C, Raffaghello L, Brandhorst S, et al. Fasting cycles retard growth of tumors and sensitize a range of cancer cell types to chemotherapy. *Sci Transl Med.* 2012;4(124):124ra127.

40. Safdie F, Brandhorst S, Wei M, et al. Fasting enhances the response of glioma to chemo- and radiotherapy. *PLoS One.* 2012;7(9):e44603.

41. Jeon H, Kim JH, Lee E, et al. Methionine deprivation suppresses triple-negative breast cancer metastasis in vitro and in vivo. *Oncotarget.* 2016.

42. Hens JR, Sinha I, Perodin F, et al. Methionine-restricted diet inhibits growth of MCF10AT1-derived mammary tumors by increasing cell cycle inhibitors in athymic nude mice. *BMC Cancer.* 2016;16:349.

43. Sugiura Y, Katsumata Y, Sano M, et al. Visualization of in vivo metabolic flows reveals accelerated utilization of glucose and lactate in penumbra of ischemic heart. *Sci Rep.* 2016;6:32361.

44. Hattori K, Kajimura M, Hishiki T, et al. Paradoxical ATP elevation in ischemic penumbra revealed by quantitative imaging mass spectrometry. *Antioxid Redox Signal.* 2010;13(8):1157-1167.

45. Nunez K, Kay J, Krotow A, et al. Cigarette Smoke-Induced Alterations in Frontal White Matter Lipid Profiles Demonstrated by MALDI-Imaging Mass Spectrometry: Relevance to Alzheimer's Disease. *J Alzheimers Dis.* 2016;51(1):151-163.

46. Sugiura Y, Honda K, Kajimura M, Suematsu M. Visualization and quantification of cerebral metabolic fluxes of glucose in awake mice. *Proteomics.* 2014;14(7-8):829-838.